

Cardiff University

School of Psychology

Doctoral Thesis

**Rhythmic neural dynamics in the
sensorimotor system: the role and
mechanism of beta oscillations**

Author:

Jacopo BARONE

Supervisors:

Prof. Krish SINGH

Dr. Holly ROSSITER

*A thesis submitted to Cardiff University
for the degree of Doctor of Philosophy*

January 2023

Summary

Oscillatory neural activity in the beta band has been consistently observed across the sensorimotor cortex. Neurological disorders that primarily affect the motor system are often linked with alterations in beta dynamics. This has led many researchers to hypothesise a key role for this rhythm in somatosensory processing and motor control. An agreement on the supposedly beta's functional role, however, is currently lacking.

This thesis studied beta oscillations while focusing on two main aspects: the role of beta in complex motor functions and the physiological mechanism behind its generation.

In the first two chapters, we explored the role of beta in the sensorimotor system by employing a joystick-reaching task while recording neural activity with MEG. We first investigated the relationship of beta oscillations with learning in a motor adaptation task. After being exposed to adaptation-inducing errors, post-movement beta activity was reduced. This effect, however, was short-lived and widely spread across a set of frontoparietal nodes, suggesting a link with generalised error monitoring. We then focused on the potential "inhibitory" role of beta in a stop-signal paradigm. We contrasted activity in IFG and pre-SMA during successful and unsuccessful stopping. Although we used standard (averaged) and beta-burst (single-trial) analyses, no differences were observable between conditions. Taken together, our findings on beta's functional role produced mixed results when compared with the existing literature.

In the third chapter, we shifted our focus to the physiological mechanisms behind beta origin. We investigated the relationship between GABA and beta in a pharmaco-MEG study. We additionally employed a set of novel techniques for power spectra parametrisation, which successfully separated neural activity into rhythmic and arrhythmic components. While we confirmed a modulation of beta oscillations after GABAergic interventions, we also showed a dynamic change in the aperiodic activity. These findings, however, were not observable across canonical averaged spectrograms, where periodic and aperiodic components conflated masking the true effect of GABA. We suggest that failing to dissociate between rhythmic and arrhythmic neural features could result in a misinterpretation of the underlying physiology of beta oscillations.

Contents

List of Figures	vi
List of Tables	viii
1 General introduction	1
1.1 The importance of rhythmic neural activity	1
1.2 The beta rhythm	2
1.2.1 The link between beta and the sensorimotor system	2
1.2.2 What is the role of beta oscillations?	5
1.2.3 Mechanisms of generating beta	7
1.3 MEG	9
1.4 Novel insights on neural oscillatory activity	13
1.4.1 The "burst-like" hypothesis	13
1.4.2 Rhythmic and arrhythmic neural signals	15
1.5 Thesis overview	17
2 Beta dynamics during motor adaptation	18
2.1 Introduction	18
2.2 Material and methods	21
2.2.1 Participants	21
2.2.2 Experimental setup	21
2.2.3 Behavioural analysis	23
2.2.4 MEG acquisition and preprocessing	24

2.2.5	Source imaging	24
2.2.6	TFRs on virtual channel time courses	25
2.2.7	Beta burst analysis	26
2.2.8	Statistical analysis	27
2.3	Results	29
2.3.1	Cursor perturbation elicits motor adaptation	29
2.3.2	Beta rebound is modulated during motor adaptation	34
2.3.3	Beta bursts amplitude is reduced during adaptation	40
2.4	Discussion	45
3	The role of beta oscillations during action-stopping	49
3.1	Introduction	49
3.2	Material and methods	52
3.2.1	Participants	52
3.2.2	Experimental setup	52
3.2.3	Behavioural analysis	54
3.2.4	MEG acquisition and preprocessing	55
3.2.5	Source imaging	56
3.2.6	TFRs on virtual channel time courses	57
3.2.7	Beta burst analysis	57
3.2.8	Statistical analysis	59
3.3	Results	60
3.3.1	Behavioural performance	60
3.3.2	Beta desynchronisation and rebound dynamics	62
3.3.3	Beta power during stopping	67
3.4	Discussion	70
4	The link between GABA and beta oscillations	73
4.1	Introduction	73
4.2	Material and methods	76
4.2.1	Design and participants	76

4.2.2	MEG acquisition and preprocessing	77
4.2.3	Source imaging	78
4.2.4	TFRs on virtual channel time courses	79
4.2.5	Statistical analysis	80
4.2.6	Power spectra parametrisation	80
4.3	Results	82
4.3.1	Behavioural features	82
4.3.2	Beta power is modulated by gaboxadol and zolpidem	82
4.3.3	Effect of pharmacological intervention on periodic and aperiodic features of power spectra	88
4.4	Discussion	93
5	General Discussion	98
5.1	The role of beta oscillations: yet unclear?	99
5.2	GABA influence on beta oscillations	100
5.3	Limitations	101
5.4	Conclusion	103
A	Appendix: Beta dynamics during motor adaptation	104
B	Appendix: The role of beta oscillations during action-stopping	107
C	Appendix: The link between GABA and beta oscillations	109
	References	111

List of Figures

1.1	Beta desynchronisation and rebound	3
1.2	Generative models of beta oscillations	8
1.3	MEG signal origin	11
1.4	Single-trial beta-bursts	14
1.5	Overview of periodic and aperiodic spectral features	16
2.1	Experimental protocol and angular perturbation	23
2.2	Behavioural features across the experiment	30
2.3	Angular error across time and phase	32
2.4	Reaction time and movement duration across phase	33
2.5	Beta dynamics during movement	34
2.6	PMBR across the experiment	36
2.7	Beta desynchronisation across the experiment	37
2.8	PMBR dynamics across left ROIs	38
2.9	PMBR dynamics across right ROIs	39
2.10	Beta bursts across time	42
2.11	Burst count across the experiment	43
3.1	Experimental protocol	53
3.2	Reaction time between conditions	61
3.3	Stimulus-locked TFRs across ROIs and conditions	63
3.4	Beta desynchronisation during GO and uSTOP trials	64
3.5	PMBR during GO and uSTOP trials	65

3.6	Beta peak timing	66
3.7	Beta power during sSTOP and uSTOP trials	68
4.1	Normalised TFRs during PRE session	83
4.2	TFRs Gaboxadol and Placebo - POST60	85
4.3	TFRs Zolpidem and Placebo - POST60	86
4.4	TFRs Gaboxadol and Zolpidem - POST60	87
4.5	Time evolving periodic and aperiodic features	88
4.6	Contrast of gaboxadol and zolpidem interventions around movement onset in M1	91
4.7	Contrast of gaboxadol and zolpidem interventions after movement offset in M1	92
A.1	Individual beta desynchronisation	104
A.2	Individual beta rebound	105

List of Tables

2.1	Descriptive statistics of behavioural features across phase	29
2.2	PMBR across phase and trial order	36
2.3	Beta desynchronisation across phase and trial order	37
2.4	Beta bursts features across phase and trial order	44
3.1	<i>Post-hoc</i> results for PMBR peak time across ROIs	66
3.2	Paired <i>t</i> -test results for burst-amplitude during stopping	69
3.3	Paired <i>t</i> -test results for burst- duration during stopping	69
3.4	Paired <i>t</i> -test results for burst-count during stopping	69
4.1	Behavioural features before and after pharmacological intervention . . .	84
A.1	Summary statistics of PMBR for each ROI	106
B.1	Beta desynchronisation during GO and uSTOP conditions	108
B.2	PMBR during GO and uSTOP conditions	108
C.1	Summary statistics for gaboxadol and zolpidem interventions around movement onset	110
C.2	Summary statistics for gaboxadol and zolpidem interventions after move- ment offset	110

Acknowledgements

I would like to express gratitude to all my colleagues, friends and family that supported me through this journey. The past four years have been the most productive, challenging and satisfying moments in my short (perhaps medium size?) life. This thesis represents only a fraction of what I achieved during this time but it serves the purpose of being a nice memorabilia of these years.

I will not provide a list of names of all the countless people that helped me or that were around when I needed them. I am aware that it is a personal preference that you (my poor reader) may dislike. But if we shared something in the past years, I want you to know that I am thankful for that.

I will make only a brief exception to the aforementioned rule, by saying thank you to Eleonora. You know me better than I do. Your presence is the key ingredient to a chilled and meaningful life. The last years have been incredible, but I am confident that we have only started our journey together.

P.S.

In the remote scenario in which one of you kids will read this in future, let me say this: of course, I am thankful for you! You are the best thing we made (although I hope we will stop at two). With love, Dad

Chapter 1

General introduction

1.1 The importance of rhythmic neural activity

Neural activity at the single-neuron level appears predominantly asynchronous. Both spike discharges of cortical cells and synaptic inputs to cortical neurons display large stochastic fluctuations, approximating a Poisson process (Destexhe and Sejnowski, 2003; Softky and Koch, 1993; Shadlen and Newsome, 1994). Interestingly, when observed at a macro-scale level, one of the most striking features of neural activity is rhythmicity. At first sight, it seems difficult to reconcile the strongly stochastic nature of neuronal spike discharges with the description of synchronised neural networks across the brain. However, an oscillatory activity could be better interpreted in the more general perspective of correlation in the timing of neural firing (Wang, 2010). Biophysical studies revealed that the intrinsic ability to resonate at multiple frequencies is observable even in single neurons (Hutcheon and Yarom, 2000). This suggests that the precise timing of their activity within neuronal networks could represent a fundamental condition for information transfer.

Theories of the functions of oscillations argue that they facilitate dynamic temporal and spatial propagation of neural signals (Fries, 2005, 2015; VanRullen, 2016; Voytek and Knight, 2015). Neural oscillations have been explored as potential biomarkers of disease status, drug efficacy, and other clinical indicators (Başar, 2013; Buzsáki and Watson, 2012; Newson and Thiagarajan, 2019). Reflecting this broad interest, a large number of investigations have reported associations between oscillations and almost every aspect of

cognition and behaviour (Başar et al., 2001; Lopes da Silva, 2013; Mazaheri et al., 2018).

Rhythmic activity is characterised by three key features: amplitude, phase and frequency. Amplitude is the amount of energy at a given time and at a given frequency. In the context of neural signals, amplitude changes are considered to result from changes in synchronisation within a neural population. Phase is a definition of the position of a point in time on a waveform cycle. Phase can be an expression of relative displacement between or among waves having the same frequency. Lastly, frequency represents the number of cycles per second, reflecting the "speed" of the oscillation. Brain oscillations are usually categorised into five frequency bands: delta (0.5-3.5 Hz), theta (4-7 Hz), alpha (8-12 Hz), beta (13-30 Hz) and gamma (>30 Hz) (Buzsáki, 2006). In this thesis, we will focus on one of these rhythms: beta oscillations.

1.2 The beta rhythm

1.2.1 The link between beta and the sensorimotor system

Neural activity in the beta range has been historically implicated in sensorimotor control (S. Baker, 2007; Pfurtscheller and Lopes da Silva, 1999). These oscillations are established during stable postures and are decreased during active states, such as motion planning and execution (Engel and Fries, 2010; Kilavik et al., 2013). A decrease in the amplitude of beta oscillations across sensorimotor areas is seen just prior to and during movement execution. Conversely, an increase in beta amplitude above the baseline level is observed following movement termination. These two phenomena are commonly referred to as movement-related beta desynchronisation and post-movement beta rebound or PMBR, respectively (**Figure 1.1**). The movement-related power decrease is typically observed bilaterally over sensorimotor areas, particularly post-central. Conversely, while some studies suggest a pre-central locus for the beta rebound, others have proposed that originates from a distributed cortical network including frontal and parietal areas, rather than a discrete cortical node. (Jurkiewicz et al., 2006; Kilavik et al., 2013; Muthukumaraswamy, Myers, et al., 2013).

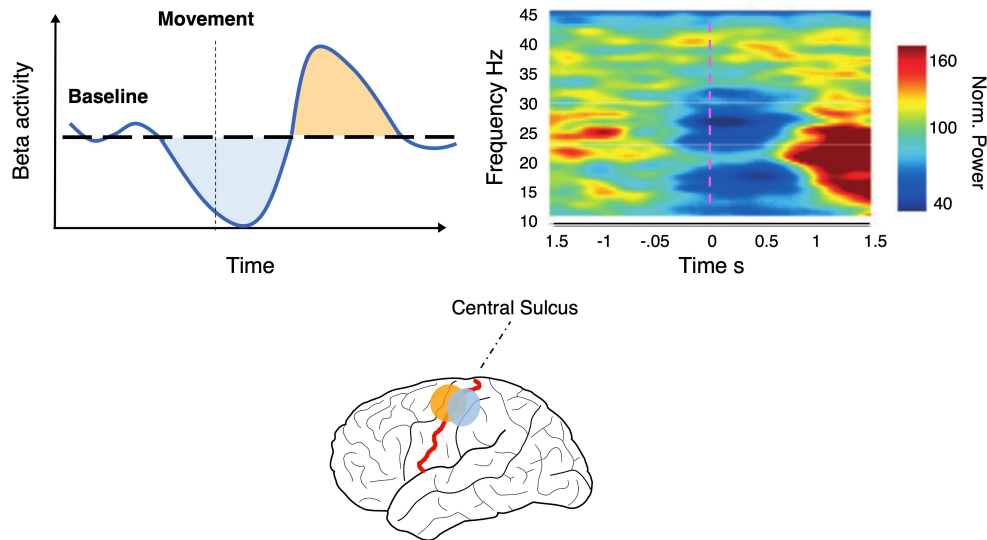


Figure 1.1: Beta desynchronisation and rebound

(*upper left*) Schematic representation of sensorimotor beta activity. During a motor task beta activity drops below baseline (**light blue shaded area**) just prior to and during movement execution. After movement ends, beta activity increases rapidly (**light orange shaded area**) before slowly returning to baseline level. (*upper right*) Example of time-frequency plot showing beta desynchronisation and rebound in the subthalamic nucleus (Alegre et al., 2005). The plot shows oscillatory activity changes specific to the beta band (13-30 Hz) in the period prior to movement and following movement termination. The colour scale indicates relative power changes with respect to baseline levels (dark colours indicate a decrease; bright colours indicate an increase). The movement begins at time 0 (**magenta dashed line**). (*bottom*) Schematic representation of beta desynchronisation and rebound spatial distribution. Beta desynchronisation (**light blue circle**) is commonly localised to the postcentral gyrus whereas rebound (**light orange circle**) is often localised to the precentral gyrus.

Sensorimotor beta oscillations have been observed across several cortical (Jensen et al., 2005; Kopell et al., 2011; Kramer et al., 2008; Roopun et al., 2006; Yamawaki et al., 2008) and sub-cortical loci (Holgado et al., 2010; McCarthy et al., 2011; Mirzaei et al., 2017; Tachibana et al., 2011). Natural modulation of beta dynamics have been reported in ageing and neurological disorders, such as Parkinson's disease (PD) and stroke. Resting and movement-related beta power has been shown to increase in older adults, alongside a concurrent deterioration of motor performance (Espenhahn et al., 2019; Heinrichs-Graham and Wilson, 2016; Rossiter, Davis, et al., 2014). PD patients consistently show an increase in beta amplitude in the basal ganglia. This alteration correlates with the severity of the motor disorders (Brown, 2006; Little and Brown, 2014). Well-established treatment options for advanced PD, such as pharmacological alteration of dopamine levels and deep-brain stimulation, act on beta levels in the subthalamic nucleus (Little et al., 2013; Tinkhauser, Pogosyan, Little, et al., 2017). Higher resting beta power in the affected hemisphere of stroke patients was associated with poorer motor function whereas the reverse relationship was found in the unaffected hemisphere (Rossiter, Boudrias, and Ward, 2014; Thibaut et al., 2017).

The above findings help to understand why beta oscillations have often been proposed as a purely motor rhythm. However, as we will see in the next paragraph, the role of beta in the sensorimotor system is more nuanced.

Beyond its established role as a sensorimotor rhythm, modulations of beta activity are also present in a range of non-motor processes, such as visual perception (Kloosterman et al., 2015; Singh et al., 2002), language processing (for review, see Weiss and Mueller, 2012), working memory (Siegel et al., 2009), long-term memory (for review, see Hanslmayr et al., 2016), decision making (Wimmer et al., 2016; Wong et al., 2016) and reward processing (for review, see Marco-Pallarés et al., 2015) ¹. For the remainder of this thesis, however, we will focus exclusively on sensorimotor beta oscillations.

¹For the interested reader we suggest two reviews encompassing several non-motor beta functions: (Schmidt et al., 2019) and (Spitzer and Haegens, 2017)

1.2.2 What is the role of beta oscillations?

As we described in the previous paragraph, one peculiarity of beta oscillations lies in the tendency to vary during movement. Beta desynchronisation is present during spontaneous and triggered movements, while successful movement cancellation is associated with an increase in beta power (N. Swann et al., 2009; N. C. Swann et al., 2012). Due to this predominant activity during rest, one of the earliest interpretations compared the activity in the beta range to an "idling rhythm" in the motor system (Pfurtscheller et al., 1996). However, other studies showed how beta desynchronisation also occurs when no muscle contraction is required (i.e., motor imagery or action observation) and how is rather insensitive to motor parameters like movement type or effector (Kilavik et al., 2013; Miller et al., 2010). These observations led Engel and Fries (2010) to propose a role for beta oscillations as an active process, which interferes with the encoding of incoming information while promoting the existing state in the system ("status-quo"). Therefore, instead of being a proxy for the level of activity of the sensorimotor network, beta oscillations act as a top-down inhibitory rhythm during motor and cognitive tasks. Following the "status-quo" hypothesis, movement-related beta desynchronisation and rebound could be interpreted as controlled fluctuations of beta level during a motor set, with the former necessary for releasing the inhibition and allowing the initiation of a motor plan, while the latter actively preserves the existing motor states from internal and external sources of noise.

PMBR has also been interpreted more specifically as an indicator of movement outcome processing (S. Baker, 2007). Supporting evidence stems from findings showing how PMBR is modulated by passive movements (Alegre et al., 2002; Cassim et al., 2001) and by kinematic errors (Tan et al., 2014). More recently, Tan et al. (2016) reported that the level of PMBR over the sensorimotor cortex serves as an index of confidence in the prediction of a motor outcome. This interpretation refers to the idea that optimal sensorimotor control requires an integration of the motor command ("efferent copy") and sensory feedback (Franklin and Wolpert, 2011). When a mismatch between the efferent copy and the sensory feedback is detected, this drives an update of the motor plan (Shadmehr et al., 2010). According to Tan, the reduction of PMBR is therefore required to dynamically

change the motor output and successfully exhibit motor learning.

Although a unifying interpretation of beta's function is currently lacking, some mechanistic aspects have been tentatively identified. In particular, oscillations in the beta frequency are physiologically well suited for facilitating long-range interactions between groups of neurons (Kopell et al., 2000, 2011; Varela et al., 2001). This characteristic could possibly make beta an ideal candidate for transmitting top-down signals from higher-executive nodes to the motor and sensory areas (Buschman and Miller, 2007; Engel and Fries, 2010; Fries, 2015; Wang, 2010).

Several reasons contribute to making sensorimotor beta's role so elusive. First, activity in the beta range is not unitary but it is actually comprised of separate rhythms (Kopell et al., 2011). PD studies show that oscillatory activity through the cortico-basal ganglia network is segregated into low (14–20 Hz) and high beta frequencies (>24 Hz) both in humans (Litvak et al., 2011; Lopez-Azcarate et al., 2010) and rats (West et al., 2018). Furthermore, each of the two rhythms shows a distinct pattern of response to variation of dopamine levels (Priori et al., 2004; Marceglia et al., 2006). Multiple studies have proposed a link between low-beta and motor dynamics, suggesting an "anti-kinetic" role (Brown, 2003; Chandrasekaran et al., 2019). High-beta, instead, seems to reflect attention and sensory cue anticipation processes (Chandrasekaran et al., 2019; Kilavik et al., 2014; Saleh et al., 2010). Secondly, some studies have observed that movement-related beta desynchronisation and PMBR have a different spatial distribution (with the first more often observed close to postcentral gyrus and the latter to precentral gyrus) and could represent independent events (Alegre et al., 2008; Gaetz et al., 2011; Jurkiewicz et al., 2006; Muthukumaraswamy, Myers, et al., 2013). Finally, recent studies returned consistent evidence towards a novel interpretation of beta activity as a burst-like phenomenon rather than sustained over time, suggesting a complete reappraisal of beta "oscillatory" nature (Little et al., 2019; Jones, 2016; Sherman et al., 2016; Shin et al., 2017). As we will discuss further below, theoretical models of beta oscillations should integrate this transient nature when accounting for its functional role.

1.2.3 Mechanisms of generating beta

Pharmacology studies have uncovered a link between GABA, the major inhibitory neurotransmitter in the brain, and beta oscillations (Jensen et al., 2005; Roopun et al., 2006; Yamawaki et al., 2008). Specifically, the administration of benzodiazepines in humans has been shown to increase the conductance of GABA-mediated currents, which in turn was correlated with an increase of beta power (Hall et al., 2009, 2011; Jensen et al., 2005; Muthukumaraswamy, Myers, et al., 2013; Nutt et al., 2015). The relation of beta and GABA was also described by several neural network models describing the mechanism by which these oscillations are generated (Whittington et al., 1995, 2000). According to these models, beta is generated by local spiking interactions among pyramidal cells and GABAergic interneurons (Jensen et al., 2005; Kopell et al., 2011; Kramer et al., 2008; Lee et al., 2013) (**Figure 1.2**). A similar generative model was also proposed for oscillations in the gamma range (30-90 Hz) (Börgers and Kopell, 2008; Olufsen et al., 2003; Whittington et al., 2000). However, some functional aspects separate these two rhythms. As described in Kopell et al. (2011), activity in the gamma range requires continuous excitation, whereas beta rhythmicity can be preserved longer, even after a decaying excitatory input. Furthermore, beta cell assemblies - groups of neurons synchronised in a beta frequency range - can concurrently co-exist with other cell assemblies. Gamma-driven spiking interactions instead, due to the large overlap in the axonal fields of inhibitory interneurons, constantly suppress each other with one assembly dominating the others. These physiological features, make beta an ideal candidate for supporting long-range network interactions (Kopell et al., 2000, 2011; Roopun et al., 2006).

An alternative model of a cortical beta generator was recently proposed by Sherman et al. (2016). According to the authors, beta oscillations can emerge from the interactions between excitatory and inhibitory neurons in deep and superficial layers (**Figure 1.2**). Specifically, the model consists of pyramidal neurons in the supragranular (layers 2/3) and infragranular (layer 5) layers coupled to inhibitory neurons. The laminar neocortical model receives further inputs from two external locations, providing excitatory drive to *proximal* and *distal* dendrites of pyramidal neurons. The authors have speculated that

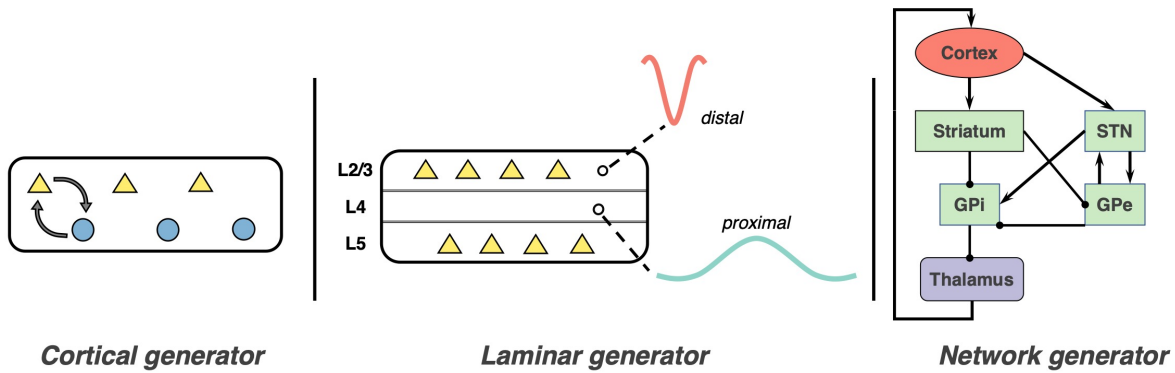


Figure 1.2: **Generative models of beta oscillations**

Schematic illustration of potential mechanisms of beta generation. (*left*) Beta oscillations can be generated in deep cortical layers by recurrent interactions between pyramidal neurons (triangles) and interneurons (circles). (*middle*) A laminar model of beta generation requires pyramidal neurons (triangles) in the supragranular (layers 2/3) and infragranular layers (layer 5). The model is complemented by two external excitatory inputs, likely originating from the thalamus (for more details see, Sherman et al., 2016). (*right*) Source model of basal ganglia beta oscillations. Arrows denote excitatory connections and lines ending with circles denote inhibitory connections. Beta can be generated in multiple ways within the basal ganglia. Most recurrent theories involve the STN-GPe loop (Holgado et al., 2010), the striatal origin (McCarthy et al., 2011) and the cortical-ganglia-thalamic loop (Moran et al., 2011). Abbreviations: STN - subthalamic nucleus; GPe/GPi - globus pallidus pars externa and interna.

both the proximal and distal drive could originate from the thalamus. The model produces beta activity which is transient (“burst-like”) and does not depend on rhythmic inputs, a finding corroborated by human and animal studies (Bonaiuto et al., 2021; Leventhal et al., 2012; Sherman et al., 2016; Shin et al., 2017).

Finally, another predominant theory on the origin of beta’s rhythm identifies the basal ganglia as a key structure (**Figure 1.2**). Consistent with this view, beta has been robustly observed from basal ganglia nuclei including the subthalamic nucleus (STN), striatum, and globus pallidus (externa - GPe; interna - GPi) (Bevan, 2002; Feingold et al., 2015; Leventhal et al., 2012). Furthermore, as we mentioned in the previous paragraphs, exaggerated beta oscillations in the basal ganglia are a common feature of PD and are believed to correlate with the degree of motor symptoms (Beck et al., 2016; Brown, 2006; Hammond et al., 2007). These pathological oscillations could be a direct consequence of changes to the underlying networks of neuronal ensembles that generate them. However, locating the origin of basal ganglia beta oscillations has been challenging, due to the complex ar-

chitecture of the system and the rich interconnections with the cortex and the thalamus. Several experimental and computational studies have reported that interactions between STN and GPe can generate beta oscillations (Bevan, 2002; Holgado et al., 2010; Kumar et al., 2011; Pavlides et al., 2015; Tachibana et al., 2011; W. Wei et al., 2015). Anatomically, STN and GPe are densely and reciprocally interconnected (Shink et al., 1996), generating recurrent excitatory-inhibitory interactions in the beta range (Plenz and Kital, 1999), which may then propagate to other regions in the cortico-basal ganglia loop. An alternative interpretation is based on a striatal-origin viewpoint (Corbit et al., 2016; McCarthy et al., 2011). Tachibana et al. (2011), however, observed that blocking the striatal input to GP did not reduce the power of beta oscillations in GPe. In contrast, blocking inputs from STN to GPe abolished beta rhythms. The amount of evidence described above suggests a complex and possibly non-unitary mechanism behind the origin of sensorimotor beta oscillations. Following this idea, some authors have proposed the integration of different models, with beta oscillations acting as an emergent property of the entire cortico-basal ganglia networks, rather than a localised phenomenon (Kumaravelu et al., 2016; Leblois, 2006; Liu et al., 2020; Moran et al., 2011; Pavlides et al., 2015; van Albada et al., 2009; West et al., 2018).

1.3 MEG

Recordings of rhythmic signatures of neural activity can be performed with a variety of techniques, such as electroencephalography (EEG), magnetoencephalography (MEG), electrocorticography (ECoG) and local field potential (LFP). In this thesis, neural recordings were obtained exclusively with a MEG system. Specifically, we used a CTF MEG system consisting of 275 first-order axial gradiometers and 29 reference magnetometers. MEG is a non-invasive imaging method based on measuring the magnetic fields that are generated by electrical brain activity. It has a relatively high spatiotemporal resolution (~ 1 ms, and 2-3 mm in principle) and reflects neural currents directly, with minimal distortion from the skull and the scalp (Hämäläinen et al., 1993).

Taking a step back, electric current from a multitude of neurons can superimpose to

generate a potential V (measured in Volts) with respect to a reference point. The difference in V between two locations gives rise to an electric field. Electric fields can be monitored by extracellularly placed electrodes with sub-millisecond time resolution and can be used to infer many facets of neural computation (Buzsáki et al., 2012). While this type of (electric) signal is recorded by EEG, ECoG and LFP, the resultant magnetic field is the target of MEG recordings.

Synchronised activity across space and time is fundamental to generating measurable magnetic fields which are detectable by the MEG (Baillet et al., 2001). The main generators of the ionic currents registered with an electrode are considered to be the postsynaptic potentials (Hämäläinen et al., 1993) (**Figure 1.3**). Although neural electric activity comprises both rapid action potentials and slower synaptic potentials, the brief nature of action potentials makes challenging signal summation on a sufficiently large scale. The slower decay rate of postsynaptic potentials instead, allows a great overlap in time without requiring rigorous synchronisation. Because of these well-defined characteristics, the largest contributor to the MEG signal is thought to be the pyramidal neuron (**Figure 1.3**). The reasons are twofold: first, the elongated morphology of the pyramidal neuron constrains the net primary current circulation along the cell, which is a factor responsible for greater signal strength compared to other kinds of neuron morphologies. Secondly, pyramidal neurons are oriented perpendicular to the brain surface with dendrites of neighbouring cells roughly parallel to each other. This results in the ionic current underlying postsynaptic potentials flowing in the same orientation across thousands of cells, thus generating large magnetic fields (Baillet, 2017; Hämäläinen et al., 1993; Vrba and Robinson, 2001).

Brain-generated magnetic fields are typically measured on a scale of 50-500 femtoteslas (fT). To put this in perspective, this number is about 10 to 100 million times smaller than Earth's static magnetic field. It follows that highly sophisticated sensor technology is required for recording. Standard systems rely on pick-up coils coupled with superconducting interference devices (SQUIDs) (D. Cohen, 1972; Hämäläinen et al., 1993). As external magnetic noise can prevent the detection of weak neural magnetic fields, several noise rejection strategies are used in modern MEG systems. The first, and largest contribution to noise suppression, comes from performing MEG recordings in magnetically shielded

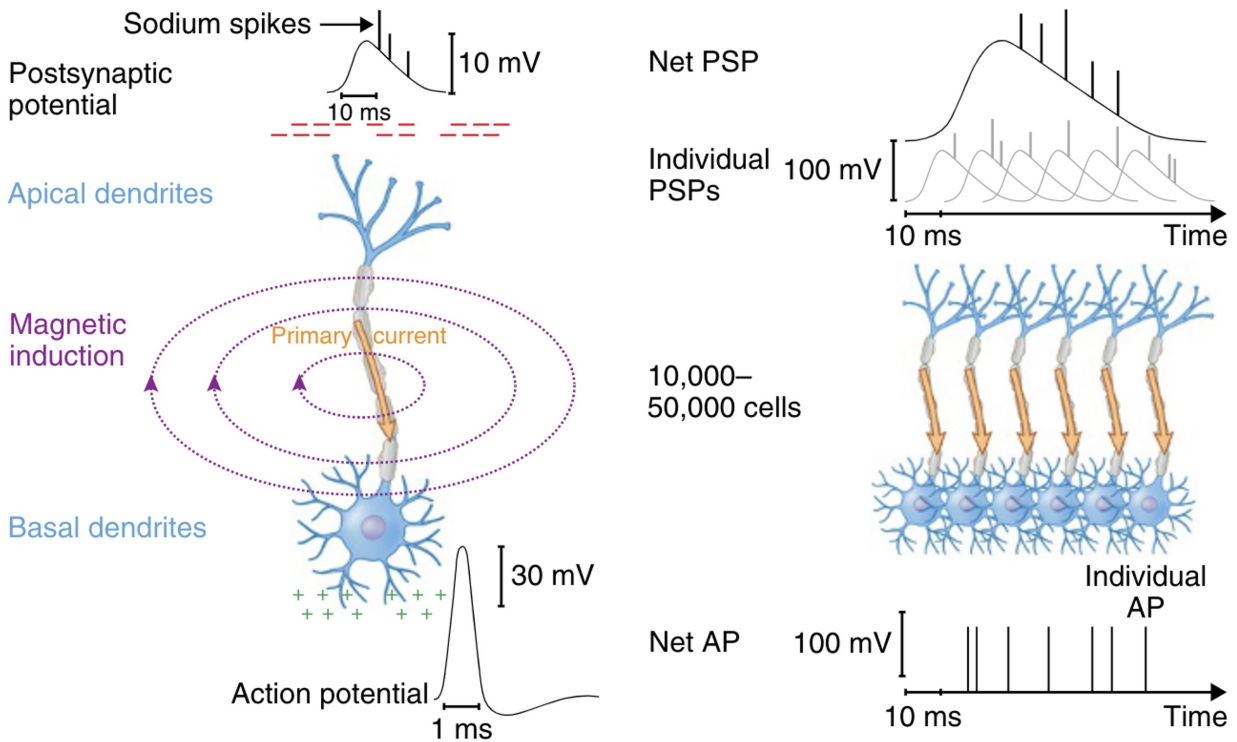


Figure 1.3: MEG signal origin

(left) Schematic representation of a cortical pyramidal neuron. Example of net primary current (**yellow arrow**) along the cell. The current is generated by an imbalance in electrical potentials between the apical dendrites and the cell body. The induced magnetic field (**purple circular arrows**) perpendicular to the primary current is the principal source of the signal recorded with the MEG. Source of activity depicted: postsynaptic potentials (PSP) and action potentials (AP). (right) At the cell assembly scale, the slow decay of PSP allows for stronger superimposition of the signal, thus increasing the detectability with MEG.

rooms. Further suppression is achieved by the specific design of MEG sensors. Two of the most common sensors are the magnetometers and the gradiometers, with the first containing a single pick-up coil while the latter contains multiple ones. Gradiometers take advantage of the fact that magnetic field strength decreases with distance from a current source as an inverse square law. Signals from noise sources at a large distance from a given gradiometer will induce similar currents in each loop, whereas the field generated by a source inside the head would induce a larger current only in the loop closer to the source (Vrba and Robinson, 2001).

The localisation of sensor-level responses can be ambiguous with MEG. Given a magnetic field measured by MEG, an infinite number of possible cortical source distributions could contribute to its generation. The problem of estimating the current density that generated the measured electric potential (or magnetic field) is described as the inverse problem (Sarvas, 1987). Source analyses in this thesis use a linearly constrained minimum-variance (LCMV) beamforming approach (Hillebrand et al., 2005; Van Veen et al., 1997), which aims to alleviate the inverse problem. This method independently estimates a solution at each source location in the brain by weighting the sensor-level contribution to the overall output so as to increase sensitivity at the target location while minimising interference from others. The only assumption of this method requires that no two macroscopic sources of neuronal activity are linearly correlated (Hillebrand et al., 2005). Beamforming has proven to successfully attenuate noise (Vrba, 2002) and it does not require assumptions on the number of active sources. Another advantage of beamformer analysis is its easy implementation since there is relatively little user interaction. The only parameters that a user needs to specify are the size of the reconstruction grid, the time-frequency window over which to run the analysis, and optionally the amount of noise regularisation (Hillebrand and Barnes, 2005).

Overall, MEG provides whole-head direct measurements of neural activity, characterised by excellent temporal and spectral resolution. Unlike EEG, MEG measures are reference-free, do not suffer from the distortive conductive effect of brain tissues, are less contaminated by muscle artifacts and are more sensitive to tangential sources (with EEG additionally sensitive to radial ones). MEG, however, is sensitive to head movements and

the correct registration of head position, which can impair data quality and comparability. Furthermore, MEG is less sensitive to the activity that occurs deeper within the brain, thus constraining a large section of MEG research to focus on activity in more superficial brain regions.

1.4 Novel insights on neural oscillatory activity

In this section, we will present recent perspectives on neural oscillations. The implications of these findings could lead to a reappraisal of the methodology used for analysing rhythmic patterns in the brain. We will show in the remainder of this thesis the potential advantage of employing these techniques when studying sensorimotor beta oscillations.

1.4.1 The "burst-like" hypothesis

Neural oscillations are typically interpreted as repeated cycles of rhythmic activity sustained over a long period of time. Accordingly, common analytical techniques consist in averaging time-frequency representations (TFRs) across multiple trials in order to improve the signal-to-noise ratio. Recent studies, however, have shown that at a single-trial level, oscillations appear only for a short period while they are also widely spread and infrequent across trials (Feingold et al., 2015; Jones et al., 2009; Leventhal et al., 2012; Lundqvist et al., 2016; Sherman et al., 2016). Therefore, it seems that the notion of brain rhythms being sustained over time is often a consequence of averaging signals in the spectral domain rather than an inherent property of oscillations (Jones, 2016). TFRs, which are the outcome of frequency analysis applied to a time series, are composed of purely non-negative values. Thus, intermittent activity occurring at different points in a time window can be accumulated without cancelling, returning a misleading picture of a "sustained" pattern of activity (**Figure 1.4**).

A group of recent studies tried to investigate if focusing on beta oscillations as a "burst-like" phenomenon could produce stronger relevance with behaviour than conventional trial averaging. Sherman et al. (2016) analysed source-localised human MEG data looking

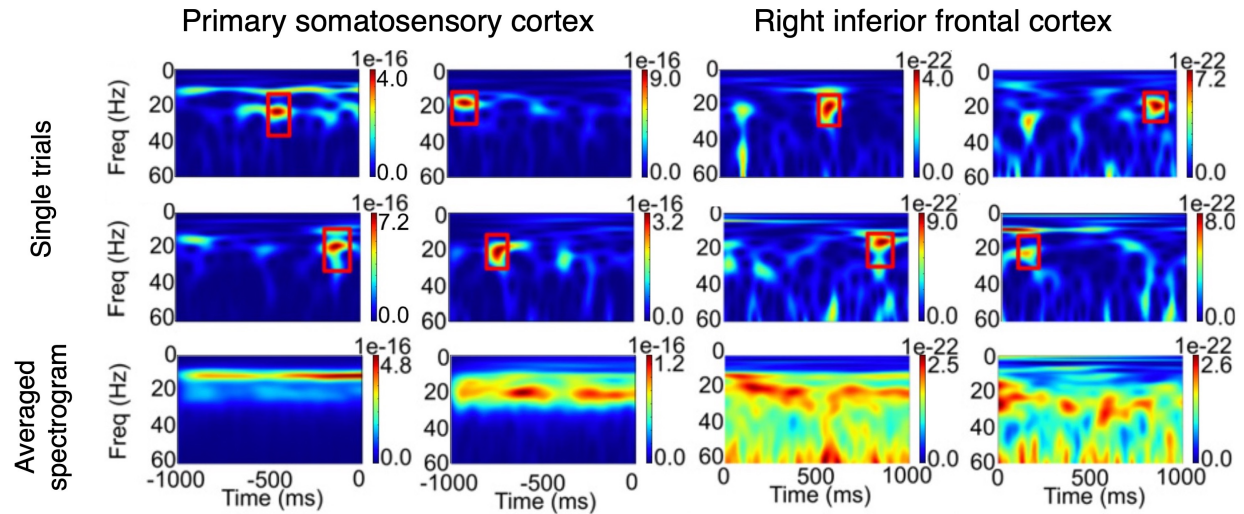


Figure 1.4: **Single-trial beta-bursts**

Examples of spontaneous oscillations and corresponding TFRs over 1-s epochs observed in MEG source-localised data from the primary somatosensory cortex (SI) and the right inferior frontal cortex (IFC). Each column shows activity from four different subjects [$units: (AM)^2$]. Across single-trials beta oscillations (**red boxes**) emerged transiently, with high-power beta events lasting approximately three periods. Sustained oscillations appear only when data are averaged over many ($N. trials = 100$) 1-s cycles. Adapted from Sherman et al. (2016).

at spontaneous activity during rest in the primary somatosensory cortex. Beta appeared transiently during single-trials as a sudden increase in power typically lasting <150 ms. When the same trials were averaged together, continuous oscillations emerged in the TFR. Similar findings in LFP recordings were reported by Feingold et al. (2015). The authors showed how beta was present reportedly in brief bursts both in the motor/premotor cortex and in the striatum of monkeys performing self-timed movement tasks. Fluctuation of averaged oscillatory power was highly correlated with variations in burst density of beta events. Thus, the authors suggested, beta synchronisation and desynchronisation could reflect the probability of occurrence of a brief bursting event, rather than representing modulation of the strength of a sustained oscillation.

Some beta-burst features however are not perfectly summarised by averaged spectrograms. Shin et al. (2017) showed that the rate of transient pre-stimulus beta events in the primary somatosensory cortex was the most consistent predictor of stimulus detection in humans and mice. Moreover, events occurring closer to the stimulus onset were more likely to result in impaired detection. Similarly, Little et al. (2019), found that the late

timing of a beta-burst closer to a preparatory cue predicted slower movement initiation. By contrast, task errors resulted in delayed onset of bursts and a reduced probability of bursting.

The cumulative evidence reviewed here supports the notion of beta as a transient event across brain areas, recording modalities and species. Trial averaged analysis may conceal the functional importance of the underlying bursting activity, thus contributing to the challenge of providing a comprehensive interpretation of beta's role in the sensorimotor system. Whilst the averaged amplitude of beta power does seem to correlate with the rate of beta events, the beta-bursts analysis could provide additional and independent measures of neural activity which could be tested experimentally and implemented in computational models.

1.4.2 Rhythmic and arrhythmic neural signals

Neural oscillation studies have often focused on predefined canonical frequency bands that are thought to capture distinct rhythms. Accordingly, standard analyses rely on the contrast of activity in narrow-band frequencies (i.e., 13–30 Hz for the beta range). This methodology, however, requires some specific sets of assumptions about the nature of neural signals. Neural recordings have reportedly shown the presence of activity which lacks defined rhythmicity. This aperiodic activity, also defined as "scale-free" or "1/f" (Freeman et al., 2003; B. J. He, 2014), is characterised in the spectrogram by exponentially decreasing power across increasing frequencies. Interestingly, this activity has been linked to several important features of brain activity, from postsynaptic integration to neural populations firing magnitude (Gao et al., 2017; Miller et al., 2009). Furthermore, aperiodic activity is always detectable in neural recordings and has large and observable variability (Freeman and Zhai, 2009; Podvalny et al., 2015).

The above findings urge caution when interpreting the results from spectral analyses. There is always non-zero power at all frequency bands, even if there is no oscillatory activity present. Therefore, it is erroneous to assume that predefined narrow-band frequency analyses would reflect the presence of physiological oscillatory activity.

A useful set of examples of how aperiodic activity could lead to misinterpretation of power spectra was displayed by Donoghue et al. (2020) (**Figure 1.5**). Different physiological processes could result in similar outcomes when inspecting narrow-band activity. For example, if we consider a reduction of power in the alpha range the most direct cause could be ascribed to a reduction of the number of neurons synchronised in that specific range. However, a reduction of alpha power can also be observed after a shift in the alpha peak frequency or by the intrinsic variability in the aperiodic activity.

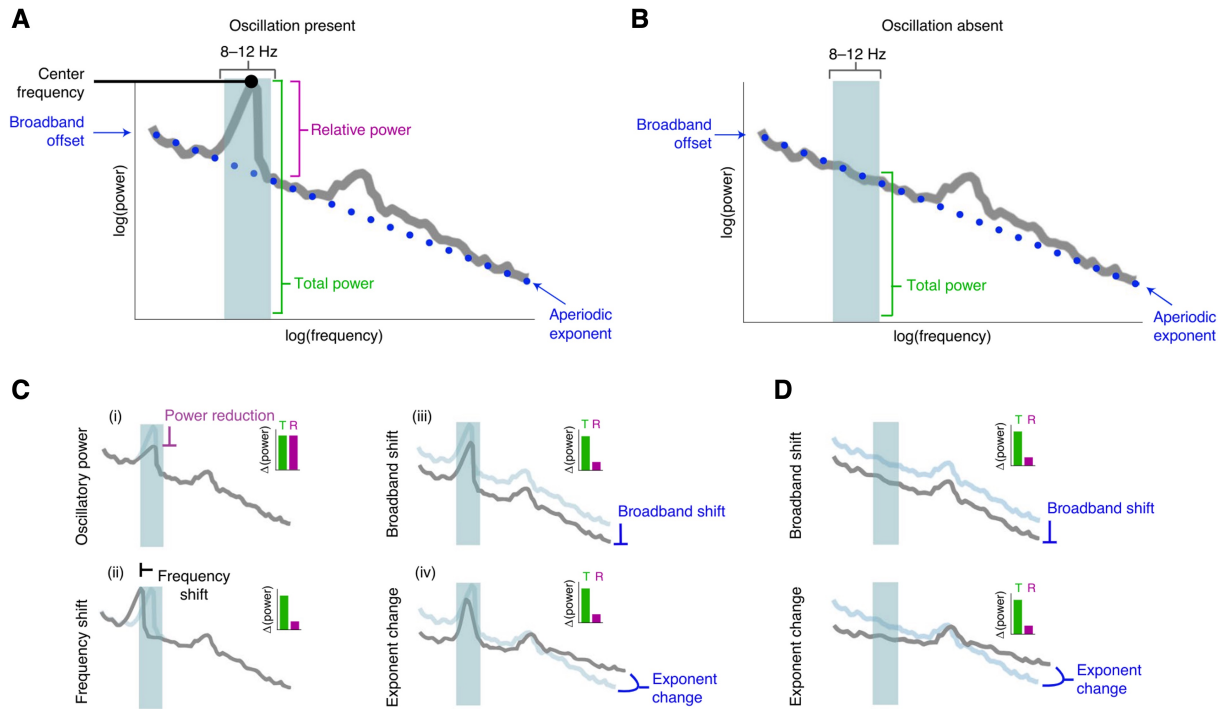


Figure 1.5: Overview of periodic and aperiodic spectral features

(A) Example of a power spectrum with a strong alpha peak in the canonical frequency range (8-12 Hz, **blue-shaded region**) and a weak beta peak (not marked). (B), Same as A, but with the alpha peak removed. (C, D), Changes in a narrow-band range (**blue-shaded region**) can be ascribed to several different physiological processes. Total power (**green bars in the inset**) reflects the total power in the frequency range, and relative power (**purple bars in the insets**) reflects the relative power of the peak, over and above the aperiodic component. (C), Example scenarios: oscillatory power reduction (i); oscillation center frequency shift (ii); broadband power shift (iii); aperiodic exponent change (iv). In each simulated case, while the total measured narrow-band power is similarly affected (inset, **green bar**), only in the power reduction case (i) the alpha power was actually changed compared to the aperiodic activity (inset, **purple bar**). (D), Examples of aperiodic dynamics with no peaks present in the spectrum. Changes in the aperiodic component can be erroneously interpreted as changes in oscillatory power when performing narrow-band analysis. R, *relative*; T, *total*. Reproduced from Donoghue et al. (2020).

Ignoring the aperiodic component when interpreting findings on neural oscillations is problematic, as this component also reflects meaningful physiological information. As we will discuss further in **Chapter 4**, avoiding spectral parametrisation in its periodic and aperiodic components, leads to a misinterpretation of the effects of beta oscillations.

1.5 Thesis overview

This thesis brings together standard and novel methods for the analysis of sensorimotor beta oscillations. In the first two chapters, we used a joystick-reaching task to explore some of the most popular interpretations of the role of beta in the sensorimotor system, specifically motor learning and action inhibition. In **Chapter 2**, we altered the visual feedback of the joystick cursor to elicit motor adaptation. This manipulation confirmed the link between beta oscillations and motor errors. In **Chapter 3**, we employed an action-stopping paradigm to test if beta oscillations are key to suppressing movement initiation. Our results, however, were inconclusive and proposed a more nuanced relationship between beta and action control.

Finally, in **Chapter 4** we tested the effect of two GABAergic modulators on beta. We showed how applying novel techniques to the analysis of beta oscillations returns more complex findings compared to standard approaches.

Chapter 2

Beta dynamics during motor adaptation

2.1 Introduction

The functional significance of beta oscillations in the sensorimotor system is still not well understood, as discussed in **Chapter 1**. One hypothesis proposes that increased beta during movement acts as an inhibitory rhythm, actively interfering with the ability of the network to encode new information (Engel and Fries, 2010). A different interpretation suggests a link between beta and the processing of movement-related sensory afferent and kinematic errors. In this context, modulation of beta promotes adaptive processes in the sensorimotor system, ultimately resulting in the update of the motor plan in the context of learning (Tan et al., 2016; Haar and Faisal, 2020).

In the first two chapters of this thesis, we will discuss both interpretations of the beta functional role. In this first chapter, we investigate whether updates in motor performance following motor learning are linked with the modulation of beta dynamics, and we explore the spatiotemporal characteristics of such an effect.

Motor learning can be defined as an improvement of motor skills through practice which is paralleled by long-lasting changes at the level of neural circuitry (Sanes and Donoghue, 2000; Muellbacher et al., 2002; Halsband and Lange, 2006). Motor learning paradigms involve goal-directed actions towards a target (reaching, pointing), while motor performance and/or sensory feedback are experimentally manipulated (force fields, prisms; for review, see Shadmehr et al., 2010).

In a visuomotor rotation paradigm, Tan et al. (2014, 2016) found that larger post-movement beta rebound (PMBR) indicates more confidence in the motor plan and the maintenance of more stable motor output, while smaller PMBR indicates the need for adaptive changes driven by sensory feedback. Recently, Haar and Faisal (2020) explored PMBR dynamics during a real-world billiards task. Across the experiment, PMBR amplitude exhibited opposite modulations, with some participants showing a reduction in learning while others showed an increase. The authors speculated that participants may opt for distinct learning strategies to complete the task during real-world paradigms. Therefore, opposing PMBR dynamics could be interpreted as neural signatures of separate underlying learning mechanisms. The link between PMBR and motor learning was also explored by Torrecillos et al. (2015). In a pointing task, the authors contrasted two types of reach errors: movement-execution errors that triggered adaptive mechanisms and errors that elicited no sensorimotor adaptation. PMBR amplitude was reduced after experiencing both kinds of errors, leading the authors to suggest a non-specific role for PMBR in error/mismatch detection. In a subsequent study, Alayrangues et al. (2019) contrasted bi-manual reaching tasks with comparable motor kinematics but different action goals. Although each task required distinct sensorimotor remapping following a mechanical perturbation, PMBR modulation was comparable across tasks. This finding supports the notion that PMBR is related to salient error-detection mechanisms which act without triggering adaptive behavioural adjustments. Together, these studies suggest a complex relationship between PMBR with outcome processing.

A growing number of studies suggest that cortical beta activity is characterised by transient bursting that may only appear to be temporally sustained if averaged over multiple trials (Sherman et al., 2016; Shin et al., 2017; Little et al., 2019; Feingold et al., 2015). These studies propose a prominent functional role for rapid beta bursts that could be concealed by conventional analysis. Bursts occur more focally in space than temporally averaged beta amplitude (Little et al., 2019), and burst timing was a better predictor of motor behaviour than average beta power (Little et al., 2019; Shin et al., 2017). Therefore, beta burst analysis could provide a better understanding of beta's role during learning.

In the present chapter, we used a joystick aiming task from Tan et al.(2014, 2016) to

test the role of beta oscillations during motor adaptation. In particular, we tested if averaged PMBR was dynamically modulated during learning and if this effect was observable in a set of frontal and parietal ROIs. We were able to identify a reduction in PMBR power when the joystick cursor visual feedback was manipulated. This effect was shown across several distinct ROIs but was stronger for M1, IFG and sPL. Finally, beta oscillations were explored at the single-trial level. These transient events appear to confirm that during adaptation the amplitude of post-movement beta bursts is reduced, but failed to produce novel insights.

2.2 Material and methods

2.2.1 Participants

22 healthy participants participated in the MEG experiment. One participant had to be excluded due to the presence of artefacts during data collection. Three participants had to be excluded because it was not possible to acquire an MR image. All of the remaining 18 participants (9 women; mean age \pm SD, 25 ± 3 years) had normal or corrected-to-normal vision. All individual participants included in the study were screened for factors contradicting MRI and MEG scanning and provided written informed consent before participation and consent to publish any research findings based on their provided data in anonymized form. Participants were financially compensated for their time.

2.2.2 Experimental setup

The task and procedure were similar to the one described in (Tan et al., 2016). Participants were seated in the MEG scanner in front of a computer monitor at 120 cm from the screen, while they held a finger-joystick with their right hand, which was rested on a padded arm support. Participants performed an out-and-back aiming task by moving the joystick to match a cursor with a target during two conditions. The cursor, which is the visual feedback of the position of the joystick, was displayed on the computer monitor in the form of a white circle that was 1.3 cm (1.2 visual degrees) in diameter. The target was a green circle (6 mm diameter) displayed on the screen. Each trial started with an empty circle at the centre of the monitor which stayed in position for 750 ms. Then the empty circle was substituted by the joystick cursor (white). After 1.5 s the target (green) appeared at one of five possible positions equally spaced around an invisible half-circle in the upper portion of the screen with a radius of 7.5 cm (6.1 visual degrees). The target remained at its new position for 750 ms before both cursor and target were removed and the empty circle was displayed for a further 1.75-2 s (uniformly distributed) before the next trial began. This summed up to a total inter-trial interval ranging from 4.75 s to 5 s. Participants were instructed to move the joystick when the green target appeared so as

to shift the white cursor from the central start position to match the position of the green target with a rapid, discrete and straight movement. The position of the white cursor was presented at rest and when the displacement of the joystick crossed 80% of the distance between the target and the starting point. The participants were explicitly told that the position of the feedback cursor would not respond to any later corrective movements and would return to the centre when the joystick position came back to the centre. This presentation strategy reduced corrective movements and encouraged more ballistic and straight movements. Perturbation was implemented by introducing an angular rotation between the cursor and the actual movement of the joystick so that the cursor deviated from its actual position. After familiarisation with the task, each subject completed a session of 310 trials. In the first 80 trials, no rotation was implemented. Thereafter, in the adaptation phase, a constant rotation was introduced (fixed perturbation of 60° , $n = 150$), followed by a washout phase without rotation ($n = 80$). Participants began with a practice session of 50 trials without rotational perturbation between the joystick and the cursor and then completed the longer experimental session after a short break. The participants were not aware of the adaptation condition and were not explicitly told that perturbation would be introduced. During the session, the experiment was paused and the participants were asked to either have a short break or to immediately return to the task. At the same time, participants were also reminded to keep trying to move the joystick so as to match the white dot with the target green dot.

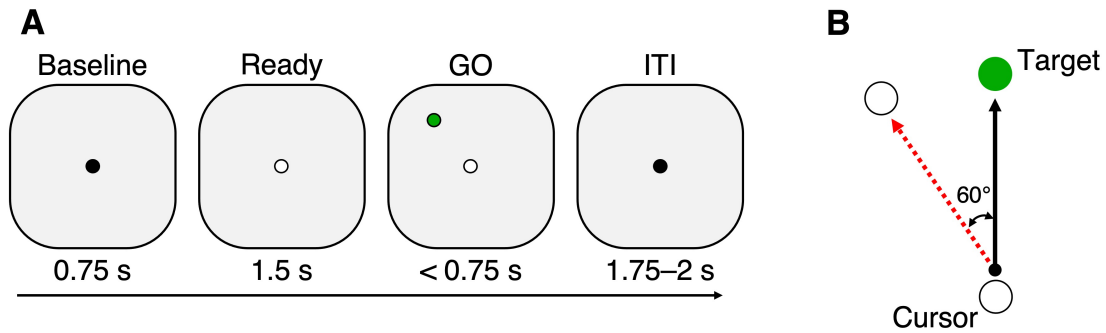


Figure 2.1: Experimental protocol and angular perturbation

(A) Participants performed an aiming task while controlling a joystick with their right hand. A typical trial consisted in a "baseline" period during which participants were instructed to remain still and fix an empty circle for 750 ms. This stage was followed by a "ready" period of 1.5 s, where the joystick white cursor was displayed. Then, in the "GO" period a green target was displayed for a maximum time of 750 ms in one of 5 possible locations in the upper half of the screen. The trial ended by displaying the same empty circle shown during "baseline" for 1.75-2 s. (B) Example of a straight outgoing movement (black line) performed when the perturbation was active. Perturbation was introduced as a rotation between the green target and actual joystick movement. A 60° angular rotation would cause the white cursor to be displaced at the end of the dashed red line

2.2.3 Behavioural analysis

Behavioural analyses were carried out with custom scripts in Python. Joystick cursor displacement was differentiated to calculate velocity and subsequently low-pass filtered through a Gaussian kernel to smooth the signal. Movement initiation was defined as the time when the joystick velocity crossed a threshold (computed as mean trial activity plus the trial standard deviation) and sustained this speed for at least 50 ms. Movement termination was the last time point the joystick velocity fell below the threshold for that trial. Joystick position error was calculated as the angular mismatch between the actual joystick position at the maximal velocity of the outgoing movement and the target position. The trial-to-trial adjustment was calculated based on the absolute change in the actual joystick position error between sequential trials. Trial-to-trial adjustment indexed motor adaptation. Reaction times (interval between stimulus onset and movement initiation), movement duration (interval between movement initiation and movement termination) and trial-to-trial adjustment were calculated for each individual trial and then averaged within subjects.

2.2.4 MEG acquisition and preprocessing

MEG signals were recorded using a CTF Omega 275-channel whole-head axial gradiometer system. The signals were recorded at a sampling rate of 1200 Hz. Fiducial coils were placed at fixed distances from three anatomical landmarks (nasion, left, and right pre-auricular) and the positions of the coils were monitored continuously throughout the session. For co-registration, these landmarks were later identified on the subjects' structural MRI. The MEG data were acquired continuously and epoched offline. All analyses were performed in MATLAB (MathWorks Inc, Natick, MA), mainly using the FieldTrip toolbox (Oostenveld et al., 2011) and custom scripts. MEG signals were first high-pass and low-pass filtered at 0.5 Hz and 150 Hz respectively. Spectral interpolation was used to remove power-line contamination and harmonics (Leske and Dalal, 2019). Data trials including large muscle artefacts were identified via a semi-automatic procedure. Trials were band-pass filtered between 110-140 Hz, z-transformed and compared against a threshold. Trials with values above the cut-off were visually inspected before exclusion. Eye movements and cardiac artefacts were projected out of the data using independent component analysis (Makeig et al., 1995). Finally, MEG signals were down-sampled to 300 Hz. Data were epoched according to three different scenarios. Stimulus-locked data were aligned from -2 s to 2 s around the GO cue (green target onset). Response-locked data were aligned from -2 s to 2 s around the start of the movement. Offset-locked data were aligned from -2 s to 1.5 s around the end of the movement.

2.2.5 Source imaging

For source localisation, each participant's anatomical MRI was divided into an irregular grid by warping the individual MRI to the MNI template brain and then applying the inverse transformation matrix to the regular MNI template grid (4mm isotropic voxel resolution), allowing source estimates at brain locations directly comparable across participants. For each grid location inside the brain, the forward model (i.e. the lead field) was calculated for a single dipole orientation by singular value decomposition, using a single-shell volume conduction model (Nolte, 2003). Since all grid locations of each subject were

aligned to the same anatomical brain compartments of the template, corresponding brain locations could be statistically compared over all subjects. Source power at each location was estimated using an LCMV (linearly constrained minimum variance) beamformer (Van Veen et al., 1997), available in FieldTrip. Beamformer analysis uses an adaptive spatial filter to estimate the power at every specific (grid) location of the brain. Virtual time courses were reconstructed for a set of cortical ROIs: the primary motor cortex (M1), the primary somatosensory cortex (S1) and the superior parietal lobule (sPL). A priori ROIs selection was based on the motor adaptation literature (Diedrichsen, 2005). ROI masks were constructed, for the left and right hemispheres, using the Harvard-Oxford atlas in FSL (Makris et al., 2005). Then, masks were thresholded to 35%, binarized and interpolated with MNI coordinates. For each participant and each ROI, a single virtual channel was extracted following a multi-step procedure. First, beamforming spatial filter weights were computed using a covariance matrix calculated by combining trials from the broadband data. The filter weights were used to reconstruct single-trial time series for each source in the ROI. Then, power spectra (PSD) were computed for each time series with Matlab Welch's method. Next, the FOOOF toolbox (Donoghue et al., 2020) was used to quantify periodic (oscillatory) activity in the beta (15-30 Hz) range. In short, the toolbox conceptualises the PSD as a combination of an aperiodic component with overlying periodic components (oscillations). These putative oscillatory components of the PSD are characterised as frequency regions of power over and above the aperiodic component. Only voxels that showed a peak in the beta range were selected for the next step. Finally, the virtual time series with maximum standard deviation was selected as the target virtual channel for that ROI.

2.2.6 TFRs on virtual channel time courses

Preprocessed MEG signals were decomposed into their time-frequency representations (TFRs) in the 8-40 Hz range using a Hanning taper with a sliding time window of 7 cycles. MEG power change was subsequently normalised as the percentage change relative to the overall average by dividing the power at each frequency and each time point by the

average power of that frequency across the whole experimental session (Tan et al., 2016; Torrecillos et al., 2015). Values >0 indicated power higher than the overall average power of that frequency and vice versa. Beta desynchronisation and PMBR were calculated for each participant trial before averaging for further analysis. Beta desynchronisation was defined as the average normalised power over a 200 ms window centred on the trough of power change in the period that goes from -0.5 to 0 s before movement onset. The same procedure was also applied to PMBR, with the difference that the window was centred on the positive peak in a time period from 0 to 0.8 s after movement offset.

2.2.7 Beta burst analysis

Beta bursts computation followed the pipeline described in Rayson et al., (2022)(for a detailed description of the analysis rationale see **Section 1.4.1**). In short, PSDs were computed for each virtual channel time-series with Matlab Welch's method and then *log*-scaled. A $1/f$ function was fitted to the spectrum and frequency bands were identified using the residuals of this fit, which represent the periodic component of the spectrum. Band peak frequencies were identified as local maxima, while the bandwidth was set to 6 Hz (± 3 Hz around the peak). Next, the amplitude threshold (standard deviations above the median) for identifying beta bursts was estimated for all participants and ROIs. The data is first band-pass filtered around the peak frequencies determined above, and then the amplitude envelope is extracted after applying the Hilbert transform to the filtered data. In order to avoid filter-related edge artefacts, the data are padded using the DC offset before applying the filter and Hilbert transform. This padding is then removed from the resulting amplitude envelope. The empirically-derived relative threshold on beta amplitude is used to identify bursts and is computed based on multiple standard deviations above the median beta amplitude (**Eq. 2.1**), with the median representing a robust measure of centrality for skewed distributions.

$$threshold = med(A) + s(A) \times k \quad (2.1)$$

where:

A = Hilbert envelope

k = range of values $\{0.1, 0.2, \dots, 3\}$

med = median

s = standard deviation

For each subject, the non-parametric correlation (Spearman's ρ) was computed between the number of bursts per trial (number of threshold crossings) and the mean amplitude per trial. This is done using a range of thresholds computed from the median and standard deviation of beta amplitude in all time points across all trials for that subject. The standard deviation multiple that maximises the mean of this correlation was selected. For M1, this resulted in a threshold of 1.6 SD above the median. The times at which beta amplitude crossed the subject-specific threshold and then returned below the threshold were found. The difference between these two time points gives the duration of the burst, and from within these, burst onset and offset times, peak amplitude, and the time at which this peak is reached were identified.

To compare the burst rate to beta amplitude, the amplitude and a smoothed measure of burst rate were normalised. The amplitude was baseline corrected by subtracting the mean amplitude over the whole experiment. The burst rate was obtained by binning the burst event timings using 10 ms bins, smoothing using a two-pass Gaussian convolution with a width of 25 bins, and then baseline correcting by subtracting the mean burst rate over the whole experiment.

2.2.8 Statistical analysis

Repeated-measures ANOVAs were used to investigate the effects of trial execution order (i.e., averages of trials 1-20, 81-100, etc) and experimental phases. Mauchly's test of sphericity was used to test the homogeneity of variance. Where Mauchly's test of sphericity was significant ($p < 0.05$) in repeated-measures ANOVAs, Greenhouse-Geisser corrections

were applied. Two-tailed paired-sample t tests were calculated for *Post-hoc* analyses, using Bonferroni correction for multiple comparisons. Mean \pm SE are presented throughout the text unless otherwise specified. Effect sizes were calculated using Cohen's d , calculated as the difference between the two means, divided by the standard deviation of the difference. 95% confidence intervals (95% CI) were calculated using accelerated bias-corrected percentile limits (number of bootstrap samples = 10000).

2.3 Results

2.3.1 Cursor perturbation elicits motor adaptation

During the priming phase (trials 1-80), the angular error between the joystick cursor and the target, was close to zero because there was no perturbation in this condition. During the adaptation phase (trials 81-230), the absolute task-relevant error was initially close to the perturbation rotation angle (mean angular error \pm SD, $42^\circ\pm 9^\circ$), and then gradually reduced with the process of adaptation ($22^\circ\pm 7^\circ$). The cursor angular error increased again ($25^\circ\pm 10^\circ$) when the constant rotation was suddenly removed (from trial 231), and then returned to baseline levels of the priming phase **Table 2.1 - Figure 2.2**.

Table 2.1: Descriptive statistics of behavioural features across phase

	<i>Phase</i>		
	<i>Priming</i>	<i>Adaptation</i>	<i>Washout</i>
<i>Angular Error °</i>			
<i>mean</i>	9	27	14
<i>median</i>	9	27	15
<i>sd</i>	1	6	3
<i>se</i>	0.4	1	1
<i>Reaction Time s</i>			
<i>mean</i>	0.41	0.46	0.43
<i>median</i>	0.42	0.47	0.45
<i>sd</i>	0.05	0.05	0.06
<i>se</i>	0.01	0.01	0.01
<i>Movement Duration s</i>			
<i>mean</i>	0.56	0.64	0.58
<i>median</i>	0.54	0.68	0.60
<i>sd</i>	0.16	0.16	0.15
<i>se</i>	0.04	0.04	0.04

A two-way repeated-measures ANOVA with factors of phase (3 levels, priming-adaptation-washout) and trial order (2 levels, start-end; an average of first and last 20 trials of each phase) was applied to the cursor angular error to test the effect of motor adaptation throughout the experiment **Figure 2.3**. This analysis showed a significant effect of phase ($F_{(1,27,21.6)} = 86.62, p < 0.001$), a significant effect of the trial order ($F_{(1,17)} = 100.35, p < 0.001$) and a significant interaction between phase and trial order ($F_{(2,34)} = 59.04, p < 0.001$). *Post-hoc* analysis showed that during the adaptation phase, the cursor angular error was reduced over trial order (start-end difference, $20^\circ \pm 2^\circ, t_{(17)} = 10.4, p < 0.001$). A similar pattern was also present in the washout phase ($12^\circ \pm 2^\circ, t_{(17)} = 8, p < 0.001$). In the priming phase instead, the cursor angular error remained stable ($-1.5^\circ \pm 1^\circ, t_{(17)} = -1, p = 0.1$).

Reaction time and movement duration showed modulations across the experiment comparable to angular error

(**Table 2.1 - Figure 2.2B-C**). A repeated measures ANOVA (**Figure 2.4**) revealed a main effect of phase for both reaction time ($F_{(2,34)} = 23.87, p < 0.001$) and movement

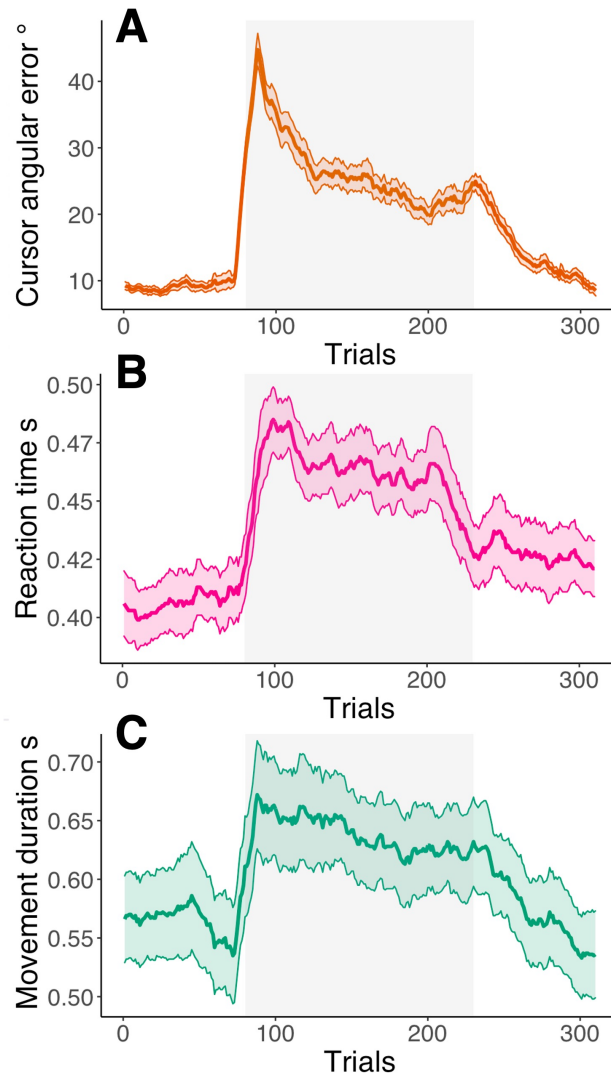


Figure 2.2: Behavioural features across the experiment

(A) Angular error across trials. Two peaks are visible at the start of the adaptation phase (trial = 80) and at the start of the washout phase (trial = 231). Each data point is the average of 15 successive trials; the solid lines and shaded area show the mean and SE across participants. A light grey shaded area marks the adaptation phase where cursor perturbation was present. (B-C) same as A for reaction time and movement duration

duration ($F_{(2,34)} = 9.41, p < 0.001$). *Post-hoc* analysis showed that during priming, participants responded faster (mean $rt \pm SD$, 410 ms \pm 50 ms) compared to both adaptation and washout (adaptation, $t_{(17)} = 6.14, p < 0.001$; washout, $t_{(17)} = 3.46, p = 0.009$). Furthermore, reaction times during the adaptation phase (460 ms \pm 50 ms) were slower compared to washout (430 ms \pm 60 ms, $t_{(17)} = 3.88, p = 0.004$). Similarly, movement duration was longer during adaptation (mean movement duration $\pm SD$, 640 ms \pm 160 ms) compared to priming (560 ms \pm 160 ms, $t_{(17)} = 3.75, p = 0.005$) and washout (580 ms \pm 150 ms, $t_{(17)} = 3.89, p = 0.004$). In contrast, no difference was found between washout and priming.

These results confirm that a visual perturbation of the joystick cursors can induce motor adaptation. The joystick angular error was initially close to the perturbation rotation angle and then was gradually reduced with the process of adaptation. The cursor angular error increased again when the constant rotation was suddenly removed, and then was reduced with the process of washout.

Both reaction time and movement duration were affected by visual perturbation. Slower responses and longer movement duration suggest a decrease in motor performance.

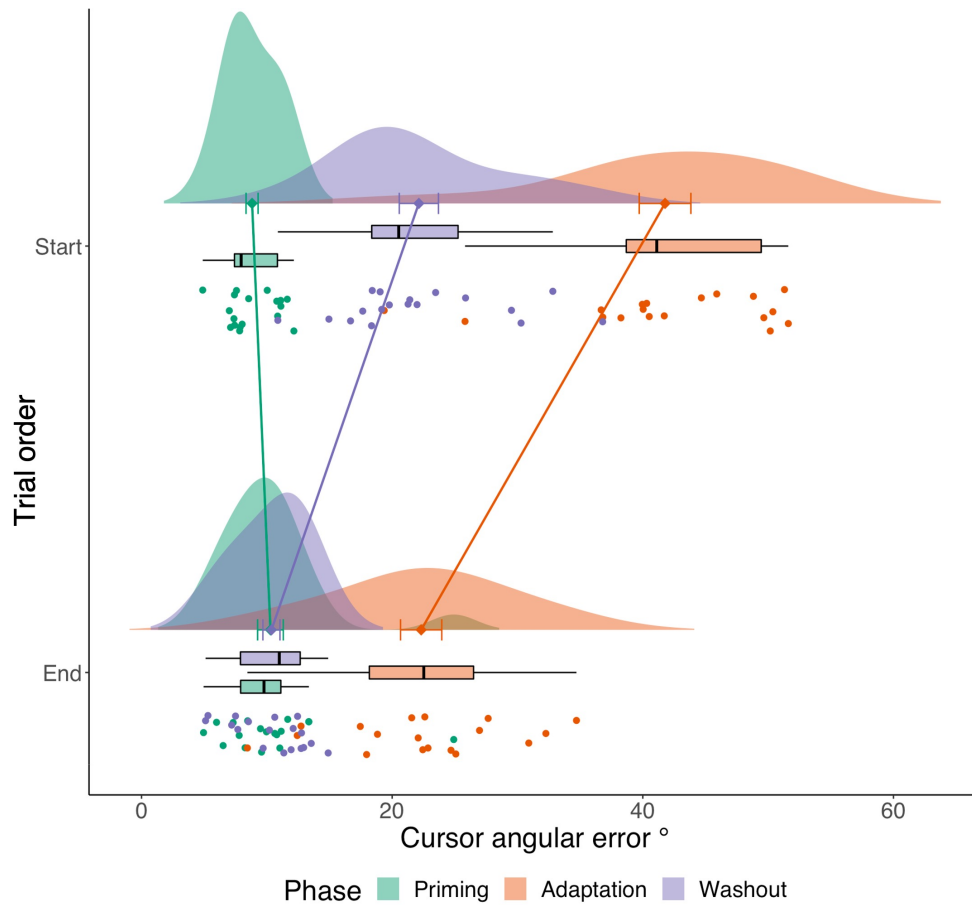


Figure 2.3: **Angular error across time and phase**

Plots of angular error at the start and end of each phase. Each raincloud plot (M. Allen et al., 2019) is composed of individual participant scores (**coloured points**), *boxplot*, data distribution (**coloured curve**) and mean with standard error (**coloured diamond point and error bars**). The x-axis reflects the cursor error. The y-axis reflects the start and the end of each phase (average of the first and last 20 trials). Individual phases are colour-coded (**light-green, priming; light-orange, adaptation; light-violet, washout**). Coloured solid lines connect the mean scores of each phase in different trial orders.

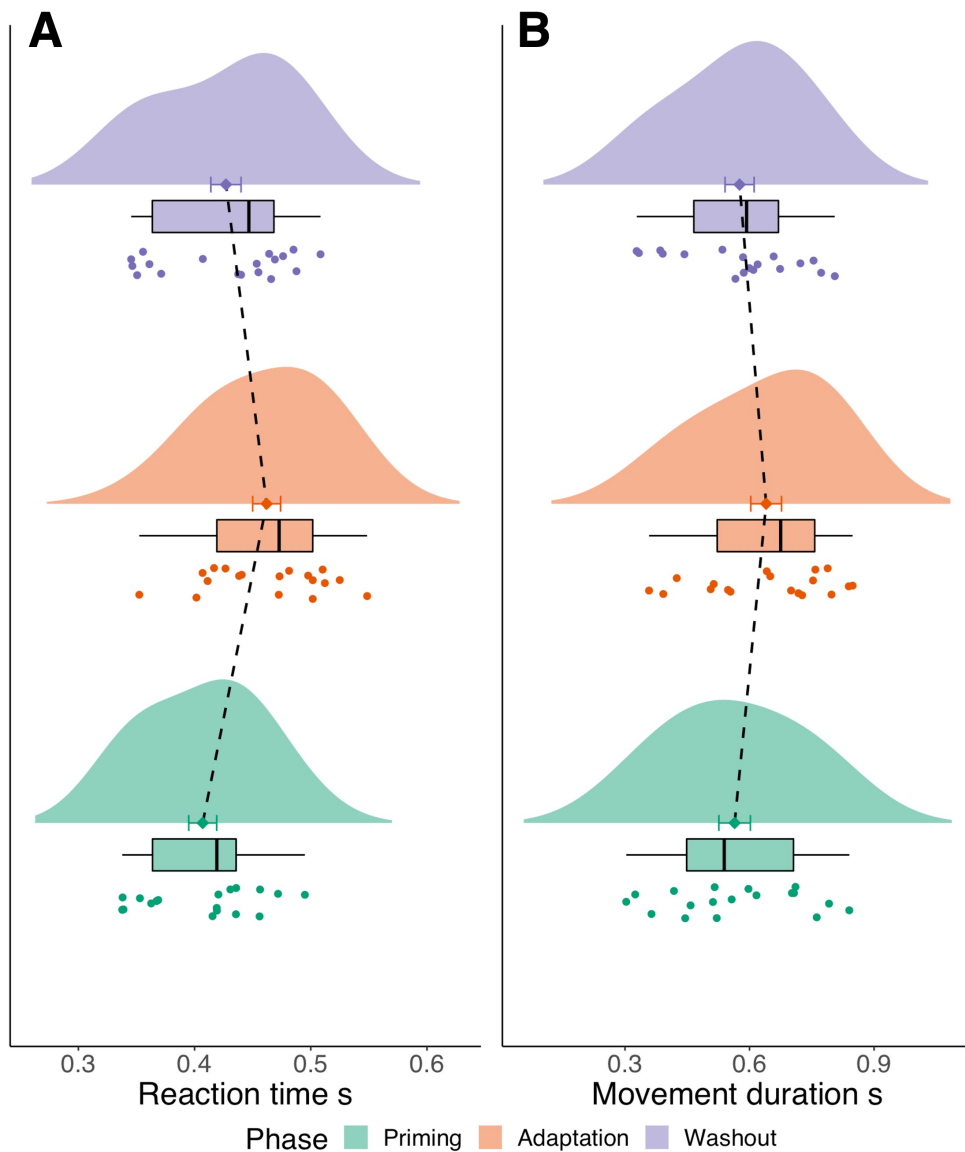


Figure 2.4: Reaction time and movement duration across phase

(A) Evolution of reaction time across phases. Each raincloud plot is composed of individual participant scores (coloured points), *boxplot*, data distribution (coloured curve) and mean with standard error (coloured diamond point and error bars). The x-axis reflects reaction time. Individual phases are colour-coded (light-green, priming; light-orange, adaptation; light-violet, washout). Dashed black lines connect the mean scores of each phase. (B) same as A for movement duration.

2.3.2 Beta rebound is modulated during motor adaptation

A relative decrease in MEG power across the beta frequency band (15-30 Hz) was consistently observed over M1 during joystick movement. The decrease in power was followed by a rebound synchronisation beginning at movement offset (**Figure 2.5**; see also **Figure A.1-A.2** in **Appendix A** for individual dynamics).

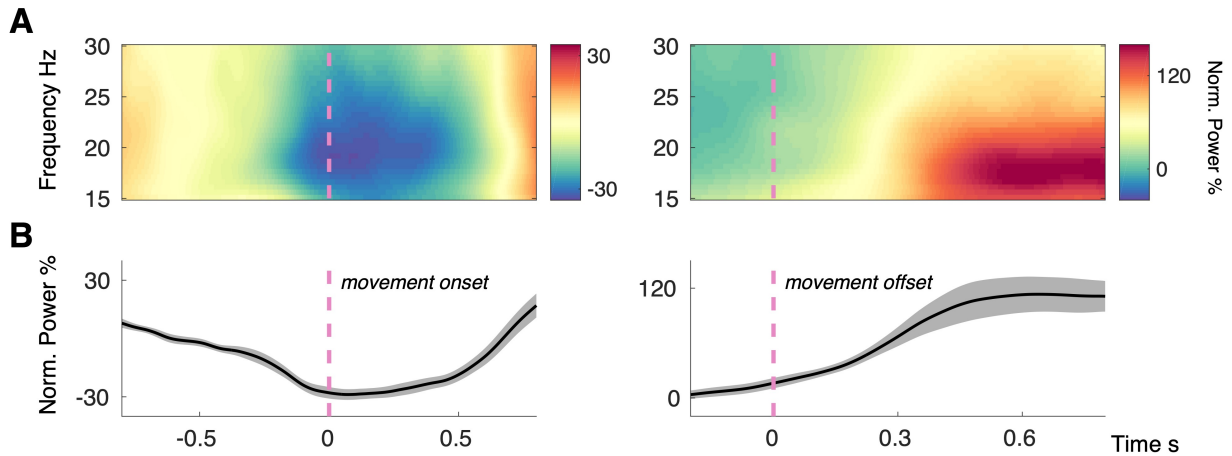


Figure 2.5: Beta dynamics during movement

(A) TFRs of a virtual sensor over M1 during movement onset (*left*) and movement offset (*right*). Pink dashed lines mark the start (*left*) and end (*right*) of movement. (B) Average normalised power across beta frequency range (15 to 30 Hz). Solid black lines and grey-shaded areas show the mean and SE across participants.

To analyse beta dynamics during learning, we split the trials across three phases (priming, adaptation and washout) and two periods (start and end). We initially run the analysis on the TFRs from M1. A two-way repeated-measures ANOVA with factors of trial order ($n = 2$) and phase ($n = 3$) was applied to the average PMBR during the first 20 trials and the last 20 trials of each phase (**Figure 2.6**; **Table 2.2**). This analysis identified a significant effect of trial order ($F_{(1,17)} = 7.16, p = 0.016$), but failed to show a significant interaction between trial order and phase ($F_{(2,34)} = 2.27, p = 0.12$). *Post-hoc* tests revealed that the PMBR was increased from start to end of the adaptation phase (mean power change \pm SD, $54 \pm 64\%$, $t_{(17)} = 3.57, p = 0.002, d = 0.84, 95\% \text{ CI } [0.48, 1.16]$). Similarly, PMBR increased during washout, but it failed to reach significance ($52 \pm 115\%$, $t_{(17)} = 1.91, p = 0.07, d = 0.45, 95\% \text{ CI } [-0.03, 0.72]$). PMBR during priming instead, remained stable ($8 \pm 64\%$, $t_{(17)} = 0.54, p = 0.6, d = 0.12, 95\% \text{ CI } [-0.41, 0.6]$).

A series of paired t tests was also run to compare beta power across phases. At the start of the phase, PMBR was lower during adaptation compared to priming ($t_{(17)} = -2.79$, $p = 0.038$, $d = -0.66$, 95% CI [-1.2, -.39]). This difference flattened at the end of the two phases ($t_{(17)} = -0.86$, $p = 1$, $d = -0.2$, 95% CI [-0.63, .28]). Comparison of PMBR between washout and priming did not return significant differences at the start ($t_{(17)} = -1.29$, $p = 0.64$, $d = -0.3$, 95% CI [-0.57, .25]), and at the end ($t_{(17)} = 0.18$, $p = 1$, $d = 0.04$, 95% CI [-0.49, .48]).

A similar analysis as the one applied to PMBR on M1, was run on the average beta desynchronisation (**Figure 2.7**). The repeated-measures ANOVA did not return any significant effect (for summary see **Table 2.3**).

Together, these results suggest that the introduction of the visual perturbation affected the dynamics of PMBR over M1. PMBR was first reduced at the start of adaptation and then, at the end, returned to activity levels comparable to the priming phase. In the washout phase, the removal of the visual perturbation was also followed by a reduction of PMBR. The magnitude of this effect, however, was smaller compared to the one observed during adaptation, making this interpretation not fully supported by the data.

The dynamics of PMBR observed in M1 were also investigated in a set of frontal and parietal ROIs (**Figure 2.8 - Figure 2.9**). An increase in beta power after movement termination was observable in all ROIs during priming. The magnitude of the increase, however, was maximal for M1 and S1 and showed lateralisation (left ROIs power > right ROIs). Comparison of PMBR at the start of adaptation with the same period during priming revealed a generalised trend. PMBR was reduced across all ROIs. However, only M1 (*left and right*), IFG (*left and right*) and sPL (*left*) survived multiple comparison corrections (for more details see **Table A.1** in **Appendix A**). The contrast of PMBR between washout and priming at the start of each phase did not return any significant findings, showing smaller differences overall (smaller effect sizes; see **Table A.1**). Similarly, no significant effect was found for the contrast of adaptation and washout.

The reduction of PMBR power in M1 during adaptation was also observed across several frontoparietal areas. The magnitude of this decrease was accentuated for ROIs in the left hemisphere and was maximal for M1, IFG and sPL.

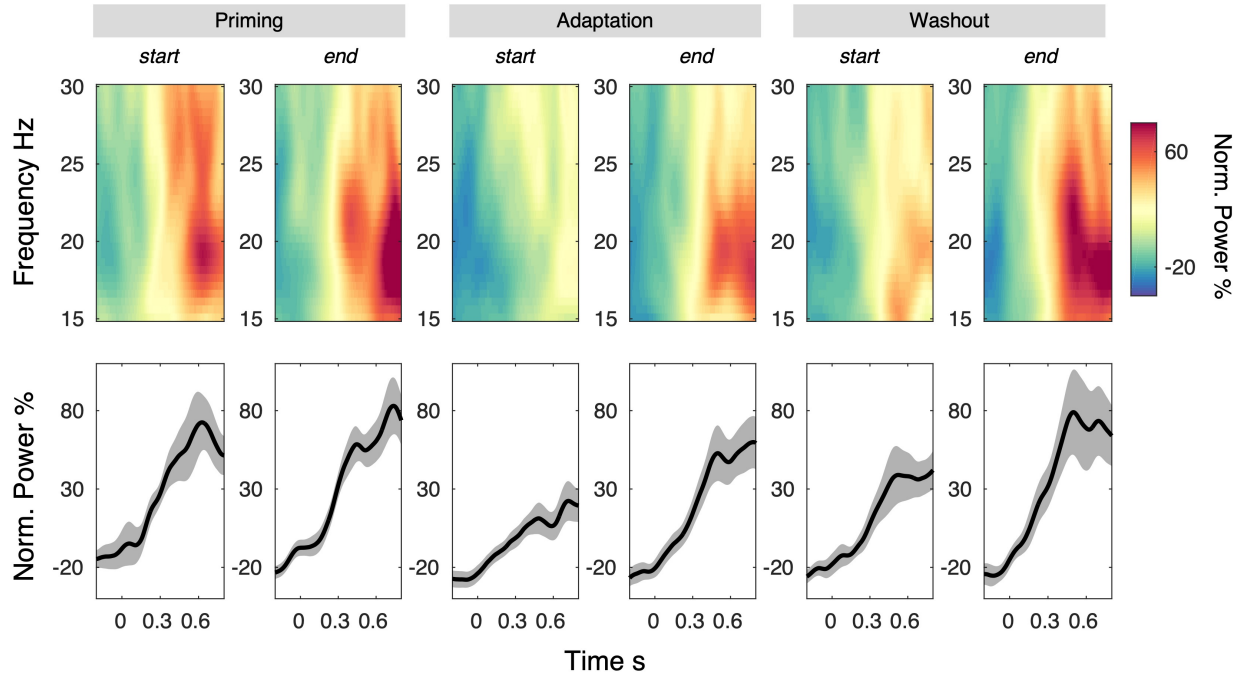


Figure 2.6: **PMBR across the experiment**

(Top) Average power change relative to the average power of the whole session at different frequencies. TFRs are aligned to movement offset at time 0, averaged across trials and then across participants. (Bottom) Average power change in the beta band (15-30 Hz) aligned to movement offset at time 0. Solid black lines and grey-shaded areas show the mean and SE across participants.

Table 2.2: **PMBR across phase and trial order**

<i>Unit=Power%</i>	<i>Phase</i>		
	<i>Priming</i>	<i>Adaptation</i>	<i>Washout</i>
Start (first 20 trials)			
<i>mean</i>	148	79	111
<i>median</i>	122	71	108
<i>sd</i>	99	52	84
<i>se</i>	23	12	20
End (last 20 trials)			
<i>mean</i>	156	133	163
<i>median</i>	119	122	110
<i>sd</i>	87	86	150
<i>se</i>	21	20	35

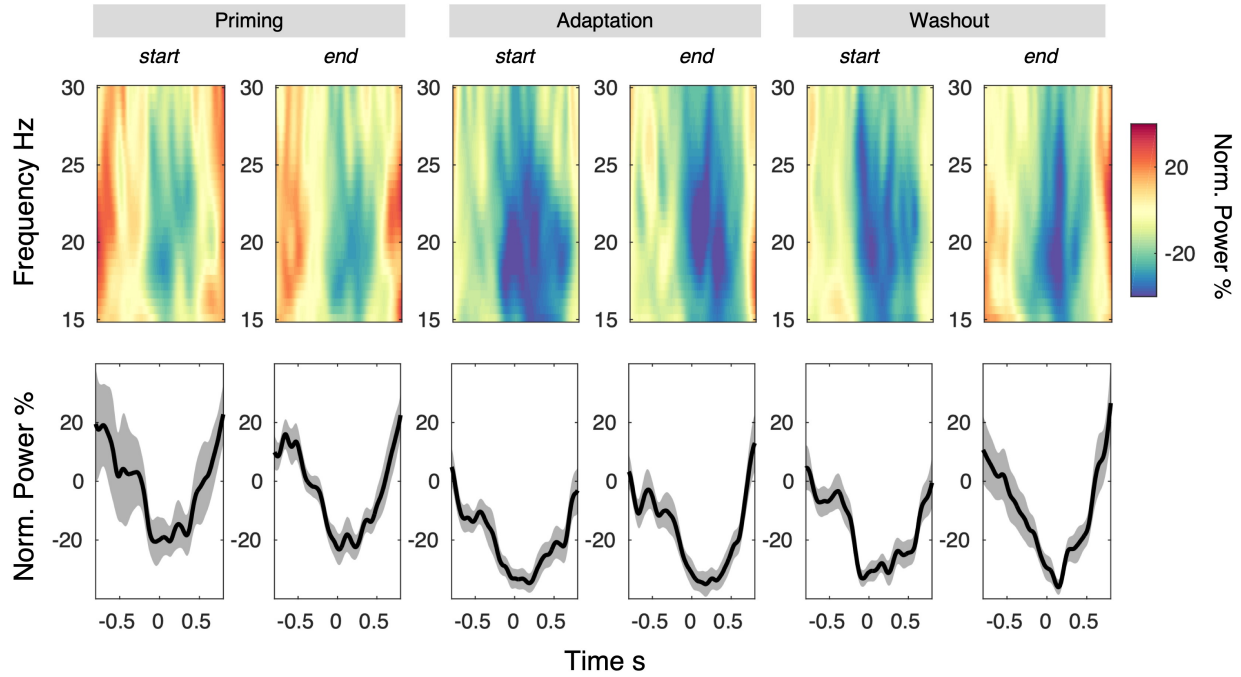


Figure 2.7: **Beta desynchronisation across the experiment**

(Top) Average power change relative to the average power of the whole session at different frequencies. TFRs are aligned to movement onset at time 0, averaged across trials and then across participants. (Bottom) Average power change in the beta band (15-30 Hz) aligned to movement onset at time 0. Solid black lines and grey-shaded areas show the mean and SE across participants.

Table 2.3: **Beta desynchronisation across phase and trial order**

<i>Unit=Power%</i>	<i>Phase</i>		
	<i>Priming</i>	<i>Adaptation</i>	<i>Washout</i>
Start (first 20 trials)			
<i>mean</i>	-43	-51	-50
<i>median</i>	-47	-48	-49
<i>sd</i>	24	11	9
<i>se</i>	6	3	2
End (last 20 trials)			
<i>mean</i>	-44	-50	-48
<i>median</i>	-42	-46	-47
<i>sd</i>	11	12	11
<i>se</i>	3	3	3

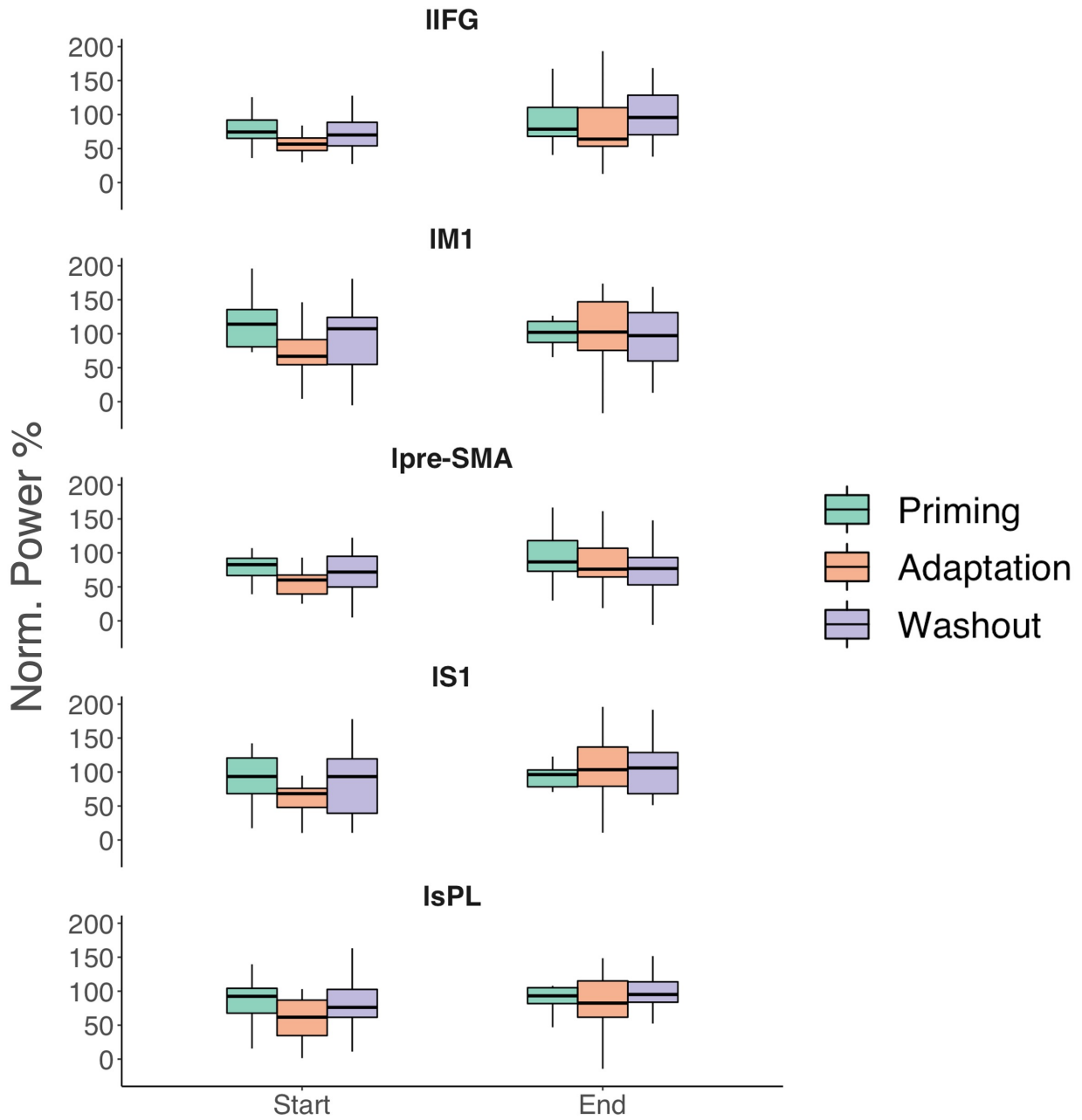


Figure 2.8: PMBR dynamics across left ROIs

Plot showing the average PMBR power across several ROIs at the start and at the end of each phase. PMBR power was normalised relative to the average power of the whole session. Individual phases are colour-coded (**light-green, priming; light-orange, adaptation; light-violet, washout**). Anatomical regions: IFG, inferior frontal gyrus, M1, primary motor cortex, pre-SMA, pre-supplementary motor area, S1, primary somatosensory cortex, sPL, superior parietal lobule.

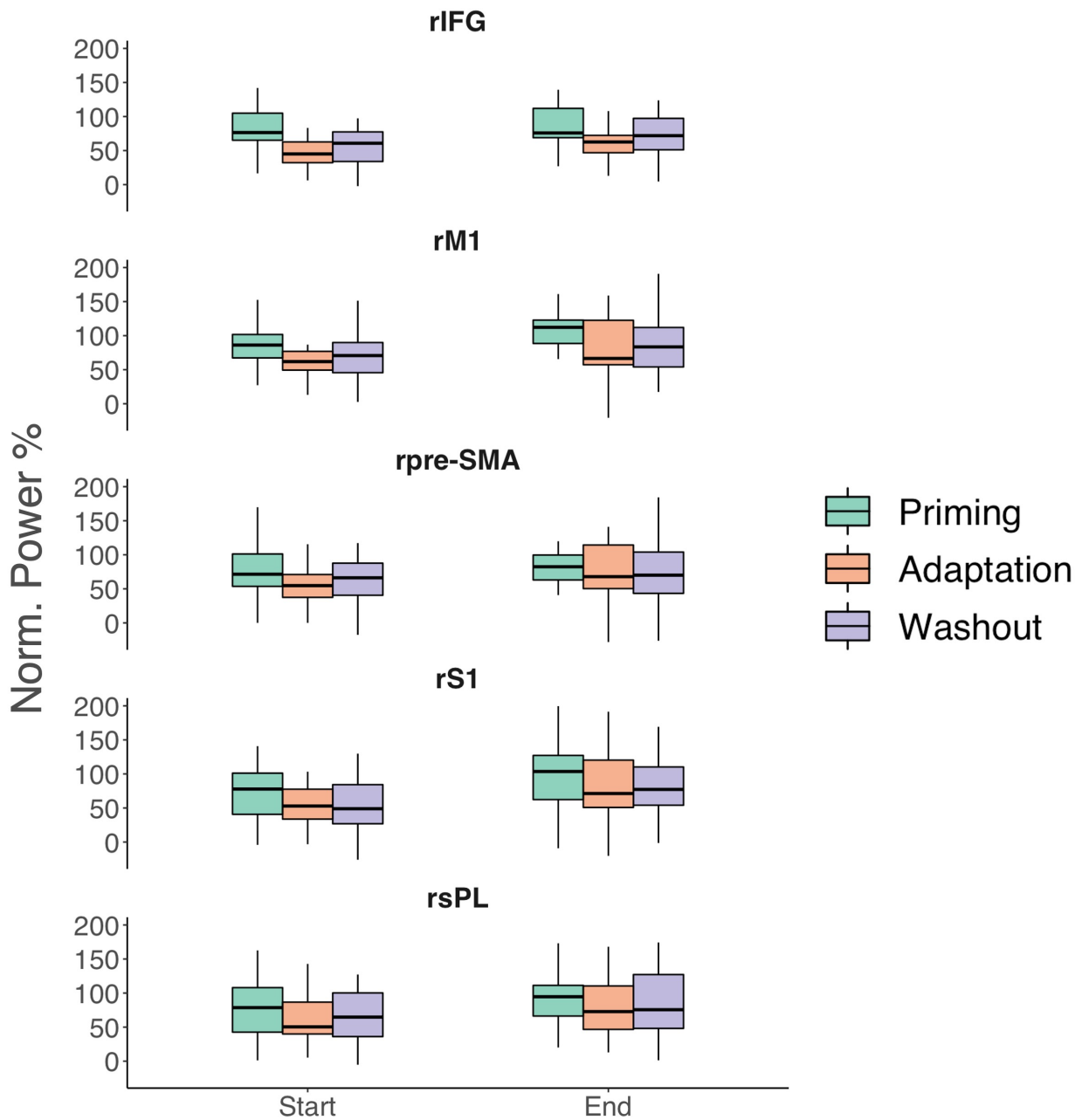


Figure 2.9: PMBR dynamics across right ROIs

Plot showing the average PMBR power across several ROIs at the start and at the end of each phase. PMBR power was normalised relative to the average power of the whole session. Individual phases are colour-coded (**light-green, priming; light-orange, adaptation; light-violet, washout**). Anatomical regions: IFG, inferior frontal gyrus, M1, primary motor cortex, pre-SMA, pre-supplementary motor area, S1, primary somatosensory cortex, sPL, superior parietal lobule.

2.3.3 Beta bursts amplitude is reduced during adaptation

The effects observed during the analysis of average beta power were further explored by looking at the characteristics of single trial beta. Specifically, the analysis focused on the behaviour of a number of beta's features (amplitude, peak time, duration and number of bursts) across phase and trial order (**Table 2.4**).

Beta burst probability gradually declines during movement and then increases after movement termination (**Figure 2.10**). These dynamics were comparable to the findings from averaged beta power. This was expected since the number of bursts extracted was designed to maximise the correlation between beta amplitude and burst count (see **Section 2.2.7**). The number of participants showing beta bursts in a time window that goes from 0 to 1 s after movement offset, was reduced at the start ($n = 14$) and at the end ($n = 8$) of the washout phase. Furthermore, the number of bursts detected for the remaining participants at the end of the washout phase (mean number of bursts \pm SD, 7 ± 4) was lower compared to the same period for priming (19 ± 9) and adaptation (17 ± 6).

In **Figure 2.11** we show the number of bursts detected across the experiment. The visualisation shows a distinct decrease in the number of bursts localised in the later stage of the experiment, overlapping with the washout phase. Due to the inconsistent number of bursts available during washout, this experimental phase was excluded from the following analysis on beta bursts.

Results from a paired t test on beta burst-amplitude showed a marked decrease at the start of adaptation compared to the same period during priming ($t_{(14)} = -2.44$, $p = 0.029$, $d = -0.63$, 95% CI [-0.91, -0.12]). At the end of both phases, the burst-amplitude difference diminished and was not significant ($t_{(14)} = -1.54$, $p = 0.146$, $d = -0.4$, 95% CI [-1.15, 0.26]).

Similar tests were run on burst peak time (*start*, $t_{(14)} = 0.61$, $p = 0.55$, $d = 0.16$, 95% CI [-0.41, 0.71]; *end*, $t_{(14)} = 0.93$, $p = 0.37$, $d = 0.24$, 95% CI [-0.36, 0.72]), burst duration (*start*, $t_{(14)} = -1.81$, $p = 0.09$, $d = -0.47$, 95% CI [-0.86, 0.11]; *end*, $t_{(14)} = -0.44$, $p = 0.67$, $d = -0.11$, 95% CI [-0.75, 0.46]) and burst count (*start*, $t_{(14)} = -1.93$, $p = 0.07$, $d = -0.5$, 95% CI [-0.89, 0.06]; *end*, $t_{(14)} = -0.63$, $p = 0.53$, $d = -0.16$, 95% CI [-0.68,

0.4]), but none showed significant differences.

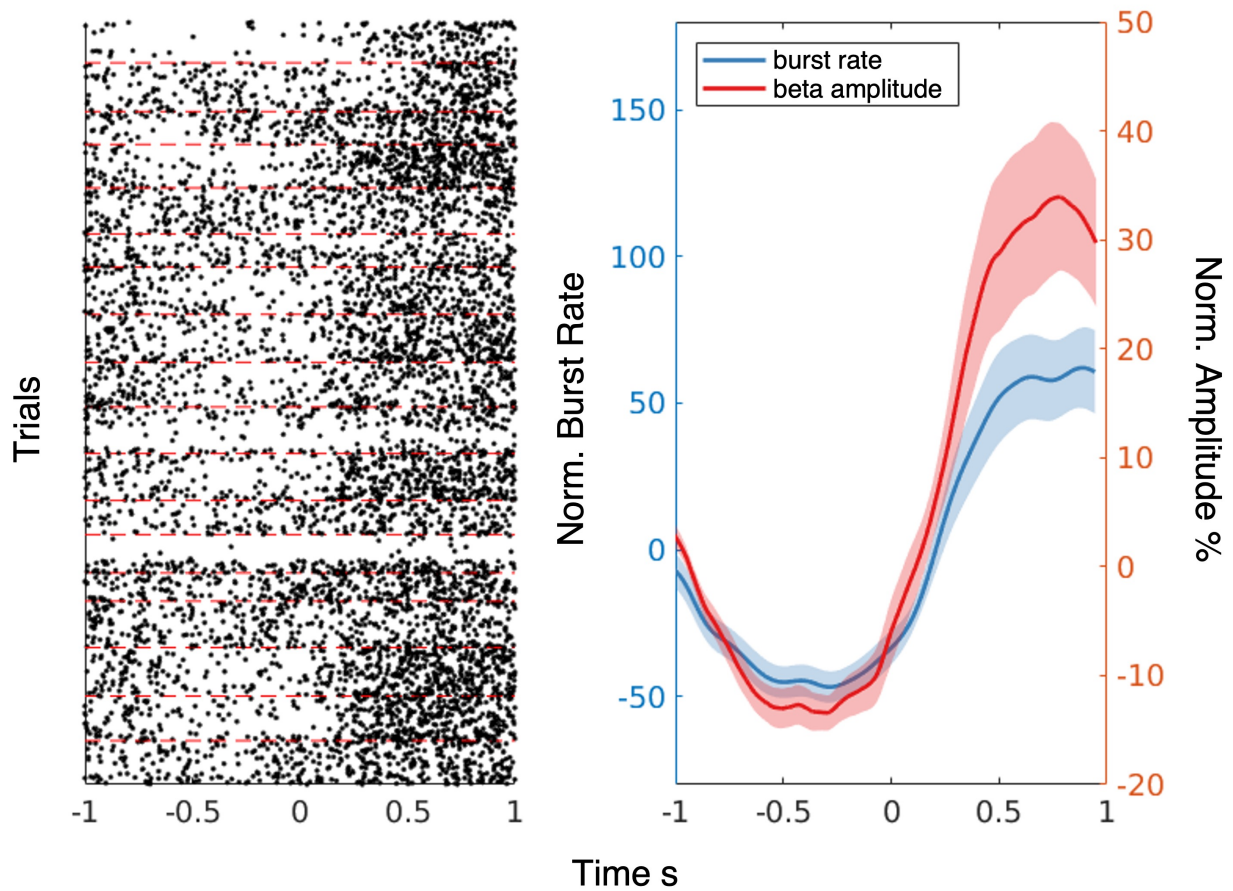


Figure 2.10: Beta bursts across time

(*Left*) Raster plots showing the timing of each individual burst (single point = peak of burst) for all trials of all 18 subjects (>5000 trials; individual subjects divided by dashed red lines). The plot is aligned to the movement offset ($t = 0$). There is a significant increase (weakly temporally locked) in burst probability after the end of the movement. (*Right*) Normalised average PMBR (*red*) is shown in the post-movement period together with burst rate probability (*blue*). The plot is aligned to the movement offset ($t = 0$). Solid coloured lines and coloured shaded areas show the mean and SE across participants.

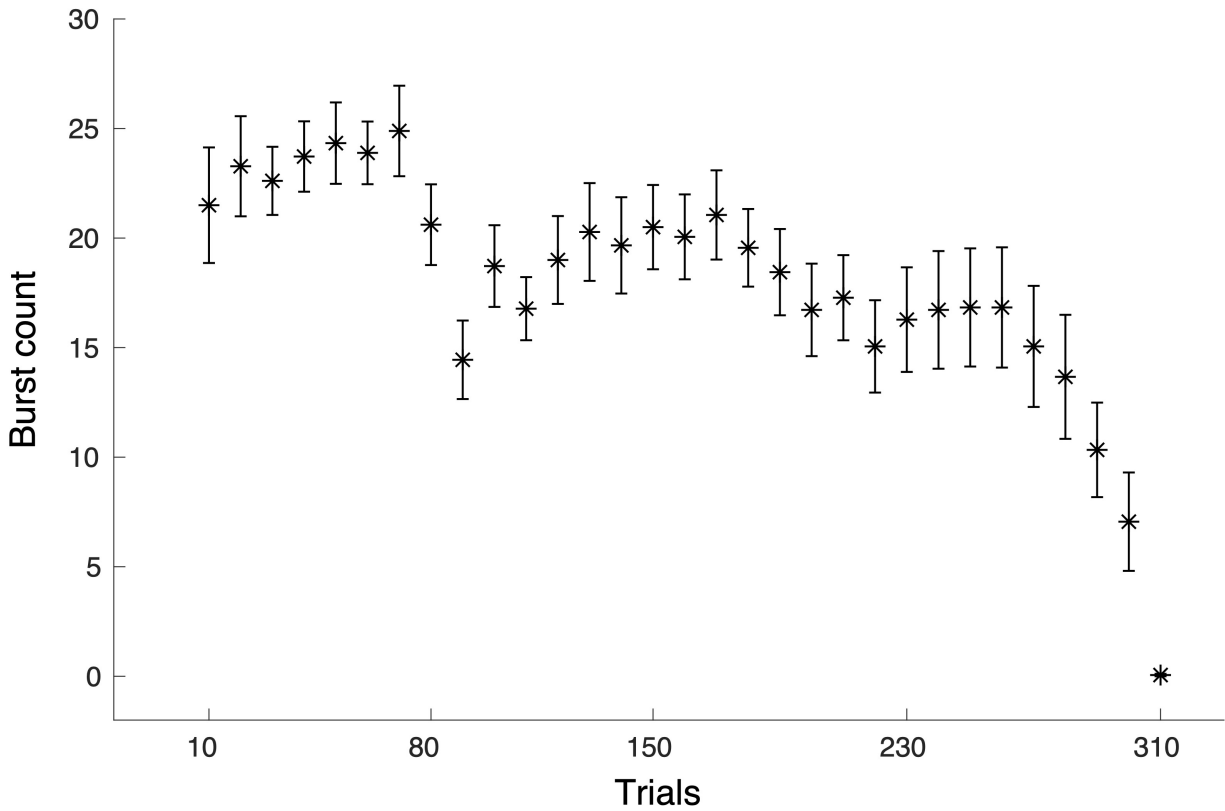


Figure 2.11: Burst count across the experiment

Average burst count across participants. Each data point is the average of the total number of bursts across 10 successive trials. * symbol shows the mean burst count while error bars show SE across 18 subjects.

Table 2.4: Beta bursts features across phase and trial order

	Burst count		Amplitude %		Peak time s		Duration s	
	<i>Priming</i>	<i>Adaptation</i>	<i>Priming</i>	<i>Adaptation</i>	<i>Priming</i>	<i>Adaptation</i>	<i>Priming</i>	<i>Adaptation</i>
Start								
<i>mean</i>	19	14	165	145	0.56	0.58	0.15	0.13
<i>median</i>	21	11	155	142	0.57	0.6	0.13	0.12
<i>sd</i>	8	8	53	40	0.08	0.06	0.07	0.05
<i>se</i>	2	2	14	10	0.02	0.02	0.02	0.01
End								
<i>mean</i>	18	17	173	155	0.57	0.6	0.16	0.15
<i>median</i>	18	16	160	140	0.56	0.62	0.15	0.14
<i>sd</i>	9	6	54	49	0.07	0.09	0.06	0.07
<i>se</i>	2	2	14	13	0.02	0.02	0.02	0.02

2.4 Discussion

In this chapter, we explored beta oscillations dynamics during motor adaptation. We found a transient reduction of PMBR during the adaptation phase, consistent with a link between beta oscillations and motor learning.

We replicated the findings in Tan et al. (2014, 2016) by employing a comparable joystick paradigm. The task successfully elicited motor adaptation. This was shown by a rapid worsening of motor performance at the start of the adaptation phase (visual perturbation ON), followed by a return to baseline performance levels at the end. A similar pattern was observable for sensorimotor beta oscillations, specifically for the PMBR, which was dynamically modulated throughout the experiment. Tan et al. have proposed a link between beta oscillations and computational models of sensorimotor control (Franklin and Wolpert, 2011; Scott, 2012). These models emphasise the importance of integrating sensory feedback with motor plans to avoid environmental instabilities. Predictions from the internal model are compared against incoming sensory information after movement termination. The mismatch between the two drives an update of the internal model and a change in the motor output (Shadmehr et al., 2010). According to the interpretation of Tan et al., a decrease in PMBR following large and consistent sensory errors indexes a low confidence in the motor plan and drives adapting behaviours. It is noteworthy that PMBR modulation was not restricted to M1. We found modulation of beta oscillations in several sensorimotor ROIs, including IFG. Extensive literature has suggested that the IFG is part of the ventral attention system, which activates in response to the detection of a salient target, particularly when the target is behaviourally relevant (Erika-Florence et al., 2014; Hampshire et al., 2009; Sharp et al., 2010; Duann et al., 2009). The PMBR reduction observed across ROIs, could be linked to generalised top-down attentional processes. This interpretation is supported by recent studies (Torrecillos et al., 2015; Alayrangues et al., 2019). These authors contrasted beta responses after two types of reach errors: errors that trigger trial-to-trial motor-command updates and errors that do not elicit sensorimotor adaptation. PMBR was similarly attenuated for both types of errors, consistent with the idea that beta attenuation relates to increased alertness due to salient events.

The cumulative evidence from both the present and the above-mentioned studies aligns with a notion of the functional role of beta during learning which reconciles two opposing views, namely relating to motor output (Engel and Fries, 2010) or sensory processing functions (Cassim et al., 2001). PMBR has consistently been shown to be modulated by movement outcomes (Alayrangues et al., 2019; Tan et al., 2014, 2016; Torrecillos et al., 2015; Haar and Faisal, 2020). Interestingly, this modulation often exhibits a negative trend following errors, resulting in a decrease in beta synchrony within crucial sensorimotor areas such as M1 and S1. Consequently, it appears that reducing beta amplitude is necessary for the sensorimotor system to respond effectively to corrective motor commands.

In our study, it remains unclear whether the link between beta and motor learning is mediated by one or more additional components, such as movement kinematics or behavioural features. Employing a correlational approach across trials to investigate the relationship between beta and multiple measures, including RTs and errors, could provide valuable insights into the primary factors driving this association. Moreover, it would be necessary to carefully and extensively manipulate various experimental features, including different movement types and specific types of errors, to try to establish a causal link between beta and learning.

To further explore beta oscillations, we analysed beta at the single-trial level. We reported a drop in the magnitude of bursts amplitude during adaptation, while burst timing and duration were mostly unaffected. Burst amplitude indicates the local synchronisation level within the beta band. Excessive synchronisation at the local and circuit level can compromise information coding capacity and thereby motor processing (Engel and Fries, 2010; Brittain and Brown, 2014). Burst count was also reduced at the start of adaptation and together with the attenuation of burst amplitude, they could contribute to the effect observed in the averaged beta spectrum. We also reported a substantial decrease in burst count in the final stage of the experiment, overlapping with the washout phase. This reduction was progressive and consistent across all participants. The interpretation of this finding is unclear. A parsimonious explanation could refer to an idiosyncratic issue within the task structure or analysis. Another interpretation could suggest a tendency for

beta burst to naturally decline throughout the experiment, as a consequence of increased fatigue or reduced attention. To date, we are not aware of any study sharing similar findings. Furthermore, the average beta power during the end of the washout was comparable to the beta power at the beginning of the experiment. This raises concerns regarding the interpretability of burst parameters and should be addressed in future studies employing similar analyses.

One major limitation of this experiment concerns the correlational nature, by design, of the results. To establish a causal effect of beta oscillations in motor learning, further studies are necessary. One potential approach to strengthen the evidence is to conduct studies involving patients with impaired beta oscillations, such as individuals with Parkinson's disease (Heinrichs-Graham et al., 2014; Tinkhauser, Pogosyan, Tan, et al., 2017) or stroke (Rossiter, Boudrias, and Ward, 2014). Another supportive line of inquiry could involve direct modulation of beta oscillations through brain stimulation techniques (Herrmann et al., 2016). While brain stimulation studies can be only consistent with a causal link, they have the potential to provide valuable insights into the underlying neural architecture and shed further light on the role of beta oscillations in motor learning.

Another source limitation of this study pertains to the choice of ROIs. Many studies of beta during movement have shown key contributions of this rhythm in sub-cortical structures, such as the basal ganglia (Leventhal et al., 2012; Feingold et al., 2015). Additionally, one key region for error-based learning is the cerebellum, viewed as a system providing predictions about upcoming movements and receiving feedback about motor errors (Shadmehr et al., 2010; Popa and Ebner, 2019). MEG has poor spatial resolution in deep structures. The distance from the sensor array and signal diffusion issues yield a low signal-to-noise ratio and linear mixing at the individual recording sites. Furthermore, it has been speculated that the neuronal architecture of the cerebellar cortex (neural arrangement) may prevent the detection of cerebellar sources due to signal cancellation (Hashimoto et al., 2003; Dalal et al., 2013). The combined implementation of new recordings techniques, such as OPM-MEG (Lin et al., 2019; Brookes et al., 2022) and optimised pipelines (Andersen et al., 2020), could return reliable data from these sources. This will be key to providing a deeper understanding of how beta is modulated across an

extended sensorimotor system.

Finally, it is crucial to acknowledge that the present study does not provide a comprehensive understanding of the adaptation process due to the lack of adequate analysis regarding accuracy and precision in motor performance. Accuracy refers to the closeness of measurements to the true value of a quantity, while precision pertains to the consistency and reproducibility of measurements under consistent conditions. In the joystick paradigm, accuracy was quantified using the mean absolute error, whereas precision could have been assessed by considering the standard deviation of signed errors. Unfortunately, our analysis focused solely on absolute errors and did not incorporate precision measurements. This limitation significantly hampers our ability to gain valuable insights into the consistency and variability of participants' movements, which are essential for understanding how individuals adapt their motor control strategies. Furthermore, the absence of precision measurements introduces uncertainty regarding the relationship between the observed beta dynamics during motor adaptation and the specific learning processes that occur in our study. It remains unclear whether the observed beta dynamics are primarily influenced by learning processes related to action execution or if they reflect modifications in the mapping between intended and actual goals, regardless of the specific motor strategies employed. Additionally, by solely prioritising accuracy, our study may have overlooked potential fluctuations or deterioration of motor performance over time. These factors could serve as confounding variables impacting the modulation of beta oscillations and their relationship to motor adaptation.

To conclude, we successfully replicated findings from previous studies (Tan et al., 2014, 2016). We confirmed how post-movement beta dynamics are linked with rapid changes in the motor performance elicited by motor adaptation, and we further showed how this effect was observable across several frontoparietal areas with similar effects. Analysis of single-trial beta bursts confirmed a modulation of beta but did not provide key additional insights.

Chapter 3

The role of beta oscillations during action-stopping

3.1 Introduction

In this chapter, we continue to discuss some of the most relevant hypotheses on the functional role of sensorimotor beta. One of the first interpretations of beta oscillations linked this rhythm to neural processes which promoted cortical idling (Pfurtscheller et al., 1996). This view was further expanded by Engel and Fries (2010), which proposed a role for beta in preserving the ongoing sensorimotor set, or “status quo”. The authors suggested that increased beta synchrony in a neural population reduced the responsiveness of that same population to incoming information, promoting *de facto* the current state. Supporting evidence comes from studies where impaired beta oscillations are linked with abnormally strong inhibition of behavioural and cognitive performance (Brown, 2006; Little and Brown, 2014; Rossiter, Boudrias, and Ward, 2014).

Motor inhibition is typically measured using the stop-signal paradigm (Logan et al., 1984). During the task, participants respond to a GO signal by initiating an action. In a minority of trials, they have to try to cancel that response following a salient STOP signal. Unlike the latency of motor responses, i.e. reaction time, response-inhibition latency cannot be observed directly. The stop-signal task is unique in allowing the estima-

tion of this covert latency, referred to as stop signal reaction times (SSRT), by modelling response-inhibition as an independent race between a GO and STOP runner (for more details see Logan et al., 1984; Verbruggen et al., 2019). Numerous studies employing the stop-signal task have consistently demonstrated that successful response inhibition relies on various cortical nodes within the frontal cortex (Schaum et al., 2021; Wessel and Aron, 2017). Specifically, two regions, namely the inferior frontal gyrus (IFG) and the pre-supplementary motor area (pre-SMA) have been identified as key candidates in the process of action-stopping. Lesions or temporary disruption via brain stimulation in these regions have provided evidence supporting their crucial roles (Aaron et al., 2003; Cai et al., 2012; Chambers et al., 2007; Flooded and Stuss, 2006). Additionally, rapid cancellation of movements has been associated with beta power increases in these nodes (C. Allen et al., 2018; Castiglione et al., 2019; Jana et al., 2020; Schaum et al., 2021; Wagner et al., 2018). A beta band power increase was also observed in the basal ganglia during stopping (N. J. Ray et al., 2012; Zavala et al., 2015; Wessel et al., 2016), perhaps underpinning a broad cortical/sub-cortical network for inhibitory control (Aron et al., 2016). Therefore, instead of being a proxy for the level of activity of the sensorimotor network, beta oscillations could act as a top-down inhibitory rhythm during motor and cognitive tasks.

Recent studies have described a higher incidence of beta-bursts recorded over medial frontal cortex with EEG (Jana et al., 2020; Wessel, 2020), further supporting the notion that beta oscillations are a valid proxy of inhibition. However, a study in macaque monkeys from Errington et al. (2020), revealed that beta bursts were neither necessary or sufficient for stopping (too infrequent) and were also observed during trials where a response was generated. This is in stark contrast from the spiking rates of neurons causally involved in movement initiation and inhibition, where a drop in accumulation discharge is observable before the SSRT (Middlebrooks et al., 2020).

The current study aims to test the role of beta oscillations during action-stopping. In particular, we focused on which beta dynamics could act as proxy of inhibition in the sensorimotor system. According to the rich literature described above, we extracted time-courses from IFG, pre-SMA and M1. We employed a joystick version of the stop-signal paradigm in combination with high temporal resolution MEG recordings. We focused

on beta during three distinct time-windows: pre-movement, post-movement and during action-stopping. Our study did not return supporting evidence for a key role of beta in inhibition for all ROIs, a finding which is in open contrast with the existing literature. This calls for an in-depth analysis of how well the role of beta during stopping is generalisable across tasks and analyses methods.

3.2 Material and methods

3.2.1 Participants

22 healthy participants participated in the MEG experiment. One participant had to be excluded due to the presence of artefacts during data collection. Three participants had to be excluded because it was not possible to acquire an MR image. All of the remaining 18 participants (9 women; mean age \pm SD, 25 ± 3 years) had a normal or corrected-to-normal vision. All individual participants included in the study were screened for factors contradicting MRI and MEG scanning and provided written informed consent before participation and consent to publish any research findings based on their provided data in anonymized form. Participants were financially compensated for their time.

3.2.2 Experimental setup

The stop-signal task followed the guidelines outlined in Verbuggen et al. (2019). The task was collected on the same day as the motor adaptation task described in **Chapter 2**. Half of the participants performed the action-stopping task first and then adaptation, the order was counter-balanced for the remaining participants. Participants were seated in the MEG scanner in front of a computer monitor at 120 cm from the screen, while they held a finger-joystick with their right hand, which was rested on a padded arm support. Participants performed an out-and-back aiming task by moving the joystick to match a cursor with a target during two conditions (**Figure 3.1**). The cursor, which is the visual feedback of the position of the joystick, was displayed on the computer monitor in the form of a white circle that was 1.3 cm (1.2 visual degrees) in diameter. The target was a green circle (GO cue, 6 mm diameter) displayed on the screen. Each trial started with an empty circle at the centre of the monitor which stayed in position for 750 ms. Then the empty circle was substituted by the joystick cursor (white). After 1.5 s the target (green) appeared at one of five possible positions equally spaced around an invisible half-circle in the upper portion of the screen with a radius of 7.5 cm (6.1 visual degrees). The target remained at its new position for 750 ms before both cursor and target were removed and

the empty circle was displayed for a further 1.75-2 s (uniformly distributed) before the next trial began. This summed up to a total inter-trial interval ranging from 4.75 s to 5 s. On a minority of trials ($n = 100$), the green target would turn to red (STOP cue) after a variable stop-signal delay (SSD). The SSD was initially set at 200 ms after the green target onset, and then continuously adjusted (in steps of 50 ms) via a standard adaptive tracking procedure: SSD increased after each successful stop and decreased after each unsuccessful stop (Verbruggen et al., 2019). The SSD was limited between a minimum of 50 ms and 750 ms, the maximum permitted reaction time. This procedure converged on a ~50% probability of stopping to the STOP cue.

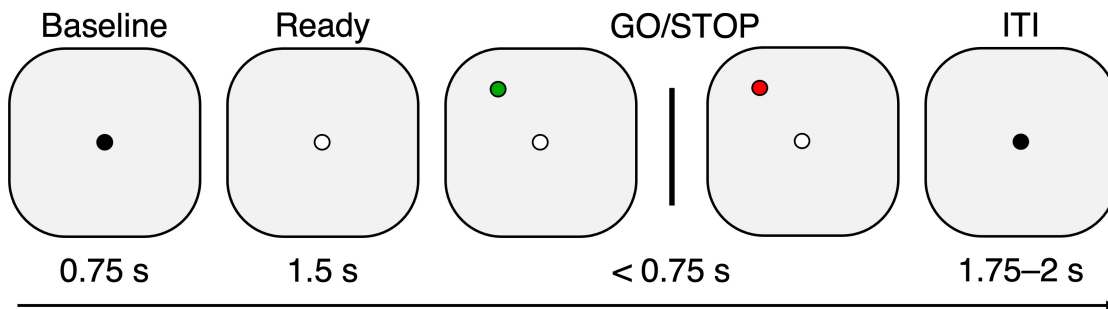


Figure 3.1: Experimental protocol

Participants performed an aiming task while controlling a joystick with their right hand. A typical trial, consisted in a "baseline" period during which participant were instructed to remain still and fix an empty circle for 750 ms. This stage was followed by a "ready" period of 1.5 s, where the joystick white cursor was displayed. Then, in the GO period a green target was displayed for a maximum time of 750 ms in one of 5 possible locations in the upper-half of the screen. On some trials, the green target turned red after a variable SSD. When this happened, participants were instructed to refrain from moving. The trial ended by displaying the same empty circle showed during "baseline" for 1.75-2 s.

Participants were instructed to move the joystick when the GO cue appeared so as to shift the white cursor from the central start position to match the position of the green target with a rapid, discrete and straight movement. Participants were informed about the presence of STOP trials and to refrain completely from moving when the STOP cue appeared. They were also informed that by design, they were expected to successfully stop only half of the time. If the participants initialised a movement and then successively stopped, that was considered an unsuccessful stopping/inhibition. The position of the

white cursor was presented at rest and when the displacement of the joystick crossed 80% of the distance between the target and the starting point. The participants were explicitly told that the position of the feedback cursor would not respond to any later corrective movements and would return to the centre when the joystick position came back to the centre. After familiarisation with the task, each subject completed a session of 310 trials with 210 GO trials and 100 STOP trials. STOP trial order was randomised. During the session, the experiment was paused two times. During the break, three task statistics were displayed on the screen: the inhibition rate, the number of GO omissions and the average reaction time. Participants were reminded to keep the number of omissions close to zero, additionally, they were reminded that the experiment was programmed to elicit a successful inhibition on 50% of the STOP trials. If the percentage was too low or too high, participants were informed to adjust their performance.

3.2.3 Behavioural analysis

Behavioural analyses were carried with custom scripts in Python. Joystick cursor displacement was differentiated to calculate velocity and subsequently low-pass filtered through a Gaussian kernel to smooth the signal. Movement initiation was defined as the time when the joystick velocity crossed a threshold (computed as mean trial activity plus the trial standard deviation) and sustained this speed for at least 50 ms. Movement termination was the last time point the joystick velocity fell below the threshold for that trial. Reaction times - RT (interval between stimulus onset and movement initiation), and movement duration (interval between movement initiation and movement termination) were calculated for each individual trial and then averaged within-subjects across three trial types: GO trials, successful stop (sSTOP) and unsuccessful stop (uSTOP) trials. An estimate of covert behavioural response inhibition was approximated with the stop-signal reaction time (SSRT), which was calculated via the integration method with the replacement of GO omissions (Verbruggen et al., 2019). In short, in the integration method, SSRT was estimated by finding the point at which the integral over the RT distribution equals the actual probability of responding during STOP trials. The integration approximately corresponds

to the n th RT of the distribution of GO trials. This is achieved by multiplying the total number of RTs in the distribution by the actual probability of responding. For example, if there are 200 GO trials and the overall probability of responding is 0.45, then the n th RT is the 90th fastest GO RT. SSRT can then be estimated by subtracting the mean SSD from the n th RT. To determine the n th RT, all go trials with a response are included (including go trials with a choice error and go trials with a premature response). GO omissions are assigned the maximum RT in order to compensate for the lacking response.

Participants were excluded from further analyses if their inhibition rate was $< 25\%$ or $> 75\%$ and if the GO omission rate was higher than 15%. According to these criteria, three participants were excluded.

3.2.4 MEG acquisition and preprocessing

MEG signals were recorded using a CTF Omega 275-channel whole-head axial gradiometer system. The signals were recorded at a sampling rate of 1200 Hz. Fiducial coils were placed at fixed distances from three anatomical landmarks (nasion, left, and right pre-auricular) and the positions of the coils were monitored continuously throughout the session. For co-registration, these landmarks were later identified on the subjects' structural MRI. The MEG data were acquired continuously and epoched offline. All analyses were performed in MATLAB (MathWorks Inc, Natick, MA), mainly using the FieldTrip toolbox (Oostenveld et al., 2011) and custom scripts. MEG signals were first high-pass and low-pass filtered at 0.5 Hz and 150 Hz respectively. Spectral interpolation was used to remove power-line contamination and harmonics (Leske and Dalal, 2019). Data trials including large muscle artefacts were identified via a semi-automatic procedure. Trials were band-pass filtered between 110-140 Hz, z-transformed and compared against a threshold. Trials with values above the cut-off were visually inspected before exclusion. Eye movements and cardiac artefacts were projected out of the data using independent component analysis (Makeig et al., 1995). Finally, MEG signals were down-sampled to 300 Hz. Data were epoched according to four different scenarios. Stimulus-locked data were aligned from -2 s to 2 s around the GO cue (green target display). Response-locked data

were aligned from -2 s to 2 s around the start of the movement. Offset-locked data were aligned from -2 s to 1.5 s around the end of the movement. Finally, SSD-locked data were aligned from -2 s to 2 s around the SSD.

3.2.5 Source imaging

For source localisation, each participant's anatomical MRI was divided into an irregular grid by warping the individual MRI to the MNI template brain and then applying the inverse transformation matrix to the regular MNI template grid (4mm isotropic voxel resolution), allowing source estimates at brain locations directly comparable across participants. For each grid location inside the brain, the forward model (i.e. the lead field) was calculated for a single dipole orientation by singular value decomposition, using a single-shell volume conduction model (Nolte, 2003). Since all grid locations of each subject were aligned to the same anatomical brain compartments of the template, corresponding brain locations could be statistically compared over all subjects. Source power at each location was estimated using an LCMV (linearly constrained minimum variance) beamformer (Van Veen et al., 1997), available in FieldTrip. Beamformer analysis uses an adaptive spatial filter to estimate the power at every specific (grid) location of the brain. Virtual time courses were reconstructed for a set of cortical ROIs: primary motor cortex (M1), primary somatosensory cortex (S1), inferior frontal gyrus (IFG) and pre-supplementary motor cortex (pre-SMA). A priori ROIs selection was based on the action-stopping literature (Jana et al., 2020). ROI masks were constructed, for the left and right hemispheres, using the Harvard-Oxford atlas in FSL (Makris et al., 2005). Then, masks were thresholded to 35%, binarized and interpolated with MNI coordinates. For each participant and each ROI, a single virtual channel was extracted following a multi-step procedure. First, beamforming spatial filter weights were computed using a covariance matrix calculated by combining trials from the broadband data. The filter weights were used to reconstruct the single-trial time series for each source in the ROI. Then, power spectra (PSD) were computed for each time series with Matlab Welch's method. Next, the FOOOF toolbox (Donoghue et al., 2020) was used to quantify periodic (oscillatory) activity in the beta (15-30 Hz) range.

In short, the toolbox conceptualises the PSD as a combination of an aperiodic component with overlying periodic components (oscillations). These putative oscillatory components of the PSD are characterised as frequency regions of power over and above the aperiodic component. Only voxels that showed a peak in the beta range were selected for the next step. Finally, the virtual time-series with maximum standard deviation was selected as the target virtual channel for that ROI.

3.2.6 TFRs on virtual channel time courses

Preprocessed MEG signals were decomposed into their time-frequency representations (TFRs) in the 8–40 Hz range using an Hanning taper with a sliding time window of 7 cycles. MEG power change was subsequently normalised as the percentage change relative to the overall average by dividing the power at each frequency and each time point by the average power of that frequency across the whole experimental session (Tan et al., 2016; Torrecillos et al., 2015). Values >0 indicated power higher than the overall average power of that frequency and vice versa. Beta desynchronisation and PMBR were calculated for each participant trial before averaging for further analysis. Beta desynchronisation was defined as the average normalised power over a 200 ms window centred on the trough of power change in the period that goes from -0.5 to 0 s before movement onset. The same procedure was also applied to PMBR, with the difference that the window was centred on the positive peak in a time period from 0 to 0.8 s after movement offset. Beta power was also analysed for a period of time from 0 to .3 s (max SSRT) after SSD to test for the dynamics of beta during action-stopping.

3.2.7 Beta burst analysis

Beta bursts computation followed the pipeline described in Rayson et al., (2022). In short, PSD was computed for each virtual channel time-series with Matlab Welch's method and then *log*-scaled. A $1/f$ function was fitted to the spectrum and frequency bands were identified using the residuals of this fit, which represent the periodic component of the spectrum. Band peak frequencies were identified as local maxima, while the bandwidth

was set to 6 Hz (± 3 Hz around the peak). Next, the amplitude threshold (standard deviations above the median) for identifying beta bursts was estimated for all participants and ROIs. The data is first band-pass filtered around the peak frequencies determined above, and then the amplitude envelope is extracted after applying the Hilbert transform to the filtered data. In order to avoid filter-related edge artefacts, the data are padded using the DC offset before applying the filter and Hilbert transform. This padding is then removed from the resulting amplitude envelope. The empirically-derived relative threshold on beta amplitude is used to identify bursts and is computed based on multiple standard deviations above the median beta amplitude (Eq. 3.1), with the median representing a robust measure of centrality for skewed distributions.

$$threshold = med(A) + s(A) \times k \quad (3.1)$$

where:

A = Hilbert envelope

k = range of values $\{0.1, 0.2, \dots, 3\}$

med = median

s = standard deviation

For each subject, the non-parametric correlation (Spearman's ρ) was computed between the number of bursts per trial (number of threshold crossings) and the mean amplitude per trial. This is done using a range of thresholds computed from the median and standard deviation of beta amplitude in all time points across all trials for that subject. The standard deviation multiple that maximises the mean of this correlation was selected. For M1, this resulted in a threshold of 1.6 SD above the median. The times at which beta amplitude crossed the subject-specific threshold and then returned below the threshold were found. The difference between these two time points gives the duration of the burst, and from within these, burst onset and offset times, peak amplitude, and the time at which this peak is reached were identified.

To compare the burst rate to beta amplitude, the amplitude and a smoothed measure of burst rate were normalised. The amplitude was baseline corrected by subtracting the

mean amplitude over the whole experiment. The burst rate was obtained by binning the burst event timings using 10 ms bins, smoothing using a two-pass Gaussian convolution with a width of 25 bins, and then baseline correcting by subtracting the mean burst rate over the whole experiment.

3.2.8 Statistical analysis

Repeated-measures ANOVAs were used to investigate the effects of trial execution order (ie, averages of trials 1–20, 81–100, etc) and experimental phases. Mauchly's test of sphericity was used to test the homogeneity of variance. Where Mauchly's test of sphericity was significant ($p < 0.05$) in repeated-measures ANOVAs, Greenhouse-Geisser corrections were applied. Two-tailed paired-sample t tests were calculated for *Post hoc* analyses, using Bonferroni correction for multiple comparisons. Mean \pm SE are presented throughout the text unless otherwise specified. Effect sizes were calculated using Cohen's d , calculated as the difference between the two means, divided by the standard deviation of the difference. 95% confidence intervals (95% CI) were calculated using accelerated bias-corrected percentile limits (number of bootstrap samples = 10000).

3.3 Results

3.3.1 Behavioural performance

Healthy participants ($n = 18$) performed a joystick stop-signal task. Three participants were excluded from further analysis according to behavioural exclusion criteria. Two participants showed a high omission rate ($> 15\%$) while one participant had an inhibition rate lower than 25%. Participants were instructed to respond with a reaching movement when they saw a GO cue, and then to try to inhibit or continue their already initiated GO response. The mean SSD was 248 ± 70 ms (mean \pm SD) and led to an average probability of responding on a STOP trial of 50% proving the adherence of participants to the task rules and the successful operation of the staircase procedure. While for sSTOP trials the mean SSD was 223 ± 68 ms, it was 274 ± 70 ms for uSTOP trials. A repeated-measures ANOVA based on RT revealed a main effect of condition (GO vs uSTOP, $F_{(1,17)} = 117.19$, $p < 0.001$), with shorter RT in uSTOP trials (443 ± 58 ms, mean \pm SD) as compared to GO trials (491 ± 55 ms) (**Figure 3.2**). Participants performed accurately as indicated by low omission error rates in GO trials with an average omission of 3%. SSRT was calculated using the integration method, resulting in a median SSRT of 235 ± 33 ms. The maximal SSRT across participants (SSRTmax) was 300 ms.

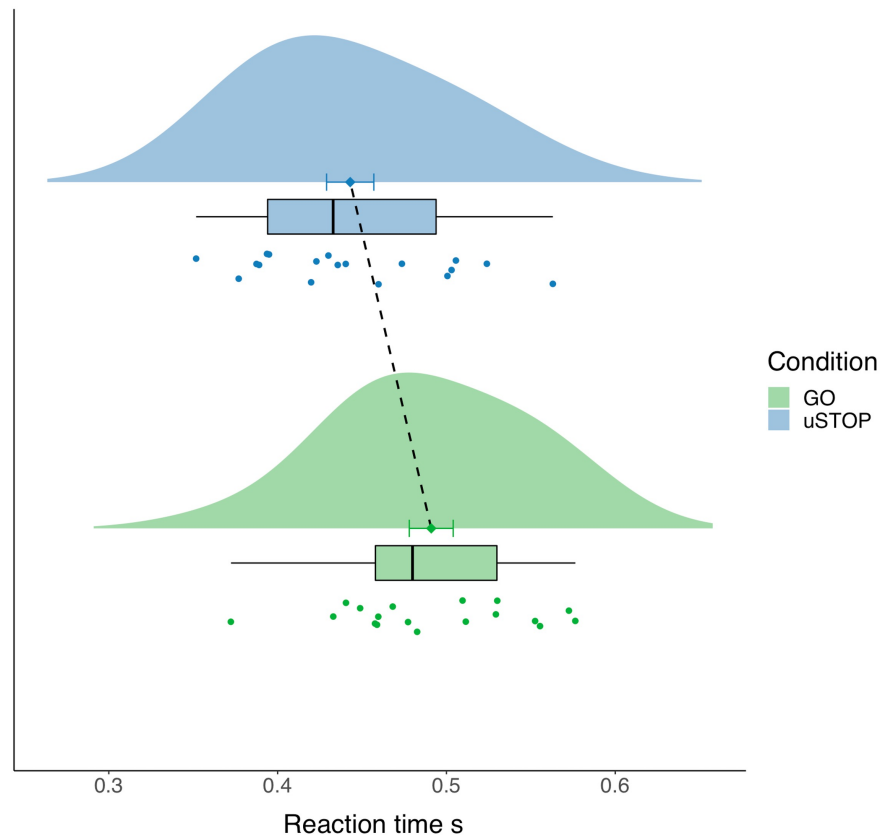


Figure 3.2: Reaction time between conditions

Plots of RT during GO and uSTOP trials. Each raincloud plot (M. Allen et al., 2019) is composed of individual participant scores (**coloured points**), *boxplot*, data distribution (**coloured curve**) and mean with standard error (**coloured diamond point and error bars**). The x-axis reflects the reaction time, expressed in seconds. Trial conditions are colour-coded (**light-green, GO; light-blue, uSTOP**)

3.3.2 Beta desynchronisation and rebound dynamics

To test for the role of beta in action inhibition, we focused on averaged beta power dynamics. First, we inspected canonical beta desynchronisation and rebound. Although these effects were more pronounced for M1 and S1, we observed similar dynamics during all three conditions and across the rest of the ROIs (**Figure 3.3**). Beta desynchronisation and rebound are classically linked to the preparation and completion of a movement. Since only GO and uSTOP trials contain a complete movement, we restricted the following analysis to these two conditions. A repeated-measures ANOVA with factors of condition (GO, uSTOP) on beta desynchronisation was independently applied to each ROI. The analysis did not return any significant effect (**Figure 3.4**, for more details see **Table B.1** in **Appendix B**). The same analysis was applied to the post-movement beta rebound which revealed a significant main effect for rIFG only ($F_{(1,14)} = 7.96, p = 0.014$), with beta rebound decreasing in the uSTOP condition compared to GO trials (**Figure 3.5**). A similar trend was also observable for the other ROIs, although it did not reach significance (see **Table B.2**). We also analysed the timing of beta desynchronisation and rebound across ROIs (**Figure 3.6**). A two-way repeated measures ANOVA with factors of condition ($n = 2$) and ROIs ($n = 5$) on peak timings of beta desynchronisation revealed a main effect of ROI ($F_{(4,56)} = 5.25, p = 0.001$). *Post-hoc* tests revealed that the beta desynchronisation started earlier in left and right pre-SMA compared to IM1 (lpre-SMA vs IM1, 23 ± 24 ms, $t_{(29)} = 3.53, p = 0.014, d = 0.65, 95\% \text{ CI } [0.3, 0.93]$; rpre-SMA vs IM1, 20 ± 26 ms, $t_{(29)} = 3.25, p = 0.03, d = 0.6, 95\% \text{ CI } [0.25, 0.9]$) (**Figure 3.6A**). The results from the same ANOVA applied to the beta rebound peak time also returned a main effect of ROI ($F_{(4,56)} = 10.04, p < 0.001$). *Post-hoc* comparisons revealed that beta rebound peaked earlier in rIFG and left/right pre-SMA compared to both M1 and S1 (**Figure 3.6B**; for a summary see **Table 3.1**). These results confirm that beta desynchronisation and rebound are widespread phenomena across the cortex. Furthermore, beta rebound data suggest an influence of trial types on its dynamics and a frontoparietal spread across time.

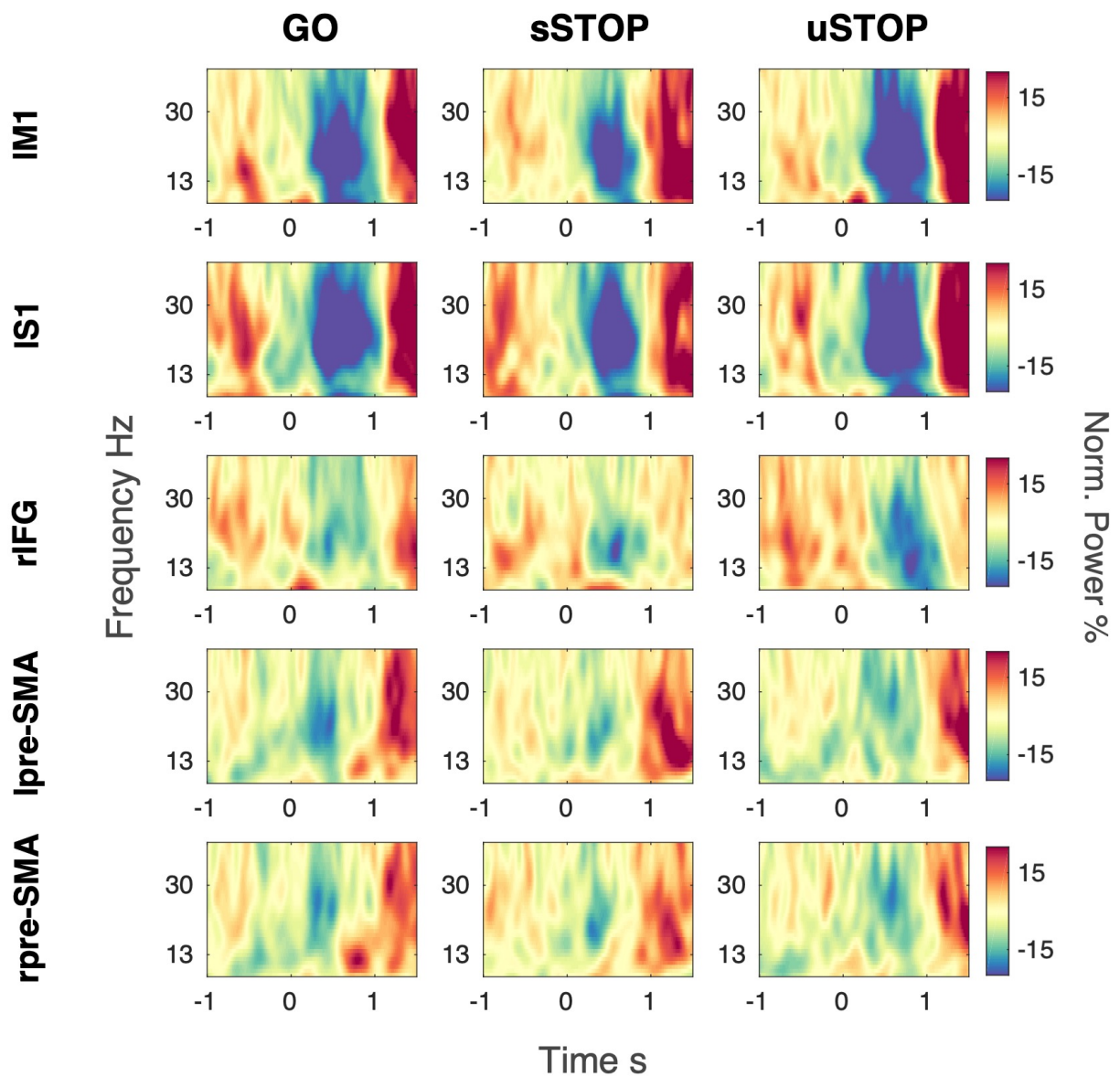


Figure 3.3: Stimulus-locked TFRs across ROIs and conditions

Normalised TFRs aligned to the GO cue onset ($t = 0$). Each column shows TFRs dynamics during a single condition (*left - GO; middle - sSTOP; right - uSTOP*). Each row shows results for a single ROI. Anatomical regions: IM1 - left primary motor cortex; IS1 - left somatosensory cortex; rIFG - right inferior frontal gyrus; lpre-SMA - left pre-supplementary motor cortex; rpre-SMA - right pre-supplementary motor cortex.

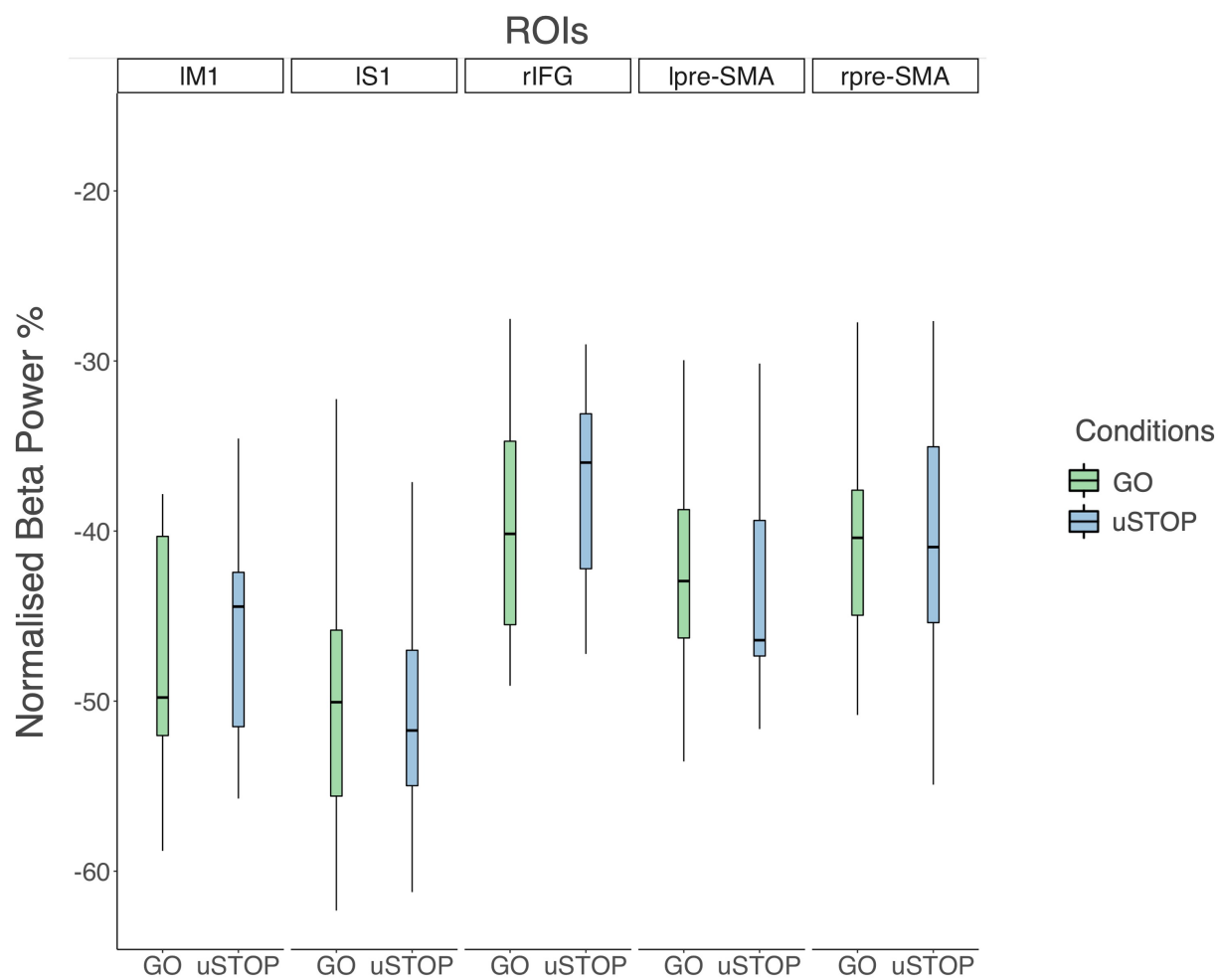


Figure 3.4: Beta desynchronisation during GO and uSTOP trials

Boxplots showing the magnitude of peak beta desynchronisation across participants during GO and uSTOP conditions. *light green* - GO; *light blue* - uSTOP. Anatomical regions: IM1 - left primary motor cortex; IS1 - left somatosensory cortex; rIFG - right inferior frontal gyrus; lpre-SMA - left pre-supplementary motor cortex; rpre-SMA - right pre-supplementary motor cortex.

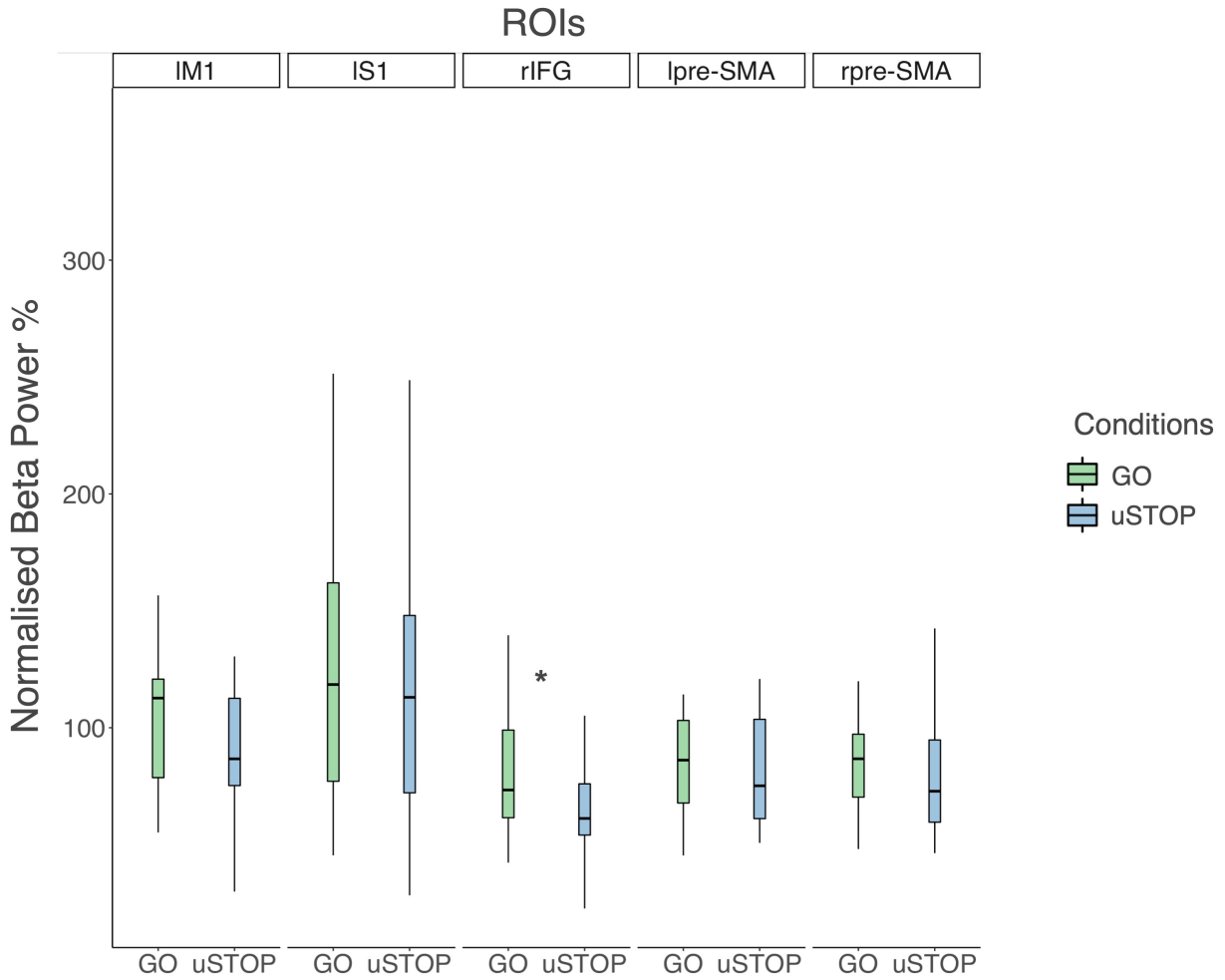


Figure 3.5: PMBR during GO and uSTOP trials

Boxplots showing the magnitude of peak beta rebound across participants during GO and uSTOP conditions. Significant effects ($p < 0.05$) are marked by the * symbol. *light green* - GO; *light blue* - uSTOP. Anatomical regions: IM1 - left primary motor cortex; IS1 - left somatosensory cortex; rIFG - right inferior frontal gyrus; lpre-SMA - left pre-supplementary motor cortex; rpre-SMA - right pre-supplementary motor cortex.

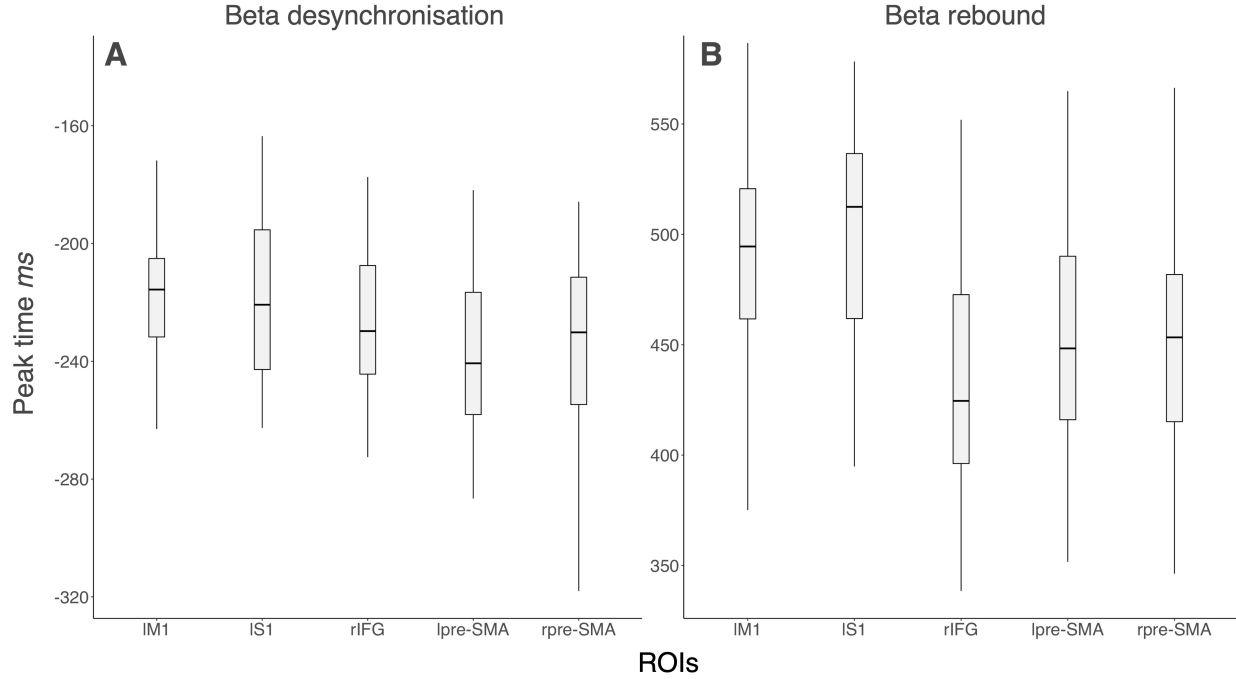


Figure 3.6: Beta peak timing

(A) Boxplots showing averaged beta desynchronisation peak timing across participants and ROIs. Peak time is expressed in *ms* before movement onset. (B) PMBR peak time. Peak time is expressed in *ms* after movement offset. Anatomical regions: IM1 - left primary motor cortex; IS1 - left somatosensory cortex; rIFG - right inferior frontal gyrus; lpre-SMA - left pre-supplementary motor cortex; rpre-SMA - right pre-supplementary motor cortex.

Table 3.1: Post-hoc results for PMBR peak time across ROIs

	<i>IM1</i>			<i>IS1</i>		
	<i>rIFG</i>	<i>lpre-SMA</i>	<i>rpre-SMA</i>	<i>rIFG</i>	<i>lpre-SMA</i>	<i>rpre-SMA</i>
<i>mean diff. (ms)</i>	51	37	41	63	49	53
<i>sd</i>	47	32	46	58	49	60
<i>t</i>	5.06	4.23	3.91	5.57	4.72	4.29
<i>Cohen's d</i>	0.92	0.77	0.72	1.02	0.86	0.78
<i>95% CI</i>	[0.48 1.33]	[0.41 1.13]	[0.34 1.1]	[0.44 1.71]	[0.42 1.34]	[0.38 1.22]

3.3.3 Beta power during stopping

Next, we inspected the role of beta during stopping. We analysed the temporal development of beta-band power across the ROIs by contrasting normalised sSTOP with uSTOP trials (**Figure 3.7**). For each ROIs, although the sSTOP condition had more power than the uSTOP, the cluster-permutation test, for a time window of 300 ms ranging from the STOP cue onset to the maximum SSRT, did not reveal any cluster differences between sSTOP and uSTOP conditions.

We then decided to further explore beta's role during stopping by to look at beta bursts. Due to their well-documented role in the stopping literature, we targeted rIFG and pre-SMA by contrasting a number of burst features between the sSTOP and uSTOP conditions during the stopping time window (from the STOP cue to the max SSRT). Instead of inspecting a broad beta range, we restricted the analysis to beta band peak frequencies (for details see Methods). This resulted in a beta range of 18-24 Hz, 17-23 Hz and 18-24 Hz for rIFG, lpre-SMA and rpre-SMA respectively. We ran a paired-*t*-test on burst-amplitude, burst-duration and burst-count independently for each ROI contrasting sSTOP vs uSTOP conditions (see **Table 3.2**, **Table 3.3**, **Table 3.4**). No significant effects were found after adjusting for multiple comparisons. These results fail to return supporting evidence towards a clear role of beta oscillations as a proxy for inhibition, particularly for frontal nodes like IFG and pre-SMA.

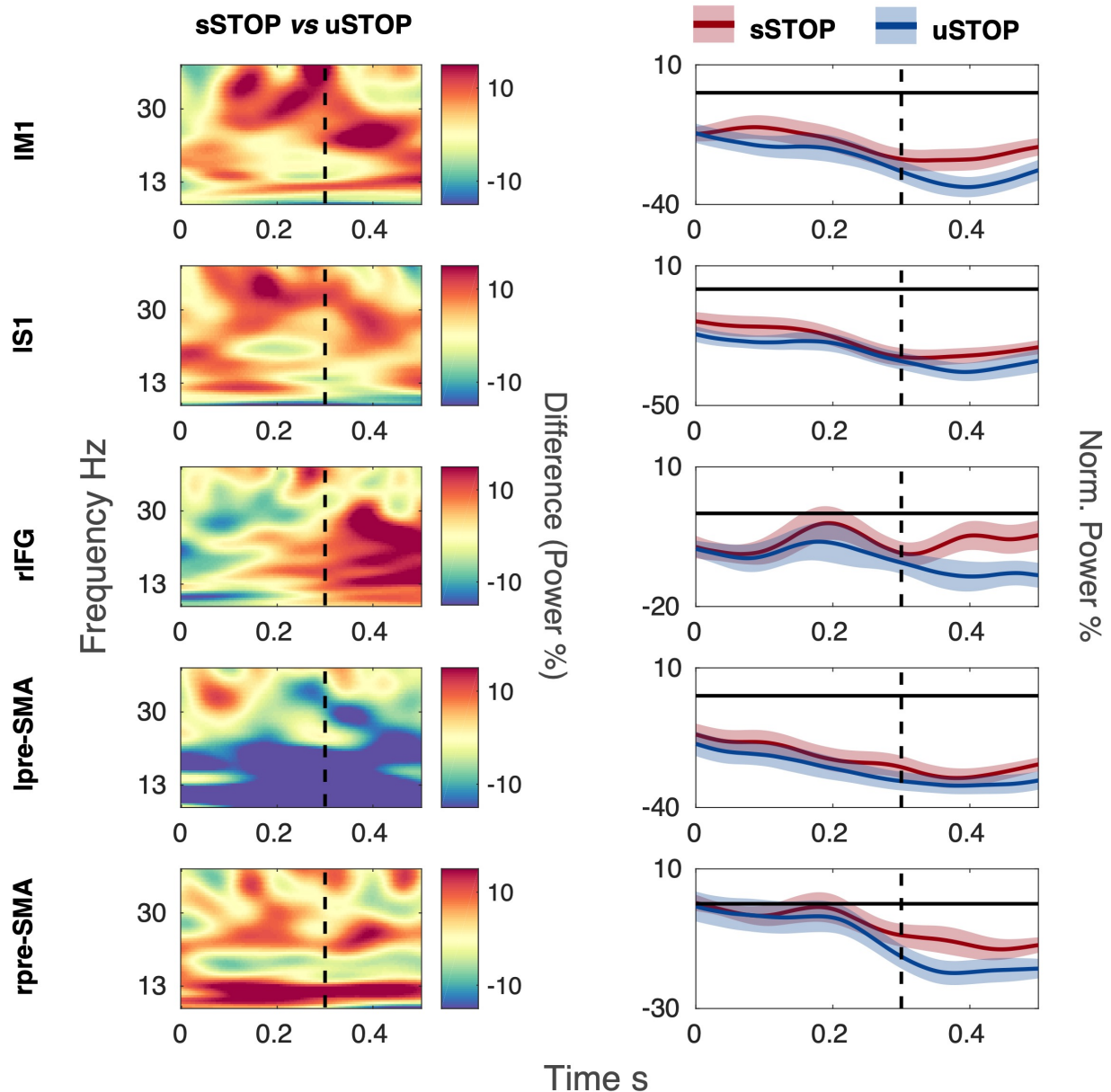


Figure 3.7: Beta power during sSTOP and uSTOP trials

(left) TFRs contrast between sSTOP and uSTOP conditions. Brighter colours signal that sSTOP trials had more power compared to uSTOP, darker colours reflect more power in the uSTOP condition. (right) Coloured solid line and shaded area represent average beta power across participants and SE respectively. *x*-axis shows time, ranging from 0 up to 500 ms after the stop-cue onset; **dashed dark vertical line** marks max SSRT ($t = 300$ ms); **dark horizontal line** marks when baseline-corrected beta power equals 0. Each row shows results for a single ROI. Anatomical regions: IM1 - left primary motor cortex; IS1 - left somatosensory cortex; rIFG - right inferior frontal gyrus; lpre-SMA - left pre-supplementary motor cortex; rpre-SMA - right pre-supplementary motor cortex.

Table 3.2: Paired *t*-test results for burst-amplitude during stopping

<i>Unit = Power %</i>	<i>Burst-amplitude</i>			
	<i>sSTOP vs uSTOP</i>	<i>rIFG</i>	<i>lpre-SMA</i>	<i>rpre-SMA</i>
<i>mean diff.</i>		-2	3.21	1.72
<i>sd</i>		14.8	11.6	10.7
<i>t</i>		-0.52	-1.07	0.62
<i>Cohen's d</i>		-0.14	-0.28	0.16
<i>95% CI</i>		[-0.66 0.43]	[-1.06 0.3]	[-0.42 0.67]

Table 3.3: Paired *t*-test results for burst- duration during stopping

<i>Unit = Duration ms</i>	<i>Burst-duration</i>			
	<i>sSTOP vs uSTOP</i>	<i>rIFG</i>	<i>lpre-SMA</i>	<i>rpre-SMA</i>
<i>mean diff.</i>		0*	0*	0*
<i>sd</i>		0.04	0.03	0.03
<i>t</i>		0.67	-0.81	-0.13
<i>Cohen's d</i>		0.17	-0.21	-0.03
<i>95% CI</i>		[-0.41 0.73]	[-0.85 0.35]	[-0.6 0.53]

* difference <10 ms

Table 3.4: Paired *t*-test results for burst-count during stopping

<i>Unit = N</i>	<i>Burst-count</i>			
	<i>sSTOP vs uSTOP</i>	<i>rIFG</i>	<i>lpre-SMA</i>	<i>rpre-SMA</i>
<i>mean diff.</i>		2	-2	-1
<i>sd</i>		5	3	4
<i>t</i>		1.46	-2.38	-1
<i>Cohen's d</i>		0.38	-0.62	-0.29
<i>95% CI</i>		[-0.22 1.01]	[-1.11 0]	[-0.8 0.3]

3.4 Discussion

In this chapter, we explored the role of beta oscillations in a stop-signal task. In our study, we could not find supporting evidence for the notion that increased beta power, particularly in frontal nodes, is key for movement inhibition. This finding is at odds with many studies in the action-stopping literature, where there is consistent evidence that response inhibition crucially depends on IFG and pre-SMA (Wessel and Aron, 2017).

ECoG studies reported increased beta power in frontal electrodes during successful stopping within 100-250 ms after the stop signal (N. Swann et al., 2009; Wessel et al., 2013). A similar pattern has also been shown in several EEG and MEG studies (Castiglione et al., 2019; Jana et al., 2020; Schaum et al., 2021; Wagner et al., 2018; Wessel, 2020). There may be several reasons for the diverse findings in our study which can be ascribed to methodological differences. First, previous studies employed standard two-choice reaction time tasks where participants responded to the GO cue by pressing a button. In our study, instead, participants were required to perform a multi-choice reaching movement with a finger joystick. Although our task was more challenging, from both a motor and visual perspective, the stop process was correctly achieved. As outlined in the guidelines for the stop-signal task (Verbruggen et al., 2019), we implemented a salient STOP cue and an adaptive tracking procedure for the SSD. This resulted in a probability of responding close to 50% while also having a low number of GO omissions. Another task difference pertained to the ratio of GO and STOP trials. In our study, 33% of the trials had a STOP cue. Interestingly, in Wagner et al. (2018) participants performed three versions of the stop-signal paradigm with varying task features, one of which was the STOP ratio. While the authors reported the canonical frontal increase in the beta band at 25% STOP ratio they failed to do so at 33%. One interpretation of this finding could be that participants might have been biased to use a different strategy to perform the task, like a waiting strategy, since the number of STOP trials was more recurrent. This interpretation is highly speculative and not necessarily supported by our behavioural data, since we reported low GO omissions and RTs in line with previous stop-signal studies. Finally, an additional difference relates to frontal node localisation. Previous studies have either

used intracranial recordings (N. Swann et al., 2009; Wessel et al., 2013) or implemented independent component analysis (ICA) to localise the frontal source of action-stopping (Castiglione et al., 2019; Wagner et al., 2018). We opted for seed-based analyses which rely on a priori-defined coordinate from an anatomical atlas. It has to be noted that a data-driven approach (i.e. source contrasting) could be generally preferred (Gross et al., 2013), however, there is a strong consensus in the field about stopping source locations, ranging from animal to fMRI studies (for a review see Wessel and Aron, 2017).

It is noteworthy that findings from a recent study returned a more complex picture of the role of beta during stopping which partially aligns with our data (Schaum et al., 2021). Schaum et al. reported a stronger increase in beta power during stopping, particularly in rIFG. Similarly, we noticed in our study an increased beta power during sSTOP vs uSTOP trials in different cortical nodes. Furthermore, the authors reported that IFG beta-band power, which started to increase shortly after the STOP signal, was not strong enough such that beta power was increased above baseline (see **Figure 3.7**). Immediately after the GO cue, we observed beta desynchronisation across multiple ROIs. In the time frame that goes from the STOP signal to the SSRT, we showed a slowing or pausing of this motor-related beta dynamic during stopping. In our study, only rIFG and rpre-SMA showed this pattern of activity, with averaged beta-power briefly approaching baseline levels but only in the sSTOP condition. This poses some open questions about the frontal beta power increase. Can these phenomena be regarded as a distinct active stopping process - operated by IFG and pre-SMA - or it is related to the attenuation of other beta phenomena, like movement desynchronisation?

A recent bursts study also questioned the causal role of beta oscillations in action inhibition (Errington et al., 2020). The authors wanted to test the role of beta bursts during a saccade-countermanding task in monkeys. They found that monkeys exhibited a small but consistent pulse of beta activity over the medial-frontal cortex during movement inhibition, similar to other bursts studies (Jana et al., 2020; Wessel, 2020). The authors also noticed how infrequently these bursts occurred (~15% of trials) and how they were observable during trials where a response was generated. When observing the time course of beta-burst incidence across trials, it was not possible to differentiate between move-

ment initiation and inhibition. Conversely, the discharge rate of target movement-related neurons showed a clear separation between trial types occurring during the stopping time frame. Although these results do not preclude beta oscillations from still being implicated in action-stopping, they point towards a more indirect influence of this rhythm on motor inhibition.

Although our burst analysis yielded inconclusive results, it is important to consider certain key caveats. Our analysis primarily concentrated on comparing the average features of beta bursts across different conditions, while neglecting to account for their connection with single-trial RTs. Notably, there exists a significant causal relationship between RTs and motor inhibition. Two experimental conditions, specifically GO and uSTOP, exhibit distinct disparities in their respective RT distributions. Failure to acknowledge this distinction poses a challenge when interpreting the results, as beta effects could potentially be confounded by the influence of RTs.

Even though our study has several limitations as outlined above (namely low sample size, unusual task choice and less powerful source localisation strategy), it suggests a more cautionary interpretation of the role of beta oscillations in motor control. Beta-burst studies have shown how beta frequency is too inconsistent for accounting for the stopping behaviour. New studies employing revised beta-bursts pipeline have recently been described (Quinn et al., 2019; Seymour et al., 2022; Zich et al., 2022). Taking advantage of these novel analyses could help clarify if the weak link between single-trial beta dynamics and behavioural performance is due to poor sensitivity/SNR or if it is representative of an alternative interpretation of beta's "canonical" role in inhibition.

Chapter 4

The link between GABA and beta oscillations

4.1 Introduction

In this chapter, we turned our focus on the mechanisms responsible for the generation of beta oscillations. Animal and modelling studies provide evidence for an essential role of GABAergic interneuronal activity for the generation of beta oscillations in the sensorimotor cortex (Roopun et al., 2006; Whittington et al., 2000; Yamawaki et al., 2008). Several studies demonstrated an increase in human beta power (Hall et al., 2009, 2011; Jensen et al., 2005; Muthukumaraswamy, Myers, et al., 2013; Nutt et al., 2015) as a result of pharmacological GABAergic modulation. Such modulations of beta power were evident at rest (Hall et al., 2009; Jensen et al., 2005) as well as during/after movement (M. Baker and Baker, 2003; Muthukumaraswamy, Myers, et al., 2013; Nutt et al., 2015).

There is compelling evidence to suggest that a reduction in cortical inhibitory tone is critical for the induction of plasticity in the motor cortex (for a review, see Bachtiar and Stagg, 2014). A recent study using magnetic resonance spectroscopy observed a significant reduction of GABA concentration during motor learning (Kolasinski et al., 2019). The authors also reported that baseline GABA levels in M1 were strongly predictive of the degree of subsequent learning, suggesting that increased inhibition was linked with poorer

learning. Similar findings are observed for beta oscillations, where a reduction in beta power is consistently observed during movement (Engel and Fries, 2010). Furthermore, impaired beta oscillations, as observed in Parkinson's disease and following stroke, are highly correlated with the severity of motor disorders (Brown, 2006; Little and Brown, 2014).

The dominant approach to the analysis of neural rhythmic activity has been to consider power changes in canonical frequency bands. In the frequency domain, oscillations manifest as narrow-band peaks of power above the aperiodic component ($1/f$). When modulations of spectral power are observed, the implicit assumption is that frequency-specific changes have occurred. However, irregular and arrhythmic activity accounts for the majority of signal power recorded with LFP, EEG and MEG (B. J. He, 2014). A growing number of studies has recently highlighted the potential importance of arrhythmic/aperiodic activity underscoring its alteration in neuropsychiatric disorders (Bruining et al., 2020; Lai et al., 2010; Maxim et al., 2005; Molina et al., 2020; Robertson et al., 2019; M. Wei et al., 2013) and ageing (W. He et al., 2019; Schaworonkow and Voytek, 2021; Voytek et al., 2015). Furthermore, this activity can dynamically change during sleep (Freeman and Zhai, 2009; Lendner et al., 2020) and with exogenous stimuli and cognitive demands (Waschke et al., 2021). Pharmacology-EEG/MEG studies have reported broadband spectral changes of cortical power, suggesting that the effect could be attributed to the underlying modulation of $1/f$ activity (Muthukumaraswamy, Myers, et al., 2013; Nutt et al., 2015). According to this interpretation, recent pharmacological manipulations of GABA-A receptors have produced alterations of aperiodic activity (Muthukumaraswamy, Carhart-Harris, et al., 2013; Muthukumaraswamy and Liley, 2018; Robertson et al., 2019; Stock et al., 2020; Waschke et al., 2021). Oscillatory and non-oscillatory activities are likely to be generated by distinct neural mechanisms and play different functional roles, which strongly calls for the necessity to disentangle them.

In this project we studied the link between the GABA system and sensorimotor beta oscillations, combining MEG recordings and pharmacological interventions. We focused on the effect of gaboxadol and zolpidem during a finger abduction task. Although the two drugs both act as GABA-A positive allosteric modulators (PAM), they show highly

specific and distinct mechanisms of action. We separated neural activity, represented in the power spectra, into two major components: periodic (rhythmic) and aperiodic ($1/f$) neural activity. We showed how employing this parametrisation could be beneficial for testing the specific effects of drugs on several markers of neural activity.

4.2 Material and methods

4.2.1 Design and participants

Twelve healthy male participants (mean age 27.7, range 21-35) took part in a randomised, single-blind, placebo-controlled study comparing single doses of zolpidem and gaboxadol. The dataset was collected at Cardiff University Brain Research Imaging Center by Suresh Muthukumaraswamy. This was part of an unpublished project. Doses of 15 mg gaboxadol and 10 mg zolpidem were chosen. This was well-tolerated and showed comparable sedative properties (Hajak et al., 2009). The elimination half-lives of these two drugs were similar at approximately 1.5-2.0 h in fasting subjects. In this experiment it was originally intended to use a mixed-sex cohort, however early in data collection, it was found that all but one female became too heavily sedated to complete the protocol; therefore females were subsequently excluded during data collection. All participants were medically screened and excluded for significant medical, psychiatric or neurological conditions and current recreational or prescription drug use. They were tested before each session for drugs of abuse (urine screen) and breath alcohol. For each session, participants were scanned on separate days, after at least a seven-day washout period, at approximately the same time of day. On each day, an initial baseline MEG recording was obtained (PRE). Participants then orally ingested a capsule containing either a placebo, 15 mg of gaboxadol or 10 mg of zolpidem. Participants were blinded to the contents of the capsules and the placebo/control session order was counterbalanced across both experiments. MEG recordings were obtained at 60 (POST60) and 160 (POST160) min time points. Zolpidem was sourced from an NHS hospital pharmacy, and gaboxadol was donated by Lundbeck as part of the ECNP Medicines Chest Initiative (Nutt et al., 2014).

For each MEG recording, the participants performed 100 trials of a cued finger movement task, comparable to that described in Muthukumaraswamy (2010). The task was chosen because of its simplicity and the ability to effectively modulate beta power. The participants were required to perform ballistic abductions of the right-hand index finger to an auditory tone pip played through insert headphones (4.5 s ISI). The participants' index fingers were lightly attached to a piece of plastic to measure finger displacement.

To maintain a constant motor performance throughout the experiment the following feedback procedure was implemented. After the auditory pip (1.5 s), the participants received on-screen feedback with a "virtual ruler", indicating how far they had moved relative to a target movement criterion (10 mm). This feedback stayed on the screen for 1 s and then was replaced with a fixation cross. The participants quickly learned to move consistently on each trial and had training trials at the beginning of each day.

4.2.2 MEG acquisition and preprocessing

MEG signals were recorded using a whole-head system with a 275-channel CTF axial gradiometer. The signals were recorded at a sampling rate of 1200 Hz. Simultaneous EMG recordings were made from the participants' right first dorsal interosseus (FDI) and digitised with the MEG data. The participants' fingers were lightly attached to a small piece of plastic, attached to an optical displacement system. This device gave a one-dimensional measure of displacement (in the direction of index-finger abduction), which was also continuously sampled with the MEG. Fiducial coils were placed at fixed distances from three anatomical landmarks (nasion, left, and right pre-auricular) and the positions of the coils were monitored continuously throughout the session. Each participant had a 1 mm isotropic FSPGR MRI scan available for source localisation analysis. To achieve MRI/MEG co-registration, the fiducial markers were placed at fixed distances from anatomical landmarks identifiable in the participants' anatomical MRIs (tragus, eye centre). The MEG data were acquired continuously and epoched offline. All analyses were performed in MATLAB (MathWorks Inc, Natick, MA), mainly using the FieldTrip toolbox (Oostenveld et al., 2011) and custom scripts. MEG signals were first high-pass and low-pass filtered at 0.5 Hz and 150 Hz respectively. Spectral interpolation was used to remove power-line contamination and harmonics (Leske and Dalal, 2019). Data trials including large muscle artefacts were identified via a semi-automatic procedure. Trials were band-pass filtered between 110-140 Hz, z-transformed and compared against a threshold. Trials with values above the cut-off were visually inspected before exclusion. Eye movements and cardiac artefacts were projected out of the data using independent component analy-

sis (Makeig et al., 1995). Finally, MEG signals were down-sampled to 300 Hz. From the continuous MEG recordings, EMG onsets were marked using an automated algorithm that marked increases in the rectified EMG signal by 1.5 SD above the noise floor, subject to the constraint that they occurred within 750 ms of the tone pip. Data were epoched from -1.5 s to 1.5 s around the start (EMG onset) and the end (EMG offset) of the movement.

Gaboxadol recordings were not available for two participants, while three participants were excluded for zolpidem. Another participant was excluded due to a high number of faulty trials in all recordings, caused by a combination of muscle artefacts and poor performance. The number of participants available after preprocessing was 9 for gaboxadol, 8 for zolpidem and 11 for placebo. Trials were adjusted at the end of each recording so that each participant had an equal number of trials between sessions (PRE, POST60). Furthermore, pharmacological interventions were contrasted in pairs (gaboxadol vs placebo; zolpidem vs placebo; gaboxadol vs zolpidem). The number of participants tested was balanced to allow within-subject comparisons.

4.2.3 Source imaging

For source localisation, each participant's anatomical MRI was divided into an irregular grid by warping the individual MRI to the MNI template brain and then applying the inverse transformation matrix to the regular MNI template grid (4mm isotropic voxel resolution), allowing source estimates at brain locations directly comparable across participants. For each grid location inside the brain, the forward model (i.e. the lead field) was calculated for a single dipole orientation by singular value decomposition, using a single-shell volume conduction model (Nolte, 2003). Since all grid locations of each subject were aligned to the same anatomical brain compartments of the template, corresponding brain locations could be statistically compared over all subjects. Source power at each location was estimated using an LCMV (linearly constrained minimum variance) beamformer (Van Veen et al., 1997). Beamformer analysis uses an adaptive spatial filter to estimate the power at every specific (grid) location of the brain. Virtual time courses were reconstructed for a set of cortical ROIs. For each ROI, the virtual time courses with the largest

SD across time were selected as the target virtual channel for the ROI.

A data-driven pipeline was employed to extract relevant ROIs. Sources were reconstructed in the beta band for the placebo intervention, with a frequency domain beamformer source analysis performed by using the dynamic imaging of coherent sources algorithm (Gross et al., 2001). The spatial filter was constructed from the individual lead fields and the cross-spectral density (CSD) matrix for each subject. CSD matrices were computed for the task period ranging from 0 to 500 ms after the auditory tone and a baseline period of the same length, with an offset of -500 ms relative to the auditory tone. CSD matrices were computed in the beta band for 25 Hz (± 10 Hz) where spectral smoothing is indicated in brackets. CSD matrix calculation was performed with the multitaper method (Percival and Walden, 1993) using four Slepian tapers (Slepian, 1978). An activation-versus-baseline *t*-statistic was calculated at a single participant level by using an analytic dependent-samples within-trial *t*-test. The source *t*-values obtained were grouped in ROIs according to the AAL atlas in FieldTrip (Tzourio-Mazoyer et al., 2002). Then *t*-values were thresholded at $\alpha = 0.05$ and the proportion of significant sources for each ROI was computed. This process was repeated for both the PRE (no drug) and the POST60 sessions. The top 10% ROIs with the highest proportion of significant sources between the two sessions were selected for extracting virtual time courses. The ROIs list according to the AAL atlas was composed of Precentral cortex (M1), Postcentral cortex (S1), Paracentral Lobule (PL), Mid Cingulum (mC) and Supplementary motor area (SMA).

4.2.4 TFRs on virtual channel time courses

Preprocessed MEG signals were decomposed into their time-frequency representations (TFRs) in the 10-35 Hz range using a Hanning taper with a sliding time window of 7 cycles. MEG power change was subsequently normalised as the percentage change relative to the overall average by dividing the power at each frequency and each time point by the average power of that frequency across the whole experimental session (Tan et al., 2016; Torrecillos et al., 2015). Values >0 indicated power higher than the overall average power of that frequency and vice versa.

4.2.5 Statistical analysis

The pre-intervention baseline spectra (PRE) were subtracted from each post-intervention spectra (POST60) and then differences between interventions were tested at two different latencies: from -0.25 to 0.25 s around movement onset and from 0.3 to 1 s after movement offset. For this purpose we used a dependent-samples permutation *t*-test and a cluster-based correction method (Maris and Oostenveld, 2007) to account for multiple comparisons across frequencies (Monte Carlo estimate). Samples whose *t*-values exceeded a threshold of cluster $\alpha = 0.05$ were considered as candidate members of clusters of adjacent samples. The sum of *t*-values within every cluster was calculated as test statistics. These cluster sizes were then tested (two-sided) against the distribution of cluster sizes obtained for 10000 repetitions.

Repeated-measures ANOVAs were used to investigate the effects of pharmacological interventions (gaboxadol vs zolpidem) and experimental sessions (PRE vs POST60). Mauchly's test of sphericity was used to test the homogeneity of variance. Where Mauchly's test of sphericity was significant ($p < 0.05$) in repeated-measures ANOVAs, Greenhouse-Geisser corrections were applied. Two-tailed paired-sample *t* tests were calculated using FDR correction for multiple comparisons. Effect sizes were calculated using Cohen's *d*, calculated as the difference between the two means, divided by the standard deviation of the difference. 95% confidence intervals (95% CI) were calculated using accelerated bias-corrected percentile limits (number of bootstrap samples = 10000).

4.2.6 Power spectra parametrisation

The Spectral Parameterisation Resolved in Time algorithm (SPRiNT) (Wilson et al., 2022) is designed to identify and model spectral features of neural activity across time. First, the algorithm performs a short-time Fourier transform (STFT) on 0.5 s sliding time windows using MATLAB's FFT. Time windows are then averaged locally in time (3 windows; 50% overlap) to generate local-mean power spectra. Power spectra are then parametrised implementing the same algorithm used in the FOOOF toolbox (Donoghue et al., 2020). The toolbox conceptualises the power spectra as a combination of an aperiodic component

with overlying periodic components (oscillations). These putative oscillatory components are characterised as frequency regions of power over and above the aperiodic component. The aperiodic component is fit as a function across the entire fitted range of the spectrum, and each oscillatory peak is individually modelled with a Gaussian. The final outputs of the algorithm are the parameters defining the best fit for the aperiodic component and the Gaussians. These are described by the exponent and offset, and periodic peaks, are described by the centre frequency, power, and bandwidth of identified peaks/Gaussians (for a detailed description of the analysis rationale see **Section 1.4.2**; see **Figure 1.5** for a visual description of each periodic and aperiodic component). The FOOOF algorithm was called with the following settings: frequency range 3-40 Hz; peak width limits 1.5-6; max peaks 4; min peak height 0.2; aperiodic mode fixed; peak threshold 2.

4.3 Results

4.3.1 Behavioural features

A series of paired t -tests were run to test the effect of the pharmacological intervention on behavioural performance. Reaction times (**Table 4.1**) were largely slower after zolpidem intervention ($t_{(7)} = -3.27, p = 0.014, d = -1.16, 95\% \text{ CI } [-2.18, -0.27]$). No effect was found for gaboxadol ($t_{(8)} = 0.262, p = 0.8, d = 0.09, 95\% \text{ CI } [-0.67, 0.98]$) and placebo ($t_{(8)} = -0.120, p = 0.9, d = -0.04, 95\% \text{ CI } [-0.7, 0.76]$). Movement duration (**Table 4.1**) remained stable after zolpidem ($t_{(7)} = -1.69, p = 0.135, d = -0.6, 95\% \text{ CI } [-1.59, 0.38]$), gaboxadol ($t_{(8)} = 0.99, p = 0.349, d = 0.33, 95\% \text{ CI } [-0.53, 0.76]$) and placebo administration ($t_{(8)} = 0.5, p = 0.634, d = 0.17, 95\% \text{ CI } [-0.69, 0.89]$).

These results suggest that zolpidem sedative effects influenced participants' responsiveness. In contrast, behavioural performance was unaltered with gaboxadol.

4.3.2 Beta power is modulated by gaboxadol and zolpidem

We tested the effects of gaboxadol and zolpidem on average beta power. In **Figure 4.1** are shown normalised TFRs located on M1, from the PRE sessions (baseline) of each drug. The canonical beta desynchronisation and post-movement beta rebound are visible. We ran a cluster-based permutation test on the normalised TFRs spanning the full time-window (-1.5 to 1.5 s around movement offset). The test did not reveal any significant cluster, suggesting that the baseline sessions were comparable.

In **Figure 4.2** we show a comparison between gaboxadol and placebo. The cluster-permutation test for a time window of 500 ms around movement onset, revealed a cluster with a significant power decrease for IM1, ISMA, IS1 and IPL. For a time window ranging from 0.3 to 1 s after movement offset, a cluster with significant power increase was observed for IM1, ISMA and ImC. The contrast of zolpidem and placebo (**Figure 4.3**), showed a cluster with a significant decrease only for IM1, ImC and IPL when tested for a latency range of 500 ms around movement onset. Direct comparison of the effects of gaboxadol and zolpidem (**Figure 4.4**), returns only a significant cluster for IM1, when

testing for the latency range of -0.25 to 0.25 ms around movement onset.

These findings suggest that gaboxadol alters beta oscillatory power. Interestingly, gaboxadol accentuates beta dynamics during movement, producing a larger desynchronisation at the movement onset and a stronger beta rebound after movement offset. Zolpidem seems to produce a more pronounced beta desynchronisation but has a less clear effect on the beta rebound.

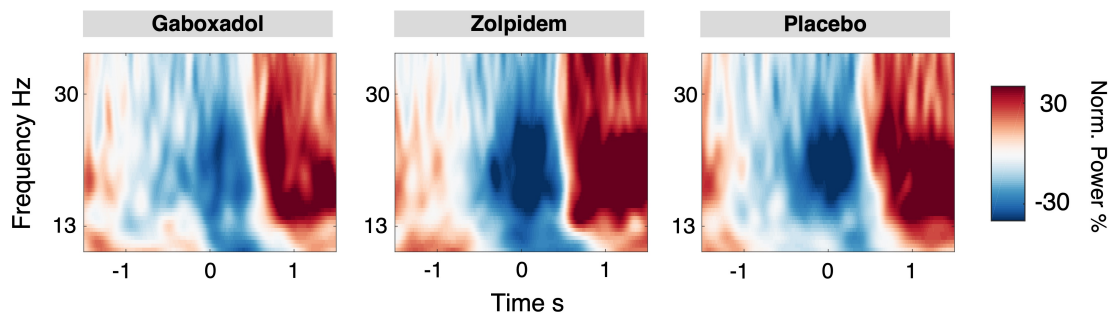


Figure 4.1: Normalised TFRs during PRE session

Power change relative to the average power of the whole session at different frequencies. TFRs are aligned to movement offset at time 0, averaged across trials and then across participants. Data from virtual channels on M1.

Table 4.1: Behavioural features before and after pharmacological intervention

	<i>Reaction time s</i>		<i>Mov. duration s</i>	
	<i>PRE</i>	<i>POST60</i>	<i>PRE</i>	<i>POST60</i>
<i>Gaboxadol</i>				
<i>mean</i>	0.241	0.237	0.204	0.186
<i>median</i>	0.232	0.224	0.156	0.141
<i>sd</i>	0.06	0.08	0.16	0.11
<i>se</i>	0.02	0.03	0.05	0.04
<i>Zolpidem</i>				
<i>mean</i>	0.271	0.323	0.208	0.230
<i>median</i>	0.255	0.313	0.189	0.187
<i>sd</i>	0.11	0.09	0.11	0.11
<i>se</i>	0.04	0.03	0.04	0.04
<i>Placebo</i>				
<i>mean</i>	0.263	0.265	0.220	0.214
<i>median</i>	0.223	0.213	0.168	0.158
<i>sd</i>	0.09	0.10	0.154	0.160
<i>se</i>	0.03	0.03	0.05	0.05

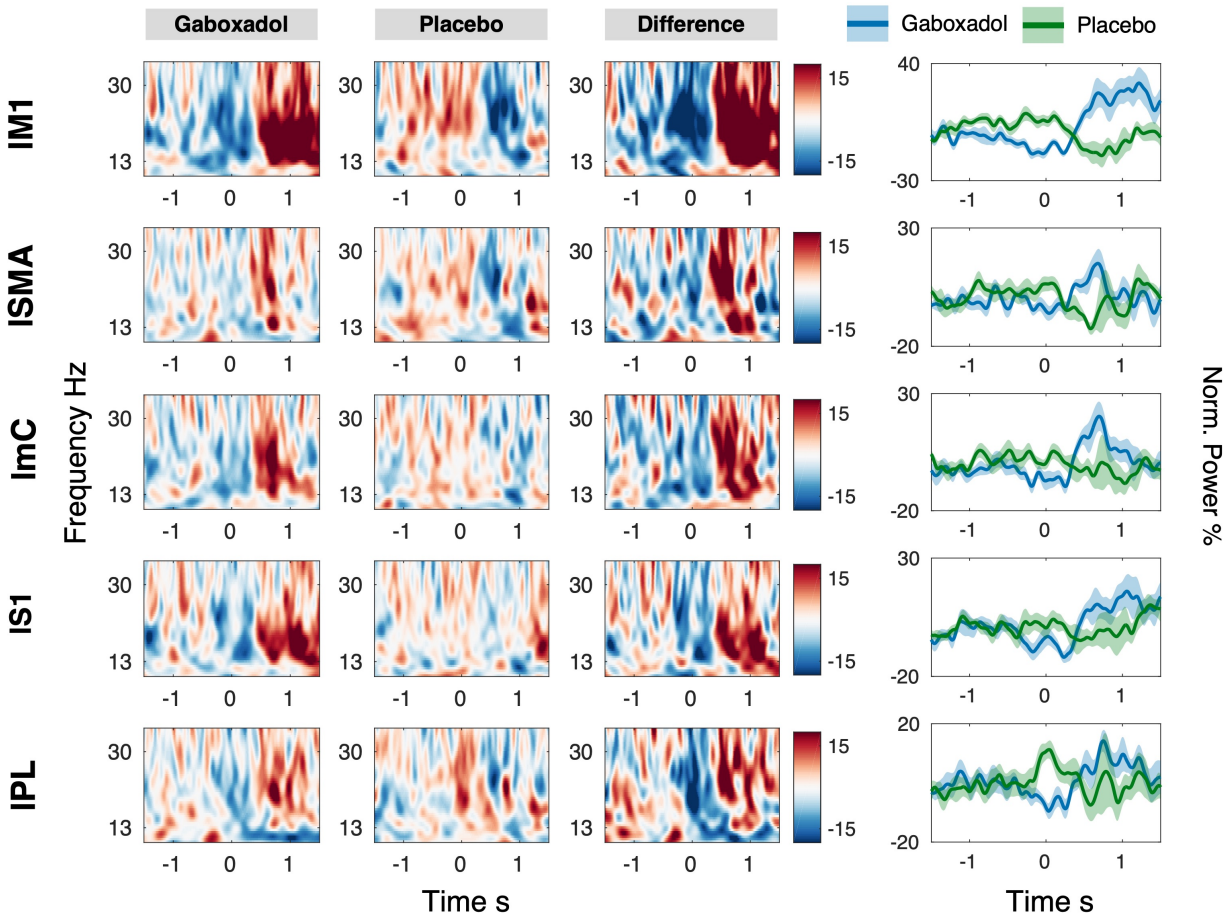


Figure 4.2: **TFRs Gaboxadol and Placebo - POST60**

First two columns show TFRs change compared to baseline (PRE session). The third column shows the TFRs difference between gaboxadol and placebo. The fourth column shows normalised power averaged in the beta range (13-30 Hz). The coloured solid line and shaded area represent average power across participants and SE respectively. Each row shows results for a single ROI. Anatomical regions: IM1 - left primary motor cortex; ISMA - left supplementary motor area; ImC - left middle cingulum; IS1 - left somatosensory cortex; IPL - left paracentral lobule.

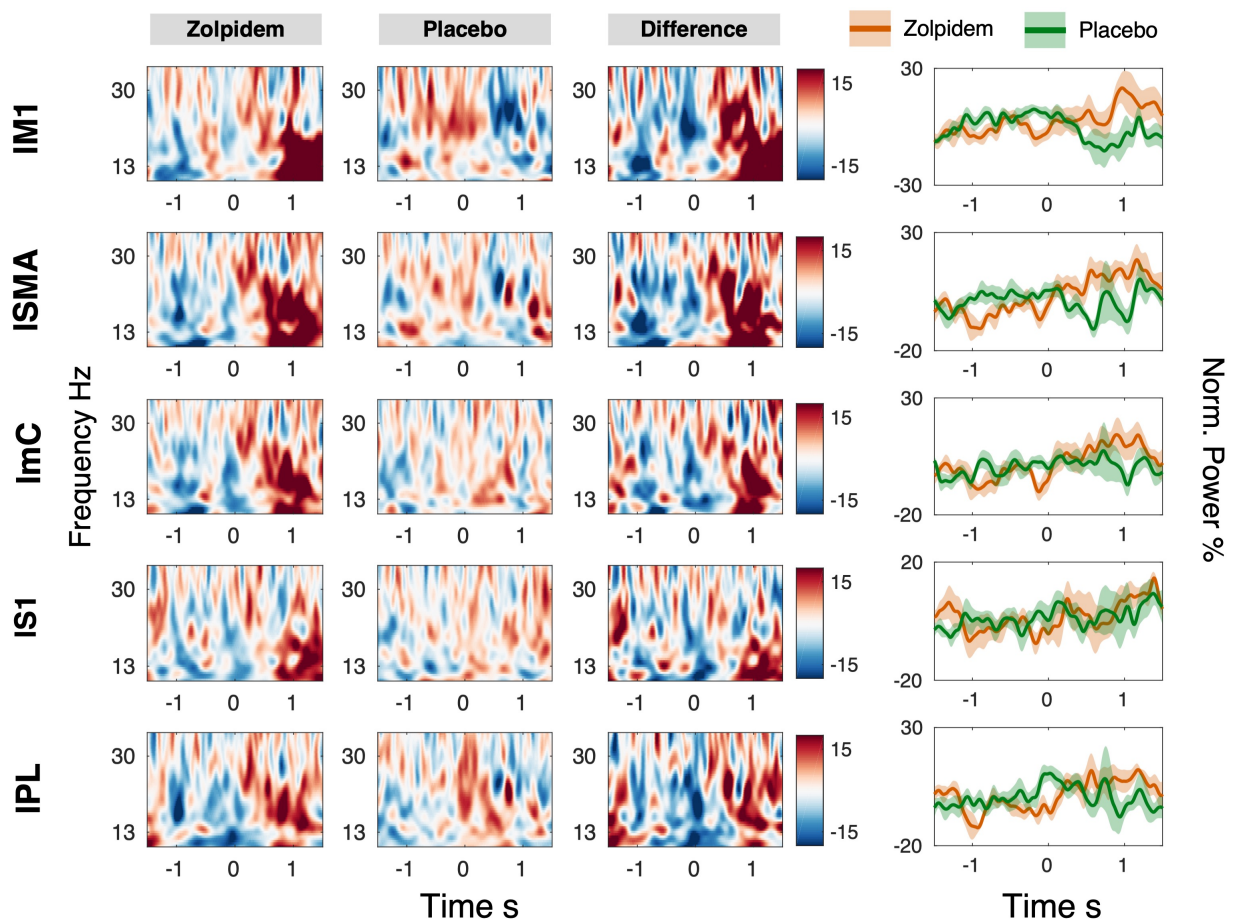


Figure 4.3: **TFRs Zolpidem and Placebo - POST60**

First two columns show TFRs change compared to baseline (PRE session). The third columns show the TFRs difference between zolpidem and placebo. The fourth column shows normalised power averaged in the beta range (13-30 Hz). The coloured solid line and shaded area represent average power across participants and SE respectively. Each row shows results for a single ROI. Anatomical regions: IM1 - left primary motor cortex; ISMA - left supplementary motor area; ImC - left middle cingulum; IS1 - left somatosensory cortex; IPL - left paracentral lobule.

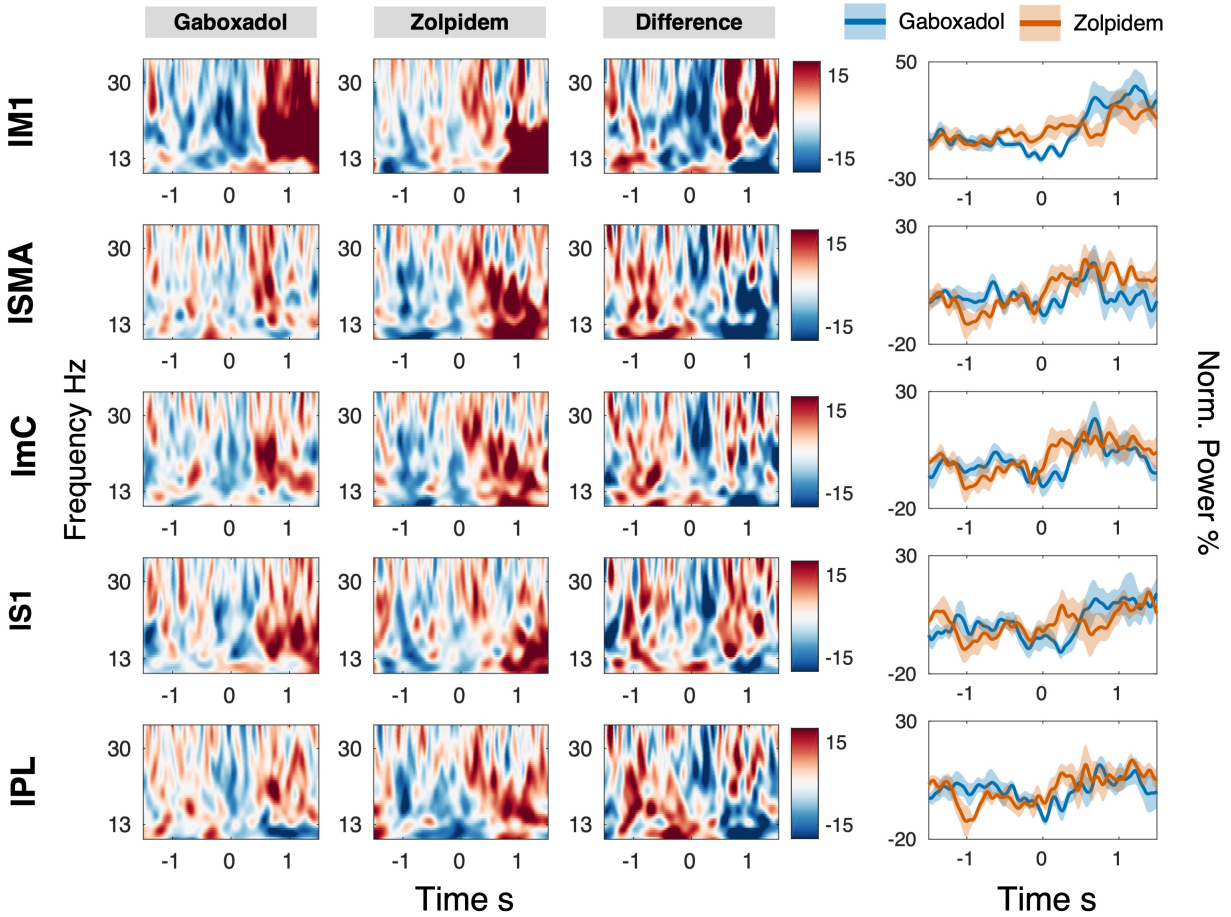


Figure 4.4: TFRs Gaboxadol and Zolpidem - POST60

First two columns show TFRs change compared to baseline (PRE session). The third columns show the TFRs difference between gaboxadol and zolpidem. The fourth column shows normalised power averaged in the beta range (13-30 Hz). The coloured solid line and shaded area represent average power across participants and SE respectively. Each row shows results for a single ROI. Anatomical regions: IM1 - left primary motor cortex; ISMA - left supplementary motor area; ImC - left middle cingulum; IS1 - left somatosensory cortex; IPL - left paracentral lobule.

4.3.3 Effect of pharmacological intervention on periodic and aperiodic features of power spectra

Results from averaged beta power were further explored by addressing the dynamics of periodic and aperiodic aspects of power spectra. Since the SPRiNT analysis allowed for a time-resolved spectra parametrisation, we visualised periodic and aperiodic dynamics during movement (**Figure 4.5**). Beta power, aperiodic-adjusted, shows comparable dynamics to the average TFRs as in **Figure 4.1**, with a pronounced decrease during movement followed by a sharp increase after movement termination. It is noteworthy that both aperiodic offset and exponent showed modulation in the opposite direction compared to beta power, increasing during movement and decreasing after movement offset.

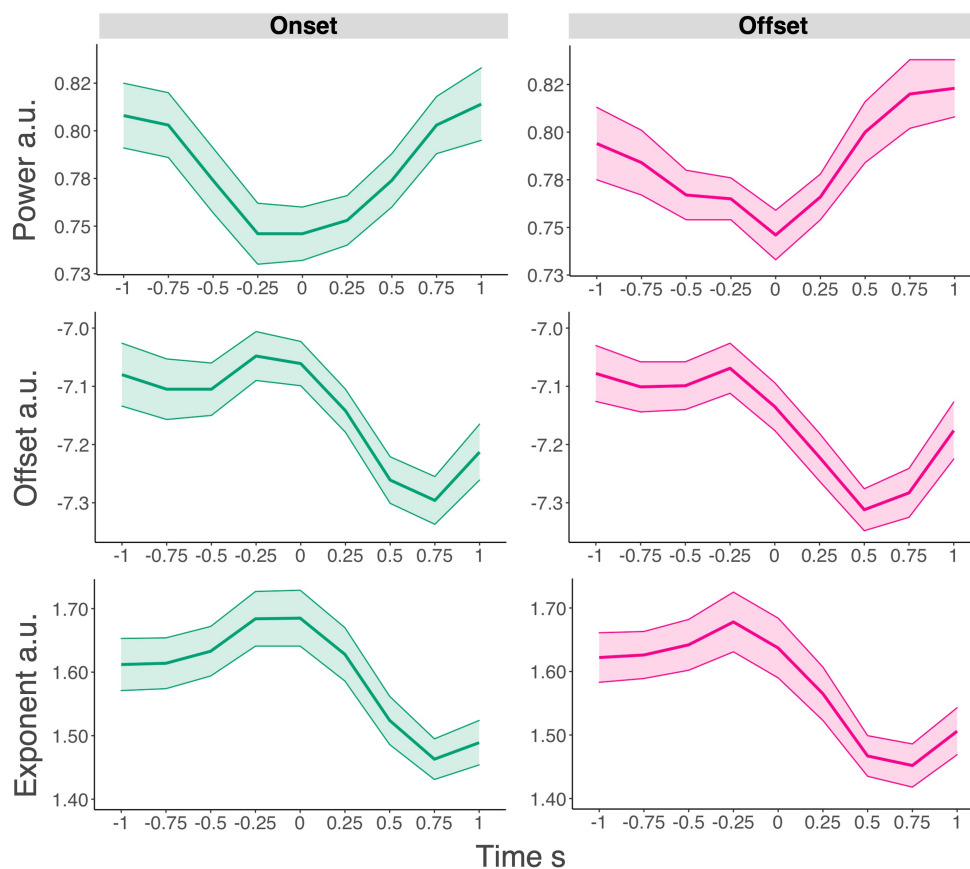


Figure 4.5: Time evolving periodic and aperiodic features

Beta power aperiodic-adjusted, aperiodic offset and exponent from spectra aligned to movement onset (*left column*) and movement offset (*right column*) from M1. The coloured solid line and shaded area represent the average across participants and SE respectively.

A two-way repeated measures ANOVA with factors of pharmacological intervention ($n = 2$; gaboxadol vs zolpidem) and recording session ($n = 2$, PRE vs POST60) was independently applied to power, peak frequency, aperiodic offset and exponent. The analysis was applied to spectra centred around a 250 ms window from -0.25 to 0 around movement onset and from 0.75 to 1 after movement offset, which match the canonical time windows for beta desynchronisation and rebound. Furthermore, the analysis was restricted to spectra from M1 which showed the largest and most consistent activation in the previous analyses (**Figure 4.6 - Figure 4.7**).

The ANOVA on the aperiodic-adjusted beta power between gaboxadol and zolpidem at the start of the movement revealed a main effect of the intervention ($F_{(1,6)} = 58.61$, $p < 0.001$) and session ($F_{(1,6)} = 12.78$, $p = 0.001$). *Post-hoc* analysis revealed increased beta power at POST60 after gaboxadol ($t_{(6)} = 3.58$, $p = 0.021$, $d = 1.35$, 95% CI [0.53, 3.62]) and zolpidem ($t_{(6)} = 3.01$, $p = 0.021$, $d = 1.17$, 95% CI [0.33, 2.53]) intervention. Zolpidem however, induced a larger beta power increase compared to gaboxadol ($t_{(6)} = 5.18$, $p = 0.004$, $d = 1.96$, 95% CI [1.07, 3.62]). Results from the ANOVA applied to the aperiodic components revealed significant interactions for offset ($F_{(1,6)} = 17.43$, $p = 0.006$) and exponent ($F_{(1,6)} = 23.76$, $p = 0.003$). *Post-hoc* tests showed a marked decrease with zolpidem at POST60, for both aperiodic offset ($t_{(6)} = -5.90$, $p = 0.004$, $d = -2.23$, 95% CI [-2.99, -1.49]) and exponent ($t_{(6)} = -5.75$, $p = 0.002$, $d = -2.17$, 95% CI [-3.11, -1.17]). In contrast, gaboxadol modulations were not significant for offset ($t_{(6)} = 1.95$, $p = 0.147$, $d = 0.73$, 95% CI [-0.22, 1.98]) and for exponent ($t_{(6)} = 1.75$, $p = 0.131$, $d = 0.66$, 95% CI [-0.28, 2.05]), although showing effects in the opposite direction compared to zolpidem. Summary metrics are available in **Table C.1** in **Appendix C**.

The results of the ANOVA on beta power after movement offset showed significant main effects of intervention ($F_{(1,6)} = 13.14$, $p = 0.011$) and session ($F_{(1,6)} = 22.13$, $p = 0.003$). Paired *t*-test showed a large beta power increase after zolpidem ($t_{(6)} = 5.71$, $p = 0.002$, $d = 2.16$, 95% CI [1.57, 3.02]), while gaboxadol was not significant ($t_{(6)} = 1.44$, $p = 0.2$, $d = 0.54$, 95% CI [-0.27, 1.13]). ANOVA on aperiodic offset ($F_{(1,6)} = 55.45$, $p < 0.001$) and exponent ($F_{(1,6)} = 29.95$, $p = 0.002$) returned significant interactions between intervention and session. *Post-hoc* comparisons reported a significant increase of

the aperiodic offset after gaboxadol ($t_{(6)} = 2.62, p = 0.04, d = 0.99, 95\% \text{ CI } [0.06, 3.6]$), while a significant decrease was observed after zolpidem ($t_{(6)} = -3.52, p = 0.04, d = -1.23, 95\% \text{ CI } [-1.92, -0.73]$). Paired t -test on the aperiodic exponent did not return significant findings after multiple comparison corrections for both gaboxadol ($t_{(6)} = 1.71, p = 0.14, d = 0.65, 95\% \text{ CI } [-0.21, 2.52]$) and zolpidem ($t_{(6)} = -2.86, p = 0.06, d = -1.08, 95\% \text{ CI } [-1.92, -0.67]$) intervention. Summary metrics are available in **Table C.2** in **Appendix C**.

The results suggest that the effects of pharmacological interventions can influence oscillatory and aperiodic features independently.

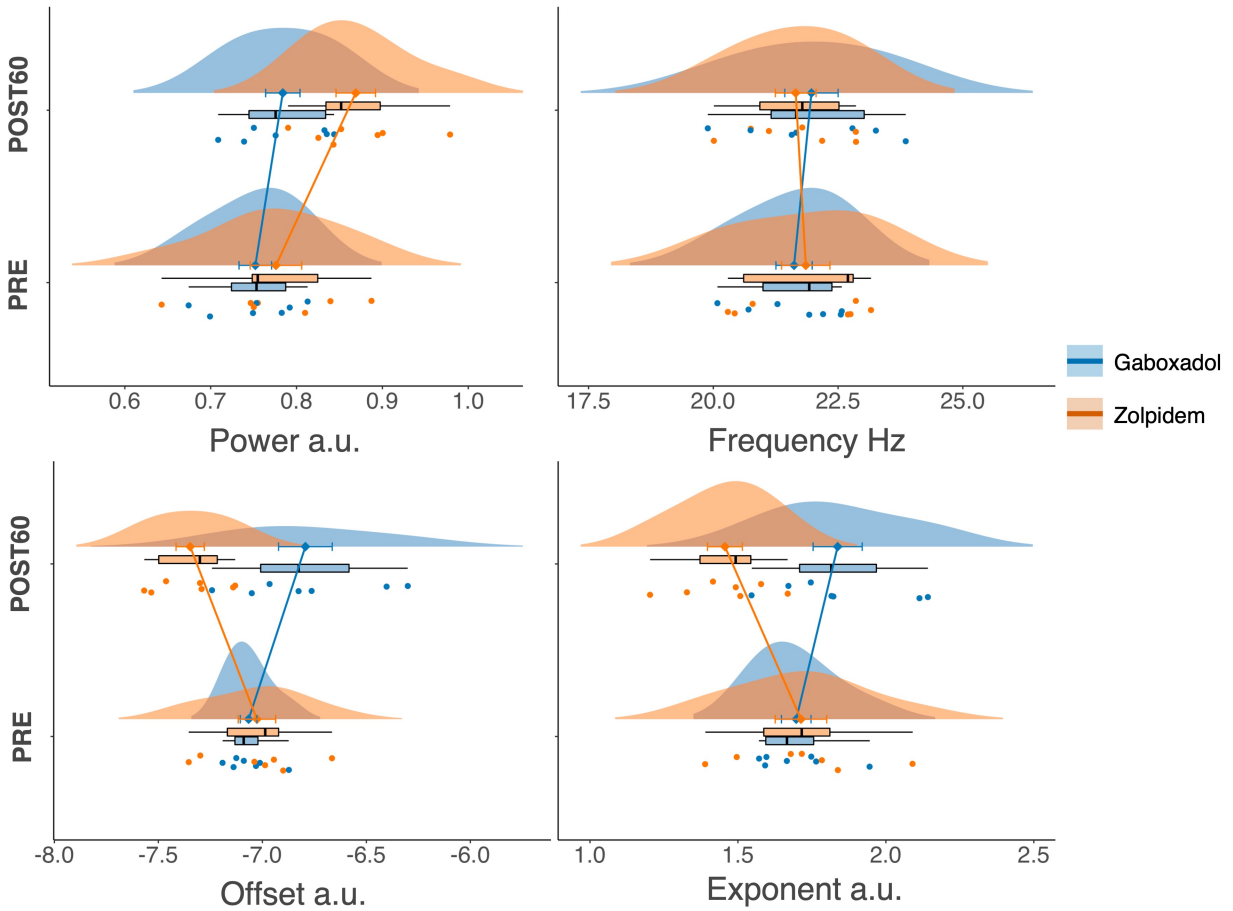


Figure 4.6: Contrast of gaboxadol and zolpidem interventions around movement onset in M1

Effects of pharmacological interventions on periodic (**beta power** - *upper left*, **beta frequency** - *upper right*) and aperiodic (**offset** - *lower left*, **exponent** - *lower right*) spectra features. Each raincloud plot is composed of individual participant scores (**coloured points**), boxplot, data distribution (**coloured curve** mean with standard error (coloured diamond point and error bars)). Observations are split across pharmacological intervention (**light-blue, gaboxadol**; **light-orange, zolpidem**) and session (PRE and POST60).

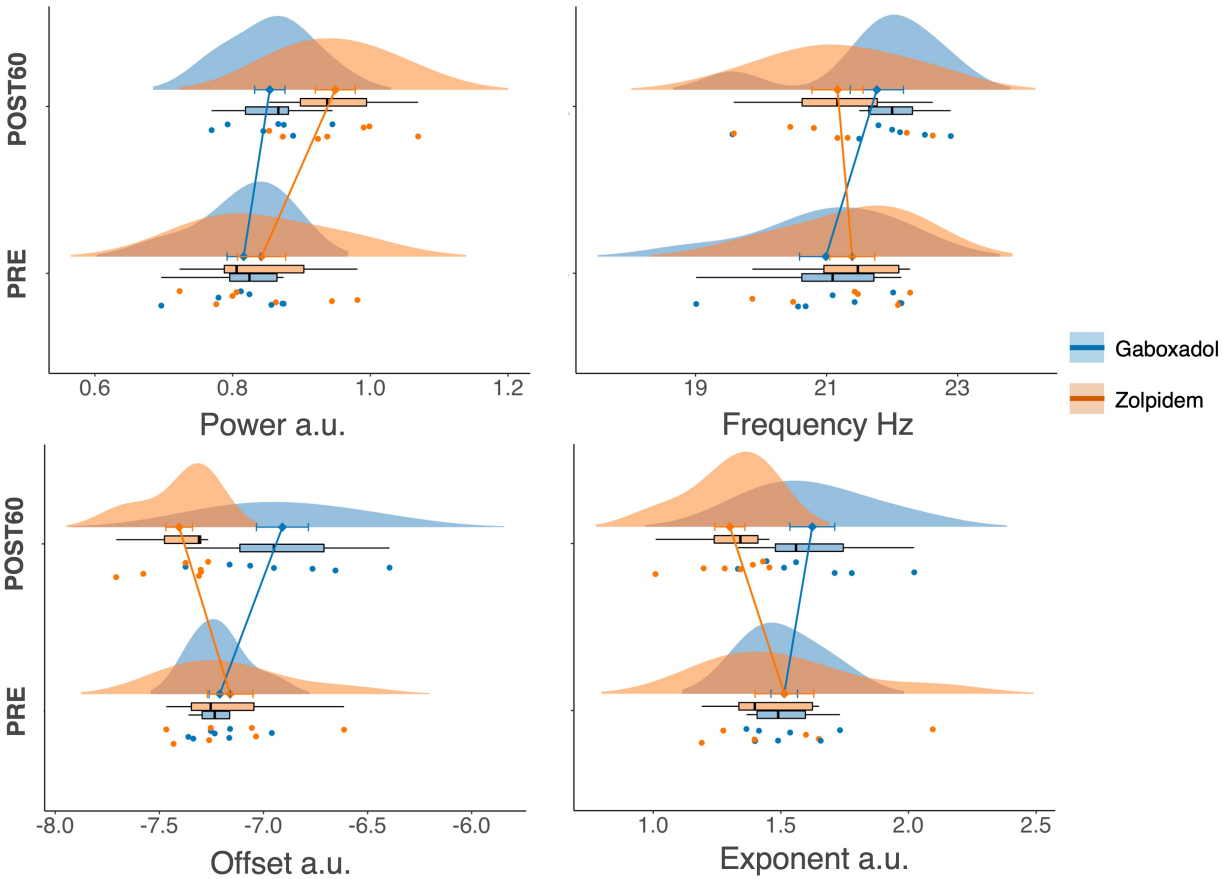


Figure 4.7: **Contrast of gaboxadol and zolpidem interventions after movement offset in M1**

Effects of pharmacological interventions on periodic (**beta power** - *upper left*, **beta frequency** - *upper right*) and aperiodic (**offset** - *lower left*, **exponent** - *lower right*) spectra features. Each raincloud plot is composed of individual participant scores (**coloured points**), boxplot, data distribution (**coloured curve**) and mean with standard error (coloured diamond point and error bars). Observations are split across pharmacological intervention (**light-blue, gaboxadol; light-orange, zolpidem**) and session (PRE and POST60).

4.4 Discussion

In this study, we evaluated the effects on sensorimotor beta oscillations of two GABAergic modulators. We showed how spectra parametrisation can differentiate between the complex effects of pharmacological intervention on rhythmic neural activity, providing additional insights into the underlying physiology.

We found selective effects on periodic spectra components after gaboxadol and zolpidem intervention. Zolpidem produced a consistent increase in the aperiodic-adjusted beta power. Gaboxadol, instead, produced only a marginal increase. These findings are partially in contrast with our results on averaged beta power. Averaged TFRs showed that gaboxadol induced a stronger modulation of beta dynamics compared to zolpidem. This translated into deeper desynchronisation during movement and increased rebound after movement termination. The nature of the discrepancy, between averaged and parameterised spectra results, could rise from the notion that rhythmic neural activity is embedded within aperiodic activity (Donoghue et al., 2020). This activity is variable and dynamic and has been linked to several contexts in which neural oscillations are usually the focus of the investigation (Bruining et al., 2020; Lendner et al., 2020; Molina et al., 2020; Muthukumaraswamy and Liley, 2018; Ouyang et al., 2020; Podvalny et al., 2015; Waschke et al., 2021; Voytek et al., 2015; Schaworonkow and Voytek, 2021). Commonly used power decomposition methods analyse neural oscillations in band-pass filtered signals. Since $1/f$ activity, by definition, will always return non-zero power for narrow-band signals, modulation of the aperiodic components could lead to a misrepresentation of the oscillatory components and misinterpretation of the underlying physiological processes (Donoghue et al., 2020, 2022; Gerster et al., 2022). In our study, pharmacological intervention produced bi-directional aperiodic modulations. Zolpidem produced a marked decrease in aperiodic offset and exponent, while the same parameters were increased after gaboxadol intervention. Aperiodic offset was proposed to reflect a population-averaged stochastic process (Miller et al., 2014). Broadband amplitude dynamics, which can be approximated by the offset component, have demonstrated a positive relationship with neuronal population spiking (Manning et al., 2009). Several studies have shown that

broadband power spectra change can be used to track local cortical activity, reflecting task-specific modulations (Manning et al., 2009; Miller et al., 2014; S. Ray and Maunsell, 2011). The aperiodic spectral exponent, in contrast, has been suggested to represent a non-invasive approximation of the excitation:inhibition (E:I) balance (Gao et al., 2017; Miller et al., 2009). In accordance with invasive work and single-cell modelling (Chini et al., 2022; Gao et al., 2017), increased inhibitory (GABAergic) activity should lead to an increase in the spectral exponent (steepening of the spectrum), while excitatory activity is linked to a decrease (flattening). Several studies have shown how substances selectively targeting inhibitory or excitatory systems have produced alterations of the aperiodic exponent, supporting the validity of this component as a marker of overall E:I balance (Muthukumaraswamy, Carhart-Harris, et al., 2013; Muthukumaraswamy and Liley, 2018; Robertson et al., 2019; Stock et al., 2020; Waschke et al., 2021). Importantly, our study revealed similar dynamics in both the aperiodic exponent and offset, indicating a possible influence or relationship between these phenomena. Although they are typically associated with distinct functions in the existing literature, investigating the correlation between the offset and exponent across participants could offer valuable insights in this regard.

Pharmacology-EEG/MEG studies in humans investigating the GABAergic system have consistently reported an increase of beta power, both at rest and during movement, after administration of a GABA-A agonist or a GABA reuptake blocker (Hall et al., 2009, 2011; Jensen et al., 2005; Muthukumaraswamy, Myers, et al., 2013; Nutt et al., 2015). Similarly, studies using gaboxadol and zolpidem have also shown a generalised effect on beta oscillations, although showing distinct spectra profiles (Nutt et al., 2015). Our results, only partially reconcile with the above-mentioned findings. When parametrised spectra are analysed, gaboxadol effects on beta oscillations are modest and apparently observable only around movement onset but not after movement termination. In an experiment using diazepam, a non-specific GABA-A receptor modulator, Hall et al. (2011) found enhancement of beta desynchronisation but no modulation of PMBR. In a subsequent study, Muthukumaraswamy et al. (2013) reported a modulation for both beta desynchronisation and rebound while using tiagabine, a GAT1 reuptake blocker. The authors speculated that the different mechanisms of action of the two drugs in the two studies could be responsi-

ble for the dissociation observed for beta dynamics during and after movement. Namely, diazepam acts primarily on the GABA-A receptor while tiagabine blocks the synaptic GABA transporter, therefore enhancing the effect of GABA on both GABA-A and GABA-B receptors. This provides supporting evidence that beta desynchronisation and PMBR are distinct phenomena with likely different generators (Gaetz et al., 2011; Jurkiewicz et al., 2006; Muthukumaraswamy, Myers, et al., 2013). Since both gaboxadol and diazepam target the same receptors, our findings could be aligned with this interpretation.

In our study beta power was drastically increased after zolpidem intervention. Evidence from rodent models demonstrates that beta is increased following zolpidem administration, through increased phasic interneuron drive (Yamawaki et al., 2008). Additional supporting evidence comes from a MEG study in which zolpidem positively modulated beta power (Nutt et al., 2015). However, studies on patients with atypical beta oscillations (Parkinson's disease, stroke), have reported that sub-sedative doses (2-5 mg) of zolpidem improve cognitive and motor abilities coincident with a reduction in beta power (Hall et al., 2010, 2014; Prokic et al., 2019). This effect was observable for Parkinson's disease patients but not for healthy controls, leading the authors to speculate that the effects of zolpidem were specific to GABAergic projections in the basal ganglia, known to be deficient in Parkinson's disease (Prokic et al., 2019). An alternative interpretation, specific to the low-dose administration of zolpidem, follows *in vitro* findings which show that low-dose zolpidem selectively augments interneuron (fast-spiking) specific GABA-A mediated tonic currents, resulting in a reduction in beta oscillatory power (Prokic et al., 2015).

We suggest that the complex effects of GABAergic drugs on beta oscillations could be partially explained by evaluating the aperiodic activity. Commonly used time-resolved signal power decomposition such as Hilbert, wavelet, and short-time Fourier signal transforms (Bruns, 2004; M. X. Cohen, 2014), do not explicitly account for the presence of aperiodic signal components, which challenge both the detection and the interpretability of spectral peaks as genuine periodic signal elements (Donoghue et al., 2020). This means that any spectral measure will always return a numerical value for power for a given frequency band, even if oscillations are absent. After gaboxadol intervention, both aperiodic

components increased in magnitude. According to previous studies (for a review see Miller et al., 2014), these findings can be interpreted as two separate co-occurring phenomena, rise in local population spiking (offset) and strengthened inhibition/reduced E:I balance (exponent). We propose that both effects could contribute to increased low-frequency power in the spectrum, even in the absence of any rhythmic/periodic activity. In contrast, the reduction of offset and exponent observed after zolpidem intervention should produce a reduction in low-frequency and an increase in high-frequency power leading to the flattening of the spectra. Interestingly, these results were reported by Nutt et al. (2015), where gaboxadol showed a general enhancement of low-frequency power from the delta through beta range while zolpidem showed enhanced beta and low gamma but reduced alpha.

It is important to interpret our findings qualitatively and exercise caution in drawing conclusions. A comprehensive understanding of the role of aperiodic activity and its relationship with rhythmic activity would require direct assessment and manipulation of key neural mechanisms (see Chini et al., 2022). Additionally, it should be noted that pharmacological interventions can influence behavioural performance. In our study, we observed slower RTs following zolpidem administration, likely due to its sedative effects. To disentangle the impact of behavioural components on our results, one potential strategy would be to compare conditions based on a subset of trials with similar RT distributions. However, this strategy was not feasible in our study due to the limited number of starting trials and the consistent performance issues associated with the interventions. Future studies should address these limitations by increasing the number of trials to enhance statistical power and account for the potential influence of behavioural factors.

The current study would greatly benefit from an exploration of the impact of GABAergic drugs on beta bursts. However, it poses challenges to directly compare burst analysis, which is performed on single trials, with spectra parametrisation, which decomposes the signal into averaged components across trials. Hence, within the scope of this thesis, it was not feasible to investigate this connection. Nevertheless, recent studies, such as the work by Seymour et al. (2022), have successfully integrated both methods. Conducting such an analysis would allow for a more comprehensive characterisation of the relationship be-

tween GABA and beta oscillations. By incorporating the modelling of aperiodic activity, we could enhance sensitivity in detecting oscillatory bursts. Furthermore, by examining burst features like power, count, or time, we can gain valuable insights into the specific physiological aspects of rhythmic neural activity that interact with GABA.

To summarise, here we highlight the importance of separating the periodic and aperiodic neuronal signals in electrophysiological recordings. We argue that when assessing spectral measures of neural oscillations the influence of aperiodic signal needs to be taken into consideration, in order to avoid erroneous interpretations. Recent development in algorithms and guidelines have made this challenge accessible (Donoghue et al., 2020, 2022; Gerster et al., 2022; Kosciessa et al., 2020; Wen and Liu, 2016; Wilson et al., 2022).

Chapter 5

General Discussion

This thesis investigated sensorimotor beta oscillations while focusing on two main aspects: the role of beta in complex motor functions and the physiological mechanism behind its generation.

In **Chapter 2** we assessed beta during a motor adaptation paradigm. Specifically, by altering the visual feedback in a joystick-reaching task, a precise modulation of PMBR was observable following errors which elicited motor adaptation. Although more pronounced in M1, this modulation was also observed across an extended network of frontoparietal areas. In contrast, when using a stop-signal task to test motor inhibition, **Chapter 3** returned inconclusive results on the role of beta. Beta activity in IFG and pre-SMA was comparable between sSTOP vs uSTOP trials. This finding, however, was noteworthy since increased beta activity in frontal nodes is often considered crucial in successful movement stopping.

In **Chapter 4**, we tested the effect of two GABAergic drugs on beta oscillations. Participants performed a finger abduction paradigm while receiving a single-dose administration of gaboxadol and zolpidem across separate sessions. Both interventions produced an increase in beta power. After applying spectra parametrisation, zolpidem only showed a strong modulation of beta power. Gaboxadol effect instead was more modest, since it was partially inflated by the aperiodic components.

In this final chapter, the main findings of this thesis are brought together to integrate the results, discuss the strength and limitations of the methods and consider future appli-

cations.

5.1 The role of beta oscillations: yet unclear?

Two chapters in the thesis investigated the roles of beta in the sensorimotor system. Beta oscillations have been consistently linked with motor learning and action stopping, often implying a causal role for this rhythm in both functions (Tan et al., 2014, 2016; Wessel and Aron, 2017). Our results only partially support this view.

In **Chapter 2** we observed a decrease in PMBR after experiencing task-related errors in the adaptation phase. This supports the idea that beta is sensitive to the outcome of a movement. It is unclear, however, whether this modulation reflects a neural signature of learning or a generalised mismatch/error signal. Our experiments were not designed to explicitly target this outstanding question but could still provide additional insights. PMBR reduction was observable in almost all the ROIs we tested during motor adaptation, but it was more pronounced in IFG and across both hemispheres. Additionally, a drop in IFG's PMBR was also observable in **Chapter 3** while contrasting GO trials with uSTOP trials. Participants in this task were aware of their incorrect performance, but no adaptive response was expected or observable in the data. The idea that PMBR modulation refers to error monitoring has been directly tested in previous studies (Alayrangues et al., 2019; Torrecillos et al., 2015), which found PMBR similarly attenuated for errors that triggered an adaptive response and for errors that did not elicit one. Therefore, our results provide additional support towards the role of PMBR modulation in signalling errors or, more generally, salient events.

In **Chapter 3** we could not differentiate beta activity during successful vs unsuccessful stopping. Even when adopting a more refined analysis focusing on beta-burst, the pattern of response was comparable across conditions. The canonical finding of increased frontal beta during stopping is normally observed in two-choice tasks. In our study, we employed instead a multi-choice joystick-reaching task. Existing guidelines advise choosing a task with a moderate level of difficulty since too complex tasks could alter the probability that the stop process is triggered (Verbruggen et al., 2019). When inspecting behavioural

performance across participants, however, we found results matching the ones described in the existing literature. This implies that our findings could not be simply interpreted in light of methodological discrepancies. Our study, then suggests that when deviating from the canonical stop-signal task a key role of beta in inhibition is less clear.

Both chapters on the beta functional role were designed following a set of well-defined paradigms. The current studies in the field of motor learning and inhibition - and by extension also our studies - often tend to suffer from a purely correlational nature and an unclear definition of beta oscillations. In light of recent studies in the field of neural oscillations (Donoghue et al., 2020, 2022; Jones, 2016), we advise a more precise and cautious interpretation of rhythmic brain activity. As we have shown in **Chapter 4**, standard analyses can obscure oscillatory dynamics and over/underemphasize its real effect. Spectral parametrisation and burst analysis will be key in disentangling neural activity in rhythmic and arrhythmic components, providing better insights into beta functional role.

5.2 GABA influence on beta oscillations

Many theories of beta generation revolve around the interaction between pyramidal neurons and interneurons (Jensen et al., 2005; Kopell et al., 2011; Sherman et al., 2016). Accordingly, the beta rhythm is the result of a balance between excitation and inhibition, with the latter being strictly dependent on GABA levels. Pharmacology-MEG studies have repeatedly reported an increase in beta activity after administration of GABA agonist or GABA reuptake inhibitor drugs (Hall et al., 2009, 2011; Jensen et al., 2005; Muthukumaraswamy, Myers, et al., 2013; Nutt et al., 2015). Therefore, the definition of beta as a GABAergic rhythm is widely accepted across the literature.

Chapter 4 showed how the link between GABA and beta oscillations is more nuanced and actually comprised of distinct, yet interactive, neural features. When relying on standard analyses, the impact of GABAergic activity on beta could easily be misinterpreted. During the investigation of average beta power fluctuations, gaboxadol showed the greatest degree of variation. Our results after spectra parameterisation while still tracing a strong association between GABA and beta also found a weaker linkage with gaboxadol.

This discrepancy stems from a significant contribution to the averaged signal from aperiodic features. These aperiodic components have been shown to vary in response to experimental demands and could be interpreted as a proxy of neural dynamics which conflate the impact of GABA on oscillatory activity. Our results, therefore, highlight the importance of carefully considering the underlying assumptions of the methods employed when studying neural activity. This statement is particularly relevant in studies where the primary goal is to uncover the physiological mechanisms behind neural oscillations.

5.3 Limitations

Within the context of this thesis project, there are several underlying behavioural assumptions that often go overlooked. One specific assumption pertains to the ecological validity of artificial laboratory tasks when studying the sensorimotor system. These tasks, commonly employed in research, allow for the isolation and individual examination of specific motor process features, thereby providing elegant experimental designs to test hypotheses. However, it is essential to critically assess the extent to which within-trial beta modulations align with the intricate nature of continuous, uninterrupted actions encountered in everyday life, which typically involve the participation of various muscle groups and occur without pauses between them.

Despite the relevance of this issue, it has received limited attention in the literature. Notably, Haar and Faisal (2020) addressed this concern in their study by recording beta activity during a game of pool table billiards using mobile EEG. Their findings revealed canonical beta modulations during movement, alongside distinct PMBR dynamics across participants, reflecting different spontaneous learning strategies observed in real-world tasks. While the study incorporated the complexity of natural motor behaviour and the presence of multiple sub-tasks, it still retained key features of laboratory-based paradigms, such as natural spatial constraints, divisibility of behaviour into trials, and clear outcomes.

However, conducting naturalistic studies poses significant challenges, partly due to the limitations associated with conventional methods for recording neural activity. Conventional MEG systems are cumbersome, static, and can only scan one person at a time,

necessitating motionless participants and being limited by the scalp-sensor separation. Encouragingly, recent advancements in MEG technologies based on optically pumped magnetometers (OPMs) (Boto et al., 2018; Brookes et al., 2022) hold promise for facilitating the exploration of naturalistic motor paradigms (Roberts et al., 2019; Seymour et al., 2021).

Thus, investigating the ecological validity of laboratory tasks and the extent to which beta modulations reflect real-world motor functions is a crucial consideration that deserves further attention in the field. Advancements in recording technologies, such as OPM-based MEG systems, present opportunities for exploring more naturalistic motor paradigms and addressing these important questions.

In **Chapter 3**, we conducted experiments to investigate the role of beta oscillations in inhibition using a stop-signal paradigm. While the latency of go responses can be directly observed, response-inhibition latency poses a challenge as it cannot be measured directly. To overcome this limitation, many researchers utilise the SSRT as an inferred measure to assess individual differences in stopping ability. SSRT is derived from a mathematical model and relies on assumptions about the underlying processes involved in inhibitory control.

It is important to recognise that SSRT while providing an estimate of the time required for cancelling an action plan, may not fully capture the complexity of inhibitory processes. For instance, it may not account for partial inhibitions or other cognitive mechanisms involved in response control. Moreover, SSRT estimates can be influenced by various factors in the decision process, rather than solely reflecting a unique construct or a compound construct primarily indexing top-down control (Bompas et al., 2020). These confounding factors can impact the interpretation and comparability of SSRT measures across different populations and experimental conditions.

It is worth noting that inferred measures like SSRT may not fully capture the real-world complexity and variability of inhibitory control. Observable measures, such as response accuracy or RTs in specific task conditions, may provide more ecologically valid assessments of inhibitory abilities. Although SSRT has been widely adopted as a convenient and practical measure of inhibitory control due to its ease of implementation and interpretation, researchers should be mindful of the potential implications of using inferred measures.

Whenever possible, complementing inferred measures with observable measures can contribute to a more comprehensive understanding of inhibitory processes.

5.4 Conclusion

As we briefly touched on above, future studies on beta would benefit from a more precise definition of neural oscillations. Are oscillations a proxy of neural activity? If so, how can we separate their contribution from multiple co-existing neural dynamics (i.e. broadband neural activity, E:I gradient)? Are oscillations fundamental for neural communication and network partition? We suggest that some of the methodologies applied in this thesis could improve our ability to answer these questions.

Our results demonstrated that beta oscillations are dynamically modulated in the sensorimotor system. We showed how beta possesses a great amount of variability when contrasting motor functions (learning vs inhibition) and also during different stages of a movement. While we confirmed a strong link between GABA and beta oscillations, we showed how arrhythmic components can bias our interpretation when using standard time-frequency analyses.

Appendix A

Appendix: Beta dynamics during motor adaptation

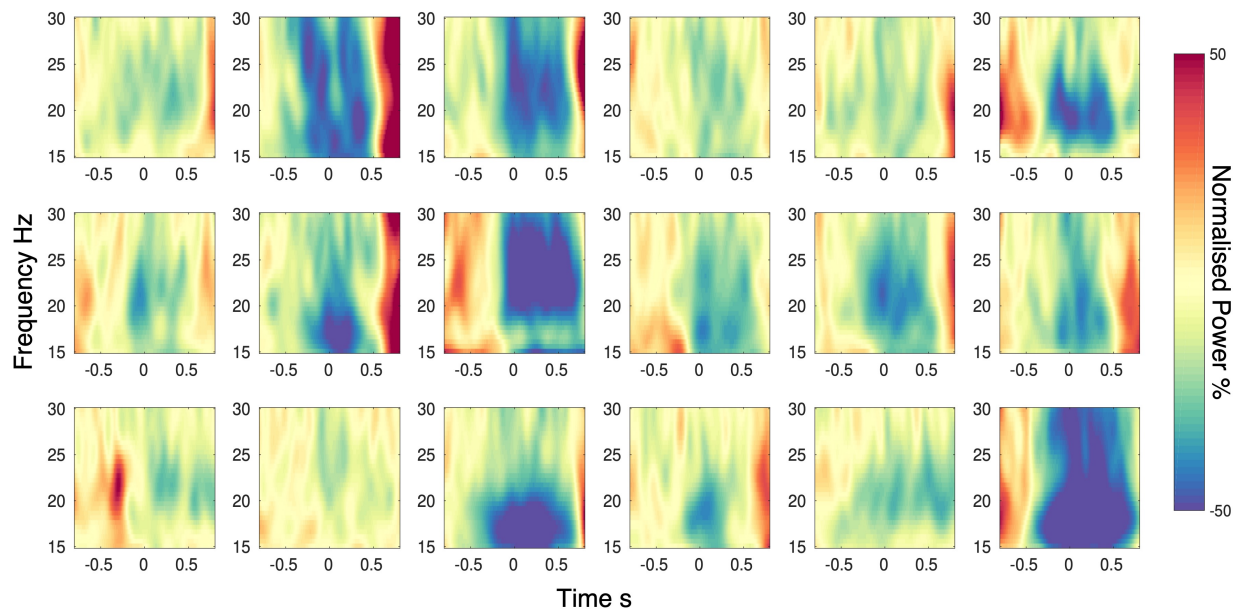


Figure A.1: Individual beta desynchronisation

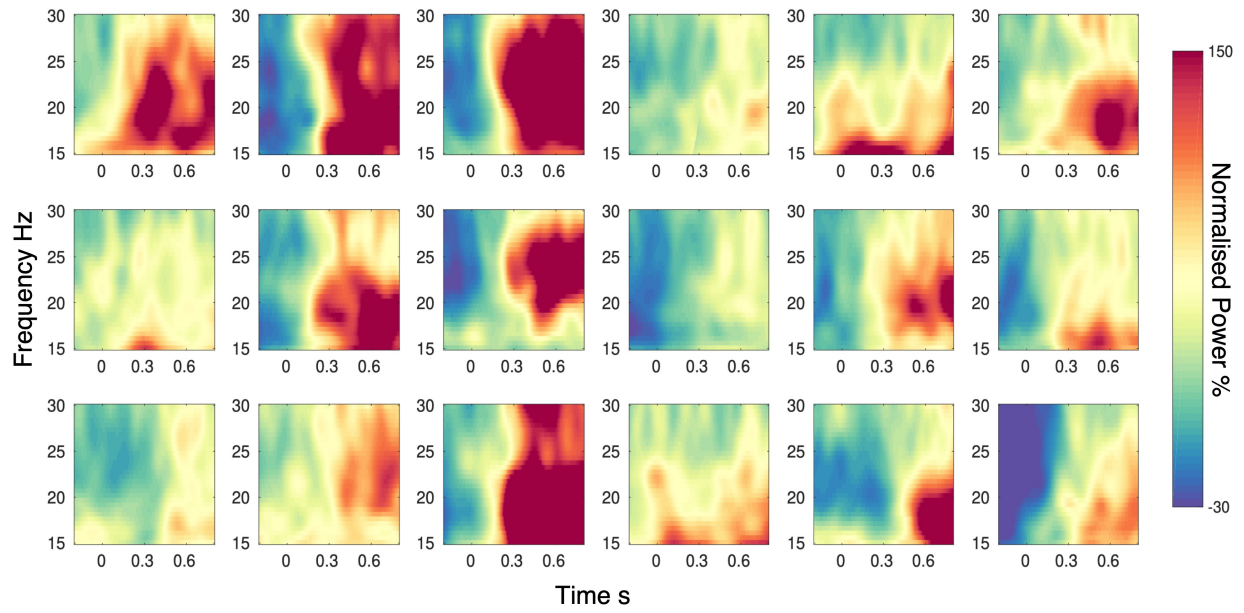


Figure A.2: Individual beta rebound

ROI	Adaptation vs Priming		Washout vs Priming		Adaptation vs Washout	
	<i>t</i>	Cohen's <i>d</i>	<i>t</i>	Cohen's <i>d</i>	<i>t</i>	Cohen's <i>d</i>
Left						
<i>IFG</i>	-2.63	-0.62 [-0.85, -0.35]	-1.72	-0.41 [-0.73, 0.10]	-1.63	-0.38 [-0.87, 0.18]
<i>M1</i>	-2.79	-0.66 [-1.2, -0.4]	-1.29	-0.30 [-0.57, 0.26]	-2.20	-0.52 [-0.86, -0.14]
<i>pre-SMA</i>	-1.86	-0.46 [-0.62, -0.1]	-1.10	-0.27 [-0.57, 0.3]	-1.09	-0.27 [-0.78, 0.25]
<i>S1</i>	-1.79	-0.42 [-0.62, 0.1]	-0.90	-0.21 [-0.54, 0.33]	-2.04	-0.48 [-0.93, -0.1]
<i>sPL</i>	-2.14	-0.52 [-0.72, -0.28]	-0.28	-0.07 [-0.53, 0.47]	-2.09	-0.51 [-0.86, -0.1]
Right						
<i>IFG</i>	-2.48	-0.59 [-0.89, -0.16]	-1.77	-0.42 [-0.66, 0.11]	-1.36	-0.32 [-0.8, 0.2]
<i>M1</i>	-2.15	-0.51 [-0.68, -0.31]	-1.41	-0.33 [-0.56, 0.27]	-1.30	-0.31 [-0.77, 0.2]
<i>pre-SMA</i>	-1.61	-0.38 [-0.51, 0.1]	-1.31	-0.31 [-0.51, 0.3]	-0.72	-0.17 [-0.62, 0.33]
<i>S1</i>	-1.98	-0.47 [-0.66, -0.15]	-1.08	-0.25 [-0.52, 0.33]	-1.44	-0.34 [-0.69, 0.16]
<i>sPL</i>	-2.10	-0.50 [-0.81, -0.02]	-0.85	-0.20 [-0.59, 0.35]	-1.62	-0.38 [-0.87, 0.13]

Table A.1: **Summary statistics of PMBR for each ROI**
Results of paired *t* test from comparisons at the start (first 20 trials) of each phase. Anatomical regions: IFG, inferior frontal gyrus, M1, primary motor cortex, pre-SMA, pre-supplementary motor area, S1, primary somatosensory cortex, sPL, superior parietal lobule.

Appendix B

Appendix: The role of beta oscillations during action-stopping

Table B.1: Beta desynchronisation during GO and uSTOP conditions

<i>Unit=Norm. Power%</i>	<i>ROIs</i>				
	<i>lM1</i>	<i>lS1</i>	<i>rIFG</i>	<i>lPRE-SMA</i>	<i>rPRE-SMA</i>
GO					
<i>mean</i>	-48	-50	-40	-42	-41
<i>median</i>	-50	-50	-40	-43	-40
<i>sd</i>	7	9	7	6	6
<i>se</i>	2	2	2	2	2
uSTOP					
<i>mean</i>	-46	-50	-37	-42	-41
<i>median</i>	-44	-52	-36	-46	-41
<i>sd</i>	7	8	8	8	7
<i>se</i>	2	2	2	2	2

Table B.2: PMBR during GO and uSTOP conditions

<i>Unit= Norm. Power%</i>	<i>ROIs</i>				
	<i>lM1</i>	<i>lS1</i>	<i>rIFG</i>	<i>lPRE-SMA</i>	<i>rPRE-SMA</i>
GO					
<i>mean</i>	117	137	79	96	91
<i>median</i>	113	118	73	86	87
<i>sd</i>	60	85	26	46	34
<i>se</i>	15	22	7	12	9
uSTOP					
<i>mean</i>	103	120	62	87	82
<i>median</i>	87	113	61	75	73
<i>sd</i>	62	68	20	34	32
<i>se</i>	16	18	5	16	8

Appendix C

Appendix: The link between GABA and beta oscillations

Table C.1: Summary statistics for gaboxadol and zolpidem interventions around movement onset

	Power a.u.		Frequency Hz		Offset a.u.		Exponent a.u.	
	<i>PRE</i>	<i>POST60</i>	<i>PRE</i>	<i>POST60</i>	<i>PRE</i>	<i>POST60</i>	<i>PRE</i>	<i>POST60</i>
Gaboxadol								
<i>mean</i>	0.75	0.78	21.61	21.96	-7.32	-6.79	1.70	1.84
<i>median</i>	0.75	0.78	21.92	21.66	-7.09	-6.82	1.67	1.82
<i>sd</i>	0.05	0.05	0.96	1.41	0.11	0.34	0.13	0.22
<i>se</i>	0.02	0.02	0.36	0.53	0.04	0.13	0.05	0.08
Zolpidem								
<i>mean</i>	0.78	0.87	21.85	21.65	-7.02	-7.34	1.71	1.45
<i>median</i>	0.78	0.85	22.69	21.78	-6.98	-7.30	1.72	1.50
<i>sd</i>	0.08	0.06	1.28	1.08	0.24	0.18	0.23	0.16
<i>se</i>	0.03	0.02	0.48	0.41	0.09	0.07	0.09	0.06

Table C.2: Summary statistics for gaboxadol and zolpidem interventions after movement offset

	Power a.u.		Frequency Hz		Offset a.u.		Exponent a.u.	
	<i>PRE</i>	<i>POST60</i>	<i>PRE</i>	<i>POST60</i>	<i>PRE</i>	<i>POST60</i>	<i>PRE</i>	<i>POST60</i>
Gaboxadol								
<i>mean</i>	0.82	0.85	20.99	21.77	-7.21	-6.91	1.51	1.62
<i>median</i>	0.82	0.87	21.01	22	-7.23	-6.96	1.49	1.56
<i>sd</i>	0.06	0.06	1.06	1.07	0.13	0.33	0.14	0.23
<i>se</i>	0.02	0.02	0.4	0.4	0.05	0.13	0.05	0.09
Zolpidem								
<i>mean</i>	0.84	0.95	21.40	21.17	-7.16	-7.41	1.51	1.3
<i>median</i>	0.81	0.94	21.48	21.16	-7.25	-7.31	1.40	1.34
<i>sd</i>	0.09	0.08	0.91	1.03	0.29	0.17	0.30	0.16
<i>se</i>	0.04	0.03	0.34	0.4	0.11	0.06	0.12	0.06

References

- Alayrangues, J., Torrecillos, F., Jahani, A., and Malfait, N. (2019). Error-related modulations of the sensorimotor post-movement and foreperiod beta-band activities arise from distinct neural substrates and do not reflect efferent signal processing. *NeuroImage*, 184, 10–24. Doi: 10.1016/j.neuroimage.2018.09.013
- Alegre, M., Alonso-Frech, F., Rodriguez-Oroz, M. C., Guridi, J., Zamarbide, I., Valencia, M., ... Artieda, J. (2005). Movement-related changes in oscillatory activity in the human subthalamic nucleus: ipsilateral vs. contralateral movements. *European Journal of Neuroscience*, 22(9), 2315–2324. Doi: 10.1111/j.1460-9568.2005.04409.x
- Alegre, M., Alvarez-Gerriko, I., Valencia, M., Iriarte, J., and Artieda, J. (2008). Oscillatory changes related to the forced termination of a movement. *Clinical Neurophysiology*, 119(2), 290–300. Doi: 10.1016/j.clinph.2007.10.017
- Alegre, M., Labarga, A., Gurtubay, I., Iriarte, J., Malanda, A., and Artieda, J. (2002). Beta electroencephalograph changes during passive movements: sensory afferences contribute to beta event-related desynchronization in humans. *Neuroscience Letters*, 331(1), 29–32. Doi: 10.1016/S0304-3940(02)00825-X
- Allen, C., Singh, K. D., Verbruggen, F., and Chambers, C. D. (2018). Evidence for parallel activation of the pre-supplementary motor area and inferior frontal cortex during response inhibition: a combined MEG and TMS study. *Royal Society Open Science*, 5(2), 171369. Doi: 10.1098/rsos.171369
- Allen, M., Poggiali, D., Whitaker, K., Marshall, T. R., and Kievit, R. A. (2019). Raincloud plots: a multi-platform tool for robust data visualization. *Wellcome Open Research*, 4, 63. Doi: 10.12688/wellcomeopenres.15191.1
- Andersen, L. M., Jerbi, K., and Dalal, S. S. (2020). Can EEG and MEG de-

- tect signals from the human cerebellum? *NeuroImage*, 215, 116817. Doi: 10.1016/j.neuroimage.2020.116817
- Aron, A. R., Herz, D. M., Brown, P., Forstmann, B. U., and Zaghoul, K. (2016). Frontosubthalamic Circuits for Control of Action and Cognition. *The Journal of Neuroscience*, 36(45), 11489–11495. Doi: 10.1523/JNEUROSCI.2348-16.2016
- Bachtiar, V., and Stagg, C. (2014). The role of inhibition in human motor cortical plasticity. *Neuroscience*, 278, 93–104. Doi: 10.1016/j.neuroscience.2014.07.059
- Baillet, S. (2017). Magnetoencephalography for brain electrophysiology and imaging. *Nature Neuroscience*, 20(3), 327–339. Doi: 10.1038/nn.4504
- Baillet, S., Mosher, J., and Leahy, R. (2001). Electromagnetic brain mapping. *IEEE Signal Processing Magazine*, 18(6), 14–30. Doi: 10.1109/79.962275
- Baker, M., and Baker, S. (2003). The effect of diazepam on motor cortical oscillations and corticomuscular coherence studied in man. *The Journal of Physiology*, 546(3), 931–942. Doi: 10.1113/jphysiol.2002.029553
- Baker, S. (2007). Oscillatory interactions between sensorimotor cortex and the periphery. *Current Opinion in Neurobiology*, 17(6), 649–655. Doi: 10.1016/j.conb.2008.01.007
- Baar, E. (2013). Brain oscillations in neuropsychiatric disease. *Dialogues in Clinical Neuroscience*, 15(3), 291–300. Doi: 10.31887/DCNS.2013.15.3/ebasar
- Baar, E., Baar-Eroglu, C., Karaka, S., and Schrmann, M. (2001). Gamma, alpha, delta, and theta oscillations govern cognitive processes. *International Journal of Psychophysiology*, 39(2-3), 241–248. Doi: 10.1016/S0167-8760(00)00145-8
- Beck, M. H., Haumesser, J. K., Khn, J., Altschler, J., Khn, A. A., and van Riesen, C. (2016). Short- and long-term dopamine depletion causes enhanced beta oscillations in the cortico-basal ganglia loop of parkinsonian rats. *Experimental Neurology*, 286, 124–136. Doi: 10.1016/j.expneurol.2016.10.005
- Bevan, M. (2002). Move to the rhythm: oscillations in the subthalamic nucleus-external globus pallidus network. *Trends in Neurosciences*, 25(10), 525–531. Doi: 10.1016/S0166-2236(02)02235-X
- Bonaiuto, J. J., Little, S., Neymotin, S. A., Jones, S. R., Barnes, G. R., and Bestmann, S.

- (2021). Laminar dynamics of high amplitude beta bursts in human motor cortex. *NeuroImage*, 242, 118479. Doi: 10.1016/j.neuroimage.2021.118479
- Brittain, J.-S., and Brown, P. (2014). Oscillations and the basal ganglia: Motor control and beyond. *NeuroImage*, 85, 637–647. Doi: 10.1016/j.neuroimage.2013.05.084
- Brookes, M. J., Leggett, J., Rea, M., Hill, R. M., Holmes, N., Boto, E., and Bowtell, R. (2022). Magnetoencephalography with optically pumped magnetometers (OPM-MEG): the next generation of functional neuroimaging. *Trends in Neurosciences*, 45(8), 621–634. Doi: 10.1016/j.tins.2022.05.008
- Brown, P. (2003). Oscillatory nature of human basal ganglia activity: Relationship to the pathophysiology of Parkinson’s disease. *Movement Disorders*, 18(4), 357–363. Doi: 10.1002/mds.10358
- Brown, P. (2006). Bad oscillations in Parkinsons disease. In P. Riederer, H. Reichmann, M. B. H. Youdim, and M. Gerlach (Eds.), *Parkinsons Disease and Related Disorders* (pp. 27–30). Vienna: Springer Vienna. Doi: 10.1007/978-3-211-45295-0_6
- Bruining, H., Hardstone, R., Juarez-Martinez, E. L., Sprengers, J., Avramiea, A.-E., Simpraga, S., ... Linkenkaer-Hansen, K. (2020). Measurement of excitation-inhibition ratio in autism spectrum disorder using critical brain dynamics. *Scientific Reports*, 10(1), 9195. Doi: 10.1038/s41598-020-65500-4
- Bruns, A. (2004). Fourier-, Hilbert- and wavelet-based signal analysis: are they really different approaches? *Journal of Neuroscience Methods*, 137(2), 321–332. Doi: 10.1016/j.jneumeth.2004.03.002
- Buschman, T. J., and Miller, E. K. (2007). Top-Down Versus Bottom-Up Control of Attention in the Prefrontal and Posterior Parietal Cortices. *Science*, 315(5820), 1860–1862. Doi: 10.1126/science.1138071
- Buzski, G. (2006). *Rhythms of the Brain*. Oxford University Press. Doi: 10.1093/acprof:oso/9780195301069.001.0001
- Buzski, G., Anastassiou, C. A., and Koch, C. (2012). The origin of extracellular fields and currents EEG, ECoG, LFP and spikes. *Nature Reviews Neuroscience*, 13(6), 407–420. Doi: 10.1038/nrn3241
- Buzski, G., and Watson, B. O. (2012). Brain rhythms and neural syntax: implications

- for efficient coding of cognitive content and neuropsychiatric disease. *Dialogues in Clinical Neuroscience*, 14(4), 345–367. Doi: 10.31887/DCNS.2012.14.4/gbuzsaki
- Brgers, C., and Kopell, N. J. (2008). Gamma Oscillations and Stimulus Selection. *Neural Computation*, 20(2), 383–414. Doi: 10.1162/neco.2007.07-06-289
- Cassim, F., Monaca, C., Szurhaj, W., Bourriez, J.-L., Defebvre, L., Derambure, P., and Guieu, J.-D. (2001). Does post-movement beta synchronization reflect an idling motor cortex?:. *Neuroreport*, 12(17), 3859–3863. Doi: 10.1097/00001756-200112040-00051
- Castiglione, A., Wagner, J., Anderson, M., and Aron, A. R. (2019). Preventing a Thought from Coming to Mind Elicits Increased Right Frontal Beta Just as Stopping Action Does. *Cerebral Cortex*, 29(5), 2160–2172. Doi: 10.1093/cercor/bhz017
- Chandrasekaran, C., Bray, I. E., and Shenoy, K. V. (2019). Frequency Shifts and Depth Dependence of Premotor Beta Band Activity during Perceptual Decision-Making. *The Journal of Neuroscience*, 39(8), 1420–1435. Doi: 10.1523/JNEUROSCI.1066-18.2018
- Chini, M., Pfeffer, T., and Hanganu-Opatz, I. (2022). An increase of inhibition drives the developmental decorrelation of neural activity. *eLife*, 11, e78811. (Publisher: eLife Sciences Publications, Ltd) Doi: 10.7554/eLife.78811
- Cohen, D. (1972). Magnetoencephalography: Detection of the Brain's Electrical Activity with a Superconducting Magnetometer. *Science*, 175(4022), 664–666. Doi: 10.1126/science.175.4022.664
- Cohen, M. X. (2014). *Analyzing Neural Time Series Data: Theory and Practice*. The MIT Press. Doi: 10.7551/mitpress/9609.001.0001
- Corbit, V. L., Whalen, T. C., Zitelli, K. T., Crilly, S. Y., Rubin, J. E., and Gittis, A. H. (2016). Pallidostriatal Projections Promote Oscillations in a Dopamine-Depleted Biophysical Network Model. *Journal of Neuroscience*, 36(20), 5556–5571. Doi: 10.1523/JNEUROSCI.0339-16.2016
- Dalal, S. S., Osipova, D., Bertrand, O., and Jerbi, K. (2013). Oscillatory activity of the human cerebellum: The intracranial electrocerebellogram revisited. *Neuroscience & Biobehavioral Reviews*, 37(4), 585–593. Doi: 10.1016/j.neubiorev.2013.02.006

- Destexhe, A., and Sejnowski, T. J. (2003). Interactions Between Membrane Conductances Underlying Thalamocortical Slow-Wave Oscillations. *Physiological Reviews*, 83(4), 1401–1453. Doi: 10.1152/physrev.00012.2003
- Diedrichsen, J. (2005). Neural Correlates of Reach Errors. *Journal of Neuroscience*, 25(43), 9919–9931. Doi: 10.1523/JNEUROSCI.1874-05.2005
- Donoghue, T., Haller, M., Peterson, E. J., Varma, P., Sebastian, P., Gao, R., ... Voytek, B. (2020). Parameterizing neural power spectra into periodic and aperiodic components. *Nature Neuroscience*, 23(12), 1655–1665. Doi: 10.1038/s41593-020-00744-x
- Donoghue, T., Schaworonkow, N., and Voytek, B. (2022). Methodological considerations for studying neural oscillations. *European Journal of Neuroscience*, 55(11-12), 3502–3527. Doi: 10.1111/ejn.15361
- Duann, J.-R., Ide, J. S., Luo, X., and Li, C.-s. R. (2009). Functional Connectivity Delineates Distinct Roles of the Inferior Frontal Cortex and Presupplementary Motor Area in Stop Signal Inhibition. *Journal of Neuroscience*, 29(32), 10171–10179. Doi: 10.1523/JNEUROSCI.1300-09.2009
- Engel, A. K., and Fries, P. (2010). Beta-band oscillations signalling the status quo? *Current Opinion in Neurobiology*, 20(2), 156–165. Doi: 10.1016/j.conb.2010.02.015
- Erika-Florence, M., Leech, R., and Hampshire, A. (2014). A functional network perspective on response inhibition and attentional control. *Nature Communications*, 5(1), 4073. Doi: 10.1038/ncomms5073
- Errington, S. P., Woodman, G. F., and Schall, J. D. (2020). Dissociation of Medial Frontal Bursts and Executive Control. *The Journal of Neuroscience*, 40(48), 9272–9282. Doi: 10.1523/JNEUROSCI.2072-20.2020
- Espenhahn, S., van Wijk, B. C., Rossiter, H. E., de Berker, A. O., Redman, N. D., Rondina, J., ... Ward, N. S. (2019). Cortical beta oscillations are associated with motor performance following visuomotor learning. *NeuroImage*, 195, 340–353. Doi: 10.1016/j.neuroimage.2019.03.079
- Feingold, J., Gibson, D. J., DePasquale, B., and Graybiel, A. M. (2015). Bursts of beta oscillation differentiate postperformance activity in the striatum and motor cortex

- of monkeys performing movement tasks. *Proceedings of the National Academy of Sciences*, 112(44), 13687–13692. Doi: 10.1073/pnas.1517629112
- Franklin, D., and Wolpert, D. (2011). Computational Mechanisms of Sensorimotor Control. *Neuron*, 72(3), 425–442. Doi: 10.1016/j.neuron.2011.10.006
- Freeman, W. J., Holmes, M. D., Burke, B. C., and Vanhatalo, S. (2003). Spatial spectra of scalp EEG and EMG from awake humans. *Clinical Neurophysiology*, 114(6), 1053–1068. Doi: 10.1016/S1388-2457(03)00045-2
- Freeman, W. J., and Zhai, J. (2009). Simulated power spectral density (PSD) of background electrocorticogram (ECoG). *Cognitive Neurodynamics*, 3(1), 97–103. Doi: 10.1007/s11571-008-9064-y
- Fries, P. (2005). A mechanism for cognitive dynamics: neuronal communication through neuronal coherence. *Trends in Cognitive Sciences*, 9(10), 474–480. Doi: 10.1016/j.tics.2005.08.011
- Fries, P. (2015). Rhythms for Cognition: Communication through Coherence. *Neuron*, 88(1), 220–235. Doi: 10.1016/j.neuron.2015.09.034
- Gaetz, W., Edgar, J., Wang, D., and Roberts, T. (2011). Relating MEG measured motor cortical oscillations to resting -Aminobutyric acid (GABA) concentration. *NeuroImage*, 55(2), 616–621. Doi: 10.1016/j.neuroimage.2010.12.077
- Gao, R., Peterson, E. J., and Voytek, B. (2017). Inferring synaptic excitation/inhibition balance from field potentials. *NeuroImage*, 158, 70–78. Doi: 10.1016/j.neuroimage.2017.06.078
- Gerster, M., Waterstraat, G., Litvak, V., Lehnertz, K., Schnitzler, A., Florin, E., ... Nikulin, V. (2022). Separating Neural Oscillations from Aperiodic 1/f Activity: Challenges and Recommendations. *Neuroinformatics*. Doi: 10.1007/s12021-022-09581-8
- Gross, J., Baillet, S., Barnes, G. R., Henson, R. N., Hillebrand, A., Jensen, O., ... Schoffelen, J.-M. (2013). Good practice for conducting and reporting MEG research. *NeuroImage*, 65, 349–363. Doi: 10.1016/j.neuroimage.2012.10.001
- Gross, J., Kujala, J., Hmlinen, M., Timmermann, L., Schnitzler, A., and Salmelin, R. (2001). Dynamic imaging of coherent sources: Studying neural interactions in the human brain. *Proceedings of the National Academy of Sciences*, 98(2), 694–699. Doi:

10.1073/pnas.98.2.694

- Haar, S., and Faisal, A. A. (2020). Brain Activity Reveals Multiple Motor-Learning Mechanisms in a Real-World Task. *Frontiers in Human Neuroscience*, 14, 354. Doi: 10.3389/fnhum.2020.00354
- Hajak, G., Hedner, J., Eglin, M., Loft, H., Strustovu, S. ., Ltolf, S., and Lundahl, J. (2009). A 2-week efficacy and safety study of gaboxadol and zolpidem using electronic diaries in primary insomnia outpatients. *Sleep Medicine*, 10(7), 705–712. Doi: 10.1016/j.sleep.2008.09.010
- Hall, S., Barnes, G. R., Furlong, P. L., Seri, S., and Hillebrand, A. (2009). Neuronal network pharmacodynamics of GABAergic modulation in the human cortex determined using pharmaco-magnetoencephalography. *Human Brain Mapping*, n/a–n/a. Doi: 10.1002/hbm.20889
- Hall, S., Prokic, E., McAllister, C., Ronnqvist, K., Williams, A., Yamawaki, N., ... Stanford, I. (2014). GABA-mediated changes in inter-hemispheric beta frequency activity in early-stage Parkinsons disease. *Neuroscience*, 281, 68–76. Doi: 10.1016/j.neuroscience.2014.09.037
- Hall, S., Stanford, I., Yamawaki, N., McAllister, C., Rnnqvist, K., Woodhall, G., and Furlong, P. (2011). The role of GABAergic modulation in motor function related neuronal network activity. *NeuroImage*, 56(3), 1506–1510. Doi: 10.1016/j.neuroimage.2011.02.025
- Hall, S., Yamawaki, N., Fisher, A. E., Clauss, R. P., Woodhall, G. L., and Stanford, I. M. (2010). GABA(A) alpha-1 subunit mediated desynchronization of elevated low frequency oscillations alleviates specific dysfunction in stroke A case report. *Clinical Neurophysiology*, 121(4), 549–555. Doi: 10.1016/j.clinph.2009.11.084
- Halsband, U., and Lange, R. K. (2006). Motor learning in man: A review of functional and clinical studies. *Journal of Physiology-Paris*, 99(4-6), 414–424. Doi: 10.1016/j.jphysparis.2006.03.007
- Hammond, C., Bergman, H., and Brown, P. (2007). Pathological synchronization in Parkinson's disease: networks, models and treatments. *Trends in Neurosciences*, 30(7), 357–364. Doi: 10.1016/j.tins.2007.05.004

- Hampshire, A., Thompson, R., Duncan, J., and Owen, A. M. (2009). Selective tuning of the right inferior frontal gyrus during target detection. *Cognitive, Affective, & Behavioral Neuroscience*, 9(1), 103–112. Doi: 10.3758/CABN.9.1.103
- Hanslmayr, S., Staresina, B. P., and Bowman, H. (2016). Oscillations and Episodic Memory: Addressing the Synchronization/Desynchronization Conundrum. *Trends in Neurosciences*, 39(1), 16–25. Doi: 10.1016/j.tins.2015.11.004
- Hashimoto, I., Kimura, T., Tanosaki, M., Iguchi, Y., and Sekihara, K. (2003). Muscle afferent inputs from the hand activate human cerebellum sequentially through parallel and climbing fiber systems. *Clinical Neurophysiology*, 114(11), 2107–2117. Doi: 10.1016/S1388-2457(03)00233-5
- He, B. J. (2014). Scale-free brain activity: past, present, and future. *Trends in Cognitive Sciences*, 18(9), 480–487. Doi: 10.1016/j.tics.2014.04.003
- He, W., Donoghue, T., Sowman, P. F., Seymour, R. A., Brock, J., Crain, S., . . . Hillebrand, A. (2019). *Co-Increasing Neuronal Noise and Beta Power in the Developing Brain* (preprint). Neuroscience. Doi: 10.1101/839258
- Heinrichs-Graham, E., and Wilson, T. W. (2016). Is an absolute level of cortical beta suppression required for proper movement? Magnetoencephalographic evidence from healthy aging. *NeuroImage*, 134, 514–521. Doi: 10.1016/j.neuroimage.2016.04.032
- Heinrichs-Graham, E., Wilson, T. W., Santamaria, P. M., Heithoff, S. K., Torres-Russotto, D., Hutter-Saunders, J. A., . . . Gendelman, H. E. (2014). Neuromagnetic Evidence of Abnormal Movement-Related Beta Desynchronization in Parkinson's Disease. *Cerebral Cortex*, 24(10), 2669–2678. Doi: 10.1093/cercor/bht121
- Herrmann, C. S., Strber, D., Helfrich, R. F., and Engel, A. K. (2016). EEG oscillations: From correlation to causality. *International Journal of Psychophysiology*, 103, 12–21. Doi: 10.1016/j.ijpsycho.2015.02.003
- Hillebrand, A., and Barnes, G. R. (2005). Beamformer Analysis of MEG Data. In *International Review of Neurobiology* (Vol. 68, pp. 149–171). Elsevier. Doi: 10.1016/S0074-7742(05)68006-3
- Hillebrand, A., Singh, K. D., Holliday, I. E., Furlong, P. L., and Barnes, G. R. (2005). A new

- approach to neuroimaging with magnetoencephalography. *Human Brain Mapping*, 25(2), 199–211. Doi: 10.1002/hbm.20102
- Holgado, A. J. N., Terry, J. R., and Bogacz, R. (2010). Conditions for the Generation of Beta Oscillations in the Subthalamic Nucleus-Globus Pallidus Network. *Journal of Neuroscience*, 30(37), 12340–12352. Doi: 10.1523/JNEUROSCI.0817-10.2010
- Hutcheon, B., and Yarom, Y. (2000). Resonance, oscillation and the intrinsic frequency preferences of neurons. *Trends in Neurosciences*, 23(5), 216–222. Doi: 10.1016/S0166-2236(00)01547-2
- Hmlinen, M., Hari, R., Ilmoniemi, R. J., Knuutila, J., and Lounasmaa, O. V. (1993). Magnetoencephalography theory, instrumentation, and applications to noninvasive studies of the working human brain. *Reviews of Modern Physics*, 65(2), 413–497. Doi: 10.1103/RevModPhys.65.413
- Jana, S., Hannah, R., Muralidharan, V., and Aron, A. R. (2020). Temporal cascade of frontal, motor and muscle processes underlying human action-stopping. *eLife*, 9, e50371. Doi: 10.7554/eLife.50371
- Jensen, O., Goel, P., Kopell, N., Pohja, M., Hari, R., and Ermentrout, B. (2005). On the human sensorimotor-cortex beta rhythm: Sources and modeling. *NeuroImage*, 26(2), 347–355. Doi: 10.1016/j.neuroimage.2005.02.008
- Jones, S. R. (2016). When brain rhythms aren't rhythmic: implication for their mechanisms and meaning. *Current Opinion in Neurobiology*, 40, 72–80. Doi: 10.1016/j.conb.2016.06.010
- Jones, S. R., Pritchett, D. L., Sikora, M. A., Stufflebeam, S. M., Hmlinen, M., and Moore, C. I. (2009). Quantitative Analysis and Biophysically Realistic Neural Modeling of the MEG Mu Rhythm: Rhythmogenesis and Modulation of Sensory-Evoked Responses. *Journal of Neurophysiology*, 102(6), 3554–3572. Doi: 10.1152/jn.00535.2009
- Jurkiewicz, M. T., Gaetz, W. C., Bostan, A. C., and Cheyne, D. (2006). Post-movement beta rebound is generated in motor cortex: Evidence from neuromagnetic recordings. *NeuroImage*, 32(3), 1281–1289. Doi: 10.1016/j.neuroimage.2006.06.005
- Kilavik, B. E., Confais, J., and Riehle, A. (2014). Signs of Timing in Motor Cortex During Movement Preparation and Cue Anticipation. In H. Merchant and V. de Lafuente

- (Eds.), *Neurobiology of Interval Timing* (Vol. 829, pp. 121–142). New York, NY: Springer New York. (Series Title: Advances in Experimental Medicine and Biology)
Doi: 10.1007/978-1-4939-1782-2_7
- Kilavik, B. E., Zaepffel, M., Brovelli, A., MacKay, W. A., and Riehle, A. (2013). The ups and downs of beta oscillations in sensorimotor cortex. *Experimental Neurology*, *245*, 15–26. Doi: 10.1016/j.expneurol.2012.09.014
- Kloosterman, N. A., Meindertsmas, T., Hillebrand, A., van Dijk, B. W., Lamme, V. A. F., and Donner, T. H. (2015). Top-down modulation in human visual cortex predicts the stability of a perceptual illusion. *Journal of Neurophysiology*, *113*(4), 1063–1076. Doi: 10.1152/jn.00338.2014
- Kolasinski, J., Hinson, E. L., Divanbeighi Zand, A. P., Rizov, A., Emir, U. E., and Stagg, C. J. (2019). The dynamics of cortical GABA in human motor learning. *The Journal of Physiology*, *597*(1), 271–282. Doi: 10.1113/JP276626
- Kopell, N., Ermentrout, G. B., Whittington, M. A., and Traub, R. D. (2000). Gamma rhythms and beta rhythms have different synchronization properties. *Proceedings of the National Academy of Sciences*, *97*(4), 1867–1872. Doi: 10.1073/pnas.97.4.1867
- Kopell, N., Whittington, M. A., and Kramer, M. A. (2011). Neuronal assembly dynamics in the beta1 frequency range permits short-term memory. *Proceedings of the National Academy of Sciences*, *108*(9), 3779–3784. Doi: 10.1073/pnas.1019676108
- Kosciessa, J. Q., Grandy, T. H., Garrett, D. D., and Werkle-Bergner, M. (2020). Single-trial characterization of neural rhythms: Potential and challenges. *NeuroImage*, *206*, 116331. Doi: 10.1016/j.neuroimage.2019.116331
- Kramer, M. A., Roopun, A. K., Carracedo, L. M., Traub, R. D., Whittington, M. A., and Kopell, N. J. (2008). Rhythm Generation through Period Concatenation in Rat Somatosensory Cortex. *PLoS Computational Biology*, *4*(9), e1000169. Doi: 10.1371/journal.pcbi.1000169
- Kumar, A., Cardanobile, S., Rotter, S., and Aertsen, A. (2011). The Role of Inhibition in Generating and Controlling Parkinson's Disease Oscillations in the Basal Ganglia. *Frontiers in Systems Neuroscience*, *5*. Doi: 10.3389/fnsys.2011.00086
- Kumaravelu, K., Brocker, D. T., and Grill, W. M. (2016). A biophysical model of

- the cortex-basal ganglia-thalamus network in the 6-OHDA lesioned rat model of Parkinsons disease. *Journal of Computational Neuroscience*, 40(2), 207–229. Doi: 10.1007/s10827-016-0593-9
- Lai, M.-C., Lombardo, M. V., Chakrabarti, B., Sadek, S. A., Pasco, G., Wheelwright, S. J., ... Suckling, J. (2010). A Shift to Randomness of Brain Oscillations in People with Autism. *Biological Psychiatry*, 68(12), 1092–1099. Doi: 10.1016/j.biopsych.2010.06.027
- Leblois, A. (2006). Competition between Feedback Loops Underlies Normal and Pathological Dynamics in the Basal Ganglia. *Journal of Neuroscience*, 26(13), 3567–3583. Doi: 10.1523/JNEUROSCI.5050-05.2006
- Lee, J. H., Whittington, M. A., and Kopell, N. J. (2013). Top-Down Beta Rhythms Support Selective Attention via Interlaminar Interaction: A Model. *PLoS Computational Biology*, 9(8), e1003164. Doi: 10.1371/journal.pcbi.1003164
- Lendner, J. D., Helfrich, R. F., Mander, B. A., Romundstad, L., Lin, J. J., Walker, M. P., ... Knight, R. T. (2020). An electrophysiological marker of arousal level in humans. *eLife*, 9, e55092. Doi: 10.7554/eLife.55092
- Leske, S., and Dalal, S. S. (2019). Reducing power line noise in EEG and MEG data via spectrum interpolation. *NeuroImage*, 189, 763–776. Doi: 10.1016/j.neuroimage.2019.01.026
- Leventhal, D., Gage, G., Schmidt, R., Pettibone, J., Case, A., and Berke, J. (2012). Basal Ganglia Beta Oscillations Accompany Cue Utilization. *Neuron*, 73(3), 523–536. Doi: 10.1016/j.neuron.2011.11.032
- Lin, C., Tierney, T. M., Holmes, N., Boto, E., Leggett, J., Bestmann, S., ... Miall, R. C. (2019). Using optically pumped magnetometers to measure magnetoencephalographic signals in the human cerebellum. *The Journal of Physiology*, 597(16), 4309–4324. Doi: 10.1113/JP277899
- Little, S., Bonaiuto, J., Barnes, G., and Bestmann, S. (2019). Human motor cortical beta bursts relate to movement planning and response errors. *PLOS Biology*, 17(10), e3000479. Doi: 10.1371/journal.pbio.3000479
- Little, S., and Brown, P. (2014). The functional role of beta oscillations in

- Parkinson's disease. *Parkinsonism & Related Disorders*, 20, S44–S48. Doi: 10.1016/S1353-8020(13)70013-0
- Little, S., Tan, H., Anzak, A., Pogosyan, A., Khn, A., and Brown, P. (2013). Bilateral Functional Connectivity of the Basal Ganglia in Patients with Parkinsons Disease and Its Modulation by Dopaminergic Treatment. *PLoS ONE*, 8(12), e82762. Doi: 10.1371/journal.pone.0082762
- Litvak, V., Jha, A., Eusebio, A., Oostenveld, R., Foltynie, T., Limousin, P., ... Brown, P. (2011). Resting oscillatory cortico-subthalamic connectivity in patients with Parkinsons disease. *Brain*, 134(2), 359–374. Doi: 10.1093/brain/awq332
- Liu, C., Zhou, C., Wang, J., Fietkiewicz, C., and Loparo, K. A. (2020). The role of coupling connections in a model of the cortico-basal ganglia-thalamocortical neural loop for the generation of beta oscillations. *Neural Networks*, 123, 381–392. Doi: 10.1016/j.neunet.2019.12.021
- Logan, G. D., Cowan, W. B., and Davis, K. A. (1984). On the ability to inhibit simple and choice reaction time responses: A model and a method. *Journal of Experimental Psychology: Human Perception and Performance*, 10(2), 276–291. Doi: 10.1037/0096-1523.10.2.276
- LopesdaSilva, F. (2013). EEG and MEG: Relevance to Neuroscience. *Neuron*, 80(5), 1112–1128. Doi: 10.1016/j.neuron.2013.10.017
- Lopez-Azcarate, J., Tainta, M., Rodriguez-Oroz, M. C., Valencia, M., Gonzalez, R., Guridi, J., ... Alegre, M. (2010). Coupling between Beta and High-Frequency Activity in the Human Subthalamic Nucleus May Be a Pathophysiological Mechanism in Parkinson's Disease. *Journal of Neuroscience*, 30(19), 6667–6677. Doi: 10.1523/JNEUROSCI.5459-09.2010
- Lundqvist, M., Rose, J., Herman, P., Brincat, S., Buschman, T., and Miller, E. (2016). Gamma and Beta Bursts Underlie Working Memory. *Neuron*, 90(1), 152–164. Doi: 10.1016/j.neuron.2016.02.028
- Makeig, S., Bell, A., Jung, T.-P., and Sejnowski, T. J. (1995). Independent Component Analysis of Electroencephalographic Data. In D. Touretzky, M. C. Mozer, and M. Haselmo (Eds.), *Advances in Neural Information Processing Systems* (Vol. 8). MIT Press.

- Makris, N., Schlerf, J. E., Hodge, S. M., Haselgrove, C., Albaugh, M. D., Seidman, L. J., ... Schmahmann, J. D. (2005). MRI-based surface-assisted parcellation of human cerebellar cortex: an anatomically specified method with estimate of reliability. *NeuroImage*, 25(4), 1146–1160. Doi: 10.1016/j.neuroimage.2004.12.056
- Manning, J. R., Jacobs, J., Fried, I., and Kahana, M. J. (2009). Broadband Shifts in Local Field Potential Power Spectra Are Correlated with Single-Neuron Spiking in Humans. *Journal of Neuroscience*, 29(43), 13613–13620. Doi: 10.1523/JNEUROSCI.2041-09.2009
- Marceglia, S., Foffani, G., Bianchi, A. M., Baselli, G., Tamma, F., Egidi, M., and Priori, A. (2006). Dopamine-dependent non-linear correlation between subthalamic rhythms in Parkinson's disease: Dopamine-dependent segregation between STN rhythms. *The Journal of Physiology*, 571(3), 579–591. Doi: 10.1113/jphysiol.2005.100271
- Marco-Pallars, J., Mnte, T. F., and Rodrguez-Fornells, A. (2015). The role of high-frequency oscillatory activity in reward processing and learning. *Neuroscience & Biobehavioral Reviews*, 49, 1–7. Doi: 10.1016/j.neubiorev.2014.11.014
- Maris, E., and Oostenveld, R. (2007). Nonparametric statistical testing of EEG- and MEG-data. *Journal of Neuroscience Methods*, 164(1), 177–190. Doi: 10.1016/j.jneumeth.2007.03.024
- Maxim, V., endur, L., Fadili, J., Suckling, J., Gould, R., Howard, R., and Bullmore, E. (2005). Fractional Gaussian noise, functional MRI and Alzheimer's disease. *NeuroImage*, 25(1), 141–158. Doi: 10.1016/j.neuroimage.2004.10.044
- Mazaheri, A., Slagter, H. A., Thut, G., and Foxe, J. J. (2018). Orchestration of brain oscillations: principles and functions. *European Journal of Neuroscience*, 48(7), 2385–2388. Doi: 10.1111/ejn.14189
- McCarthy, M. M., Moore-Kochlacs, C., Gu, X., Boyden, E. S., Han, X., and Kopell, N. (2011). Striatal origin of the pathologic beta oscillations in Parkinson's disease. *Proceedings of the National Academy of Sciences*, 108(28), 11620–11625. Doi: 10.1073/pnas.1107748108
- Middlebrooks, P. G., Zandbelt, B. B., Logan, G. D., Palmeri, T. J., and Schall, J. D. (2020). Countermanding Perceptual Decision-Making. *iScience*, 23(1), 100777. Doi: 10.1016/j.isci.2020.100777

10.1016/j.isci.2019.100777

- Miller, K. J., Honey, C. J., Hermes, D., Rao, R. P., denNijs, M., and Ojemann, J. G. (2014). Broadband changes in the cortical surface potential track activation of functionally diverse neuronal populations. *NeuroImage*, 85, 711–720. Doi: 10.1016/j.neuroimage.2013.08.070
- Miller, K. J., Schalk, G., Fetz, E. E., den Nijs, M., Ojemann, J. G., and Rao, R. P. N. (2010). Cortical activity during motor execution, motor imagery, and imagery-based online feedback. *Proceedings of the National Academy of Sciences*, 107(9), 4430–4435. Doi: 10.1073/pnas.0913697107
- Miller, K. J., Sorensen, L. B., Ojemann, J. G., and den Nijs, M. (2009). Power-Law Scaling in the Brain Surface Electric Potential. *PLoS Computational Biology*, 5(12), e1000609. Doi: 10.1371/journal.pcbi.1000609
- Mirzaei, A., Kumar, A., Leventhal, D., Mallet, N., Aertsen, A., Berke, J., and Schmidt, R. (2017). Sensorimotor Processing in the Basal Ganglia Leads to Transient Beta Oscillations during Behavior. *The Journal of Neuroscience*, 37(46), 11220–11232. Doi: 10.1523/JNEUROSCI.1289-17.2017
- Molina, J. L., Voytek, B., Thomas, M. L., Joshi, Y. B., Bhakta, S. G., Talledo, J. A., . . . Light, G. A. (2020). Memantine Effects on Electroencephalographic Measures of Putative Excitatory/Inhibitory Balance in Schizophrenia. *Biological Psychiatry: Cognitive Neuroscience and Neuroimaging*, 5(6), 562–568. Doi: 10.1016/j.bpsc.2020.02.004
- Moran, R. J., Mallet, N., Litvak, V., Dolan, R. J., Magill, P. J., Friston, K. J., and Brown, P. (2011). Alterations in Brain Connectivity Underlying Beta Oscillations in Parkinsonism. *PLoS Computational Biology*, 7(8), e1002124. Doi: 10.1371/journal.pcbi.1002124
- Muellbacher, W., Ziemann, U., Wissel, J., Dang, N., Kofler, M., Facchini, S., . . . Hallett, M. (2002). Early consolidation in human primary motor cortex. *Nature*, 415(6872), 640–644. Doi: 10.1038/nature712
- Muthukumaraswamy, S. (2010). Functional Properties of Human Primary Motor Cortex Gamma Oscillations. *Journal of Neurophysiology*, 104(5), 2873–2885. Doi: 10.1152/jn.00607.2010

- Muthukumaraswamy, S., Carhart-Harris, R. L., Moran, R. J., Brookes, M. J., Williams, T. M., Errtizoe, D., ... Nutt, D. J. (2013). Broadband Cortical Desynchronization Underlies the Human Psychedelic State. *Journal of Neuroscience*, *33*(38), 15171–15183. Doi: 10.1523/JNEUROSCI.2063-13.2013
- Muthukumaraswamy, S., and Liley, D. T. (2018). 1/f electrophysiological spectra in resting and drug-induced states can be explained by the dynamics of multiple oscillatory relaxation processes. *NeuroImage*, *179*, 582–595. Doi: 10.1016/j.neuroimage.2018.06.068
- Muthukumaraswamy, S., Myers, J., Wilson, S., Nutt, D., Lingford-Hughes, A., Singh, K., and Hamandi, K. (2013). The effects of elevated endogenous GABA levels on movement-related network oscillations. *NeuroImage*, *66*, 36–41. Doi: 10.1016/j.neuroimage.2012.10.054
- Newson, J. J., and Thiagarajan, T. C. (2019). EEG Frequency Bands in Psychiatric Disorders: A Review of Resting State Studies. *Frontiers in Human Neuroscience*, *12*, 521. Doi: 10.3389/fnhum.2018.00521
- Nolte, G. (2003). The magnetic lead field theorem in the quasi-static approximation and its use for magnetoencephalography forward calculation in realistic volume conductors. *Physics in Medicine and Biology*, *48*(22), 3637–3652. Doi: 10.1088/0031-9155/48/22/002
- Nutt, D., Kilpatrick, G., and Hayes, A. (2014). The extinction of drugs for clinical research: Can the ECNP medicines chest save them? *European Neuropsychopharmacology*, *24*(4), 487–490. Doi: 10.1016/j.euroneuro.2014.01.018
- Nutt, D., Wilson, S., Lingford-Hughes, A., Myers, J., Papadopoulos, A., and Muthukumaraswamy, S. (2015). Differences between magnetoencephalographic (MEG) spectral profiles of drugs acting on GABA at synaptic and extrasynaptic sites: A study in healthy volunteers. *Neuropharmacology*, *88*, 155–163. Doi: 10.1016/j.neuropharm.2014.08.017
- Olufsen, M. S., Whittington, M. A., Camperi, M., and Kopell, N. (2003). New Roles for the Gamma Rhythm: Population Tuning and Preprocessing for the Beta Rhythm. *Journal of Computational Neuroscience*, *14*(1), 33–54. Doi: 10.1023/A:1021124317706

- Oostenveld, R., Fries, P., Maris, E., and Schoffelen, J.-M. (2011). FieldTrip: Open Source Software for Advanced Analysis of MEG, EEG, and Invasive Electrophysiological Data. *Computational Intelligence and Neuroscience*, 2011, 1–9. Doi: 10.1155/2011/156869
- Ouyang, G., Hildebrandt, A., Schmitz, F., and Herrmann, C. S. (2020). Decomposing alpha and 1/f brain activities reveals their differential associations with cognitive processing speed. *NeuroImage*, 205, 116304. Doi: 10.1016/j.neuroimage.2019.116304
- Pavlidis, A., Hogan, S. J., and Bogacz, R. (2015). Computational Models Describing Possible Mechanisms for Generation of Excessive Beta Oscillations in Parkinsons Disease. *PLOS Computational Biology*, 11(12), e1004609. Doi: 10.1371/journal.pcbi.1004609
- Percival, D. B., and Walden, A. T. (1993). *Spectral Analysis for Physical Applications* (1st ed.). Cambridge University Press. Doi: 10.1017/CBO9780511622762
- Pfurtscheller, G., and Lopes da Silva, F. (1999). Event-related EEG/MEG synchronization and desynchronization: basic principles. *Clinical Neurophysiology*, 110(11), 1842–1857. Doi: 10.1016/S1388-2457(99)00141-8
- Pfurtscheller, G., Stanck, A., and Neuper, C. (1996). Post-movement beta synchronization. A correlate of an idling motor area? *Electroencephalography and Clinical Neurophysiology*, 98(4), 281–293. Doi: 10.1016/0013-4694(95)00258-8
- Plenz, D., and Kital, S. T. (1999). A basal ganglia pacemaker formed by the subthalamic nucleus and external globus pallidus. *Nature*, 400(6745), 677–682. Doi: 10.1038/23281
- Podvalny, E., Noy, N., Harel, M., Bickel, S., Chechik, G., Schroeder, C. E., ... Malach, R. (2015). A unifying principle underlying the extracellular field potential spectral responses in the human cortex. *Journal of Neurophysiology*, 114(1), 505–519. Doi: 10.1152/jn.00943.2014
- Popa, L. S., and Ebner, T. J. (2019). Cerebellum, Predictions and Errors. *Frontiers in Cellular Neuroscience*, 12, 524. Doi: 10.3389/fncel.2018.00524
- Priori, A., Foffani, G., Pesenti, A., Tamma, F., Bianchi, A., Pellegrini, M., ... Viliani, R. (2004). Rhythm-specific pharmacological modulation of subthalamic ac-

- tivity in Parkinson's disease. *Experimental Neurology*, 189(2), 369–379. Doi: 10.1016/j.expneurol.2004.06.001
- Prokic, E. J., Stanford, I. M., Woodhall, G. L., Williams, A. C., and Hall, S. D. (2019). Bradykinesia Is Driven by Cumulative Beta Power During Continuous Movement and Alleviated by Gabaergic Modulation in Parkinson's Disease. *Frontiers in Neurology*, 10, 1298. Doi: 10.3389/fneur.2019.01298
- Prokic, E. J., Weston, C., Yamawaki, N., Hall, S. D., Jones, R. S., Stanford, I. M., . . . Woodhall, G. L. (2015). Cortical oscillatory dynamics and benzodiazepine-site modulation of tonic inhibition in fast spiking interneurons. *Neuropharmacology*, 95, 192–205. Doi: 10.1016/j.neuropharm.2015.03.006
- Quinn, A. J., van Ede, F., Brookes, M. J., Heideman, S. G., Nowak, M., Seedat, Z. A., . . . Woolrich, M. W. (2019). Unpacking Transient Event Dynamics in Electrophysiological Power Spectra. *Brain Topography*, 32(6), 1020–1034. Doi: 10.1007/s10548-019-00745-5
- Ray, N. J., Brittain, J.-S., Holland, P., Joundi, R. A., Stein, J. F., Aziz, T. Z., and Jenkinson, N. (2012). The role of the subthalamic nucleus in response inhibition: Evidence from local field potential recordings in the human subthalamic nucleus. *NeuroImage*, 60(1), 271–278. Doi: 10.1016/j.neuroimage.2011.12.035
- Ray, S., and Maunsell, J. H. R. (2011). Different Origins of Gamma Rhythm and High-Gamma Activity in Macaque Visual Cortex. *PLoS Biology*, 9(4), e1000610. Doi: 10.1371/journal.pbio.1000610
- Rayson, H., Debnath, R., Alavizadeh, S., Fox, N., Ferrari, P. F., and Bonaiuto, J. J. (2022). Detection and analysis of cortical beta bursts in developmental EEG data. *Developmental Cognitive Neuroscience*, 54, 101069. Doi: 10.1016/j.dcn.2022.101069
- Robertson, M. M., Furlong, S., Voytek, B., Donoghue, T., Boettiger, C. A., and Sheridan, M. A. (2019). EEG power spectral slope differs by ADHD status and stimulant medication exposure in early childhood. *Journal of Neurophysiology*, 122(6), 2427–2437. Doi: 10.1152/jn.00388.2019
- Roopun, A. K., Middleton, S. J., Cunningham, M. O., LeBeau, F. E. N., Bibbig, A., Whittington, M. A., and Traub, R. D. (2006). A beta2-frequency (2030 Hz) oscillation in

- nonsynaptic networks of somatosensory cortex. *Proceedings of the National Academy of Sciences*, 103(42), 15646–15650. Doi: 10.1073/pnas.0607443103
- Rossiter, H. E., Boudrias, M.-H., and Ward, N. S. (2014). Do movement-related beta oscillations change after stroke? *Journal of Neurophysiology*, 112(9), 2053–2058. Doi: 10.1152/jn.00345.2014
- Rossiter, H. E., Davis, E. M., Clark, E. V., Boudrias, M.-H., and Ward, N. S. (2014). Beta oscillations reflect changes in motor cortex inhibition in healthy ageing. *NeuroImage*, 91, 360–365. Doi: 10.1016/j.neuroimage.2014.01.012
- Saleh, M., Reimer, J., Penn, R., Ojakangas, C. L., and Hatsopoulos, N. G. (2010). Fast and Slow Oscillations in Human Primary Motor Cortex Predict Oncoming Behaviorally Relevant Cues. *Neuron*, 65(4), 461–471. Doi: 10.1016/j.neuron.2010.02.001
- Sanes, J. N., and Donoghue, J. P. (2000). Plasticity and primary motor cortex. *Annual review of neuroscience*, 23(1), 393–415.
- Sarvas, J. (1987). Basic mathematical and electromagnetic concepts of the biomagnetic inverse problem. *Physics in Medicine and Biology*, 32(1), 11–22. Doi: 10.1088/0031-9155/32/1/004
- Schaum, M., Pinzuti, E., Sebastian, A., Lieb, K., Fries, P., Mobascher, A., ... Tscher, O. (2021). Right inferior frontal gyrus implements motor inhibitory control via beta-band oscillations in humans. *eLife*, 10, e61679. Doi: 10.7554/eLife.61679
- Schaworonkow, N., and Voytek, B. (2021). Longitudinal changes in aperiodic and periodic activity in electrophysiological recordings in the first seven months of life. *Developmental Cognitive Neuroscience*, 47, 100895. Doi: 10.1016/j.dcn.2020.100895
- Schmidt, R., Herrojo Ruiz, M., Kilavik, B. E., Lundqvist, M., Starr, P. A., and Aron, A. R. (2019). Beta Oscillations in Working Memory, Executive Control of Movement and Thought, and Sensorimotor Function. *The Journal of Neuroscience*, 39(42), 8231–8238. Doi: 10.1523/JNEUROSCI.1163-19.2019
- Scott, S. H. (2012). The computational and neural basis of voluntary motor control and planning. *Trends in Cognitive Sciences*, 16(11), 541–549. Doi: 10.1016/j.tics.2012.09.008
- Seymour, R. A., Alexander, N., and Maguire, E. A. (2022). Robust estimation of 1/f activity

- improves oscillatory burst detection. *European Journal of Neuroscience*, ejn.15829. Doi: 10.1111/ejn.15829
- Shadlen, M. N., and Newsome, W. T. (1994). Noise, neural codes and cortical organization. *Current Opinion in Neurobiology*, 4(4), 569–579. Doi: 10.1016/0959-4388(94)90059-0
- Shadmehr, R., Smith, M. A., and Krakauer, J. W. (2010). Error Correction, Sensory Prediction, and Adaptation in Motor Control. *Annual Review of Neuroscience*, 33(1), 89–108. Doi: 10.1146/annurev-neuro-060909-153135
- Sharp, D. J., Bonnelle, V., De Boissezon, X., Beckmann, C. F., James, S. G., Patel, M. C., and Mehta, M. A. (2010). Distinct frontal systems for response inhibition, attentional capture, and error processing. *Proceedings of the National Academy of Sciences*, 107(13), 6106–6111. Doi: 10.1073/pnas.1000175107
- Sherman, M. A., Lee, S., Law, R., Haegens, S., Thorn, C. A., Hmlinen, M. S., ... Jones, S. R. (2016). Neural mechanisms of transient neocortical beta rhythms: Converging evidence from humans, computational modeling, monkeys, and mice. *Proceedings of the National Academy of Sciences*, 113(33). Doi: 10.1073/pnas.1604135113
- Shin, H., Law, R., Tsutsui, S., Moore, C. I., and Jones, S. R. (2017). The rate of transient beta frequency events predicts behavior across tasks and species. *eLife*, 6, e29086. Doi: 10.7554/eLife.29086
- Shink, E., Bevan, M., Bolam, J., and Smith, Y. (1996). The subthalamic nucleus and the external pallidum: two tightly interconnected structures that control the output of the basal ganglia in the monkey. *Neuroscience*, 73(2), 335–357. Doi: 10.1016/0306-4522(96)00022-X
- Siegel, M., Warden, M. R., and Miller, E. K. (2009). Phase-dependent neuronal coding of objects in short-term memory. *Proceedings of the National Academy of Sciences*, 106(50), 21341–21346. Doi: 10.1073/pnas.0908193106
- Singh, K. D., Barnes, G. R., Hillebrand, A., Forde, E. M., and Williams, A. L. (2002). Task-Related Changes in Cortical Synchronization Are Spatially Coincident with the Hemodynamic Response. *NeuroImage*, 16(1), 103–114. Doi: 10.1006/nimg.2001.1050

- Slepian, D. (1978). Prolate Spheroidal Wave Functions, Fourier Analysis, and Uncertainty-V: The Discrete Case. *Bell System Technical Journal*, 57(5), 1371–1430. Doi: 10.1002/j.1538-7305.1978.tb02104.x
- Softky, W., and Koch, C. (1993). The highly irregular firing of cortical cells is inconsistent with temporal integration of random EPSPs. *The Journal of Neuroscience*, 13(1), 334–350. Doi: 10.1523/JNEUROSCI.13-01-00334.1993
- Spitzer, B., and Haegens, S. (2017). Beyond the Status Quo: A Role for Beta Oscillations in Endogenous Content (Re)Activation. *eneuro*, 4(4), ENEURO.0170–17.2017. Doi: 10.1523/ENEURO.0170-17.2017
- Stock, A., Pertermann, M., Mckschel, M., and Beste, C. (2020). Highdose ethanol intoxication decreases 1/f neural noise or scalefree neural activity in the resting state. *Addiction Biology*, 25(6). Doi: 10.1111/adb.12818
- Swann, N., Tandon, N., Canolty, R., Ellmore, T. M., McEvoy, L. K., Dreyer, S., ... Aron, A. R. (2009). Intracranial EEG Reveals a Time- and Frequency-Specific Role for the Right Inferior Frontal Gyrus and Primary Motor Cortex in Stopping Initiated Responses. *Journal of Neuroscience*, 29(40), 12675–12685. Doi: 10.1523/JNEUROSCI.3359-09.2009
- Swann, N. C., Cai, W., Conner, C. R., Pieters, T. A., Claffey, M. P., George, J. S., ... Tandon, N. (2012). Roles for the pre-supplementary motor area and the right inferior frontal gyrus in stopping action: Electrophysiological responses and functional and structural connectivity. *NeuroImage*, 59(3), 2860–2870. Doi: 10.1016/j.neuroimage.2011.09.049
- Tachibana, Y., Iwamuro, H., Kita, H., Takada, M., and Nambu, A. (2011). Subthalamo-pallidal interactions underlying parkinsonian neuronal oscillations in the primate basal ganglia: BG oscillations in Parkinsons disease. *European Journal of Neuroscience*, 34(9), 1470–1484. Doi: 10.1111/j.1460-9568.2011.07865.x
- Tan, H., Jenkinson, N., and Brown, P. (2014). Dynamic Neural Correlates of Motor Error Monitoring and Adaptation during Trial-to-Trial Learning. *Journal of Neuroscience*, 34(16), 5678–5688. Doi: 10.1523/JNEUROSCI.4739-13.2014
- Tan, H., Wade, C., and Brown, P. (2016). Post-Movement Beta Activity in Sensorimotor

- Cortex Indexes Confidence in the Estimations from Internal Models. *The Journal of Neuroscience*, 36(5), 1516–1528. Doi: 10.1523/JNEUROSCI.3204-15.2016
- Thibaut, A., Simis, M., Battistella, L. R., Fanciullacci, C., Bertolucci, F., Huerta-Gutierrez, R., ... Fregni, F. (2017). Using Brain Oscillations and Corticospinal Excitability to Understand and Predict Post-Stroke Motor Function. *Frontiers in Neurology*, 8, 187. Doi: 10.3389/fneur.2017.00187
- Tinkhauser, G., Pogosyan, A., Little, S., Beudel, M., Herz, D. M., Tan, H., and Brown, P. (2017). The modulatory effect of adaptive deep brain stimulation on beta bursts in Parkinsons disease. *Brain*, 140(4), 1053–1067. Doi: 10.1093/brain/awx010
- Tinkhauser, G., Pogosyan, A., Tan, H., Herz, D. M., Khn, A. A., and Brown, P. (2017). Beta burst dynamics in Parkinsons disease OFF and ON dopaminergic medication. *Brain*, 140(11), 2968–2981. Doi: 10.1093/brain/awx252
- Torreccillos, F., Alayrangues, J., Kilavik, B. E., and Malfait, N. (2015). Distinct Modulations in Sensorimotor Postmovement and Foreperiod -Band Activities Related to Error Saliency Processing and Sensorimotor Adaptation. *Journal of Neuroscience*, 35(37), 12753–12765. Doi: 10.1523/JNEUROSCI.1090-15.2015
- Tzourio-Mazoyer, N., Landeau, B., Papathanassiou, D., Crivello, F., Etard, O., Delcroix, N., ... Joliot, M. (2002). Automated Anatomical Labeling of Activations in SPM Using a Macroscopic Anatomical Parcellation of the MNI MRI Single-Subject Brain. *NeuroImage*, 15(1), 273–289. Doi: 10.1006/nimg.2001.0978
- van Albada, S., Gray, R., Drysdale, P., and Robinson, P. (2009). Mean-field modeling of the basal ganglia-thalamocortical system. II. *Journal of Theoretical Biology*, 257(4), 664–688. Doi: 10.1016/j.jtbi.2008.12.013
- VanRullen, R. (2016). Perceptual Cycles. *Trends in Cognitive Sciences*, 20(10), 723–735. Doi: 10.1016/j.tics.2016.07.006
- Van Veen, B., Van Drongelen, W., Yuchtman, M., and Suzuki, A. (1997). Localization of brain electrical activity via linearly constrained minimum variance spatial filtering. *IEEE Transactions on Biomedical Engineering*, 44(9), 867–880. Doi: 10.1109/10.623056
- Varela, F., Lachaux, J.-P., Rodriguez, E., and Martinerie, J. (2001). The brainweb: Phase

- synchronization and large-scale integration. *Nature Reviews Neuroscience*, 2(4), 229–239. Doi: 10.1038/35067550
- Verbruggen, F., Aron, A. R., Band, G. P., Beste, C., Bissett, P. G., Brockett, A. T., . . . Boehler, C. N. (2019). A consensus guide to capturing the ability to inhibit actions and impulsive behaviors in the stop-signal task. *eLife*, 8, e46323. Doi: 10.7554/eLife.46323
- Voytek, B., and Knight, R. T. (2015). Dynamic Network Communication as a Unifying Neural Basis for Cognition, Development, Aging, and Disease. *Biological Psychiatry*, 77(12), 1089–1097. Doi: 10.1016/j.biopsych.2015.04.016
- Voytek, B., Kramer, M. A., Case, J., Lepage, K. Q., Tempesta, Z. R., Knight, R. T., and Gazzaley, A. (2015). Age-Related Changes in 1/f Neural Electrophysiological Noise. *Journal of Neuroscience*, 35(38), 13257–13265. Doi: 10.1523/JNEUROSCI.2332-14.2015
- Vrba, J. (2002). Magnetoencephalography: the art of finding a needle in a haystack. *Physica C: Superconductivity*, 368(1-4), 1–9. Doi: 10.1016/S0921-4534(01)01131-5
- Vrba, J., and Robinson, S. E. (2001). Signal Processing in Magnetoencephalography. *Methods*, 25(2), 249–271. Doi: 10.1006/meth.2001.1238
- Wagner, J., Wessel, J. R., Ghahremani, A., and Aron, A. R. (2018). Establishing a Right Frontal Beta Signature for Stopping Action in Scalp EEG: Implications for Testing Inhibitory Control in Other Task Contexts. *Journal of Cognitive Neuroscience*, 30(1), 107–118. Doi: 10.1162/jocn_a_01183
- Wang, X.-J. (2010). Neurophysiological and Computational Principles of Cortical Rhythms in Cognition. *Physiological Reviews*, 90(3), 1195–1268. Doi: 10.1152/physrev.00035.2008
- Waschke, L., Donoghue, T., Fiedler, L., Smith, S., Garrett, D. D., Voytek, B., and Obleser, J. (2021). Modality-specific tracking of attention and sensory statistics in the human electrophysiological spectral exponent. *eLife*, 10, e70068. Doi: 10.7554/eLife.70068
- Wei, M., Qin, J., Yan, R., Li, H., Yao, Z., and Lu, Q. (2013). Identifying major depressive disorder using Hurst exponent of resting-state brain networks. *Psychiatry Research: Neuroimaging*, 214(3), 306–312. Doi: 10.1016/j.psychresns.2013.09.008

- Wei, W., Rubin, J. E., and Wang, X.-J. (2015). Role of the Indirect Pathway of the Basal Ganglia in Perceptual Decision Making. *Journal of Neuroscience*, 35(9), 4052–4064. Doi: 10.1523/JNEUROSCI.3611-14.2015
- Weiss, S., and Mueller, H. M. (2012). Too Many betas do not Spoil the Broth: The Role of Beta Brain Oscillations in Language Processing. *Frontiers in Psychology*, 3. Doi: 10.3389/fpsyg.2012.00201
- Wen, H., and Liu, Z. (2016). Separating Fractal and Oscillatory Components in the Power Spectrum of Neurophysiological Signal. *Brain Topography*, 29(1), 13–26. Doi: 10.1007/s10548-015-0448-0
- Wessel, J. R. (2020). -Bursts Reveal the Trial-to-Trial Dynamics of Movement Initiation and Cancellation. *The Journal of Neuroscience*, 40(2), 411–423. Doi: 10.1523/JNEUROSCI.1887-19.2019
- Wessel, J. R., and Aron, A. R. (2017). On the Globality of Motor Suppression: Unexpected Events and Their Influence on Behavior and Cognition. *Neuron*, 93(2), 259–280. Doi: 10.1016/j.neuron.2016.12.013
- Wessel, J. R., Conner, C. R., Aron, A. R., and Tandon, N. (2013). Chronometric Electrical Stimulation of Right Inferior Frontal Cortex Increases Motor Braking. *Journal of Neuroscience*, 33(50), 19611–19619. Doi: 10.1523/JNEUROSCI.3468-13.2013
- Wessel, J. R., Ghahremani, A., Udupa, K., Saha, U., Kalia, S. K., Hodaie, M., . . . Chen, R. (2016). Stop-related subthalamic beta activity indexes global motor suppression in Parkinson's disease: STN Indexes Global Motor Suppression. *Movement Disorders*, 31(12), 1846–1853. Doi: 10.1002/mds.26732
- West, T. O., Berthouze, L., Halliday, D. M., Litvak, V., Sharott, A., Magill, P. J., and Farmer, S. F. (2018). Propagation of beta/gamma rhythms in the cortico-basal ganglia circuits of the parkinsonian rat. *Journal of Neurophysiology*, 119(5), 1608–1628. Doi: 10.1152/jn.00629.2017
- Whittington, M. A., Traub, R. D., and Jefferys, J. G. R. (1995). Synchronized oscillations in interneuron networks driven by metabotropic glutamate receptor activation. *Nature*, 373(6515), 612–615. Doi: 10.1038/373612a0
- Whittington, M. A., Traub, R. D., Kopell, N., Ermentrout, B., and Buhl, E. H. (2000).

- Inhibition-based rhythms: experimental and mathematical observations on network dynamics. *International Journal of Psychophysiology*, 38(3), 315–336. Doi: 10.1016/S0167-8760(00)00173-2
- Wilson, L. E., da Silva Castanheira, J., and Baillet, S. (2022). *Time-resolved parameterization of aperiodic and periodic brain activity* (preprint). Neuroscience. Doi: 10.1101/2022.01.21.477243
- Wimmer, K., Ramon, M., Pasternak, T., and Compte, A. (2016). Transitions between Multiband Oscillatory Patterns Characterize Memory-Guided Perceptual Decisions in Prefrontal Circuits. *The Journal of Neuroscience*, 36(2), 489–505. Doi: 10.1523/JNEUROSCI.3678-15.2016
- Wong, Y. T., Fabiszak, M. M., Novikov, Y., Daw, N. D., and Pesaran, B. (2016). Coherent neuronal ensembles are rapidly recruited when making a look-reach decision. *Nature Neuroscience*, 19(2), 327–334. Doi: 10.1038/nn.4210
- Yamawaki, N., Stanford, I., Hall, S., and Woodhall, G. (2008). Pharmacologically induced and stimulus evoked rhythmic neuronal oscillatory activity in the primary motor cortex in vitro. *Neuroscience*, 151(2), 386–395. Doi: 10.1016/j.neuroscience.2007.10.021
- Zavala, B., Zaghloul, K., and Brown, P. (2015). The subthalamic nucleus, oscillations, and conflict. *Movement Disorders*, 30(3), 328–338. Doi: 10.1002/mds.26072
- Zich, C., Quinn, A. J., Bonaiuto, J. J., O'Neill, G., Mardell, L. C., Ward, N. S., and Bestmann, S. (2022). *Spatiotemporal organization of human sensorimotor beta burst activity* (preprint). Neuroscience. Doi: 10.1101/2022.05.19.492617